# Study on Fatigue Resistance of Corroded Steel Girder Ends Retrofitted with Carbon Fiber Reinforced Polymer

炭素繊維強化ポリマー補修された腐食鋼桁端部の疲労耐久性に関する研究

Rusandi Noor

YOKOHAMA NATIONAL UNIVERSITY
March 2023

# Study on Fatigue Resistance of Corroded Steel Girder Ends Retrofitted with Carbon Fiber Reinforced Polymer

炭素繊維強化ポリマー補修された腐食鋼桁端部の疲労耐久性に関する研究

Rusandi Noor
19wa912

A dissertation submitted in partial fulfillment of the requirements
for the degree in Doctor of Engineering

Academic Supervisor

Assoc. Prof. Dr. Hiroshi Tamura
Prof. Dr. Hiroshi Katsuchi
Dr. Wang Jiaqi
Dr. Kensei Hirao

Department of Civil Engineering
Institute of Urban Innovation
YOKOHAMA NATIONAL UNIVERSITY
March 2023

Abstract

Post-retrofit inspection of retrofitted steel bridges can be particularly challenging due to the lack of visual accessibility by the inspector. It should be necessary for the bridge reinforcement elements should meet the durability standard in service life performance. Moreover, the prediction of damage type and damage initiation process should be characterized to provide an accurate understanding of the retrofit part's life.

This study was initiated by numerical investigation of the CFRP (Carbon Fiber Reinforced Polymer) reinforcement for local-corroded steel girder ends. The modeling consists of 3 configurations of bracing types of simple supported steel bridges. Local stress transformation studies are conducted so that the steel girder ends stresses due to various types of loading can be predicted. The CFRP retrofit model was validated with CFRP in the existing system to evaluate the modeling approach parameter. Then, the modeling and field loading test validation reached a good agreement. The validated corroded girder model showed high-stress values under the design loads. The result has been studied based on a computational model to gain the shape of the elastic local stress distribution of CFRP to capture the response in different loading types. The contribution of the 50 mm curved shapes of reinforcement member parts significantly affects the compressive stress distribution shape and out-of-plane displacement of the corroded steel part. Simulating and predicting these local stress and deformation modes characteristics based on actual conditions will support the need for field measurement of local stresses.

There could be the possibility of insufficient fatigue machine specification to applicate a full-size retrofitted bridge target part. Then, only a small effective (practical) part was constructed as a compact specimen to interpret the fatigue experiment complexity. The fixture and specimen design became key parameters to replicate the CFRP retrofit girder ends element conditions. The novel design method contained various functions: fixture layout strategy and applied the CFRP retrofit guidelines. Therefore, the fixturing layout is essential to identify the technical parameter configuration in eccentric fatigue cyclic loading, which is the configuration of the retrofit specimens following the limitation of the fatigue machine. In addition, the filler plate also contributed to eccentricity reproduction during the fatigue experiment. Therefore, the simplification approach of the corroded specimen part was conducted: corroded bead adjustment and specimen narrowing width. Due to the limitation of duplicability of the corroded girder ends part, e.g., stiffener, scallop parts. The simplification design was generated under the reproduction of local stress distribution methods to maintain the elastic behavior of

the retrofit specimen. These fixtures and compact specimen design have not produced a CFRP retrofit specimen bearing failure to date (elastic condition). With this challenge, the novel fatigue experimental design is appropriate for developing accuracy in various applications.

The experimental fatigue scale evaluated the strengthened damaged part of steel girder ends by recognizing the resistance behavior under long-run elastic loading. The study aims to make it possible to consider the location of fatigue initiation due to low-durability section parts. Retrofit specimens were designed to replicate the inner side corrosion of the exterior steel girder web ends. Applicability of a new bending fixture design to reproduce a service load bridge was performed by considering the compact specimen shape and dimensions. Also, a strategy for fatigue strength evaluation is outlined, including polyurea putty application (FU-Z), loading frequency, and data collection methods. Lifecycles-oriented investigations of local stress showed a damage initiation characteristic of retrofit specimens without polyurea putty was detected at $3 \times 10^6$ cycles. The results also showed the redistributed local stress that the shifted local stress ($\sigma_{SLS}$) detection of the edge joint was identified at one point from four strain gauge points observations. The damage initiation is discovered in elastic constant amplitude load fluctuation. Thus, this phenomenon became the main discussion in this study. A slight local stress inclination was established at $3.5 \times 10^6$ cycles to observe and analyze the damage propagation characteristics. In addition, significant delamination was confirmed from a cut-off section. Delamination was observed at the surrounding location of detachment at the end of the corroded web edge. However, the fatigue experiment results showed that polyurea putty (FU-Z) was a low-strength material with elastic high-elongation properties (300%－500%) involved in the durability parameter. That flexibility benefit was to prevent delamination and detachment under extended cyclic concentration stress. Due to long compressive fatigue loading, the damage initiation characteristics could give a better view of the relationship between the durability of bonding strength in each material component.

Through this study, durability observation indicated that the CFRP-repaired steel girder end specimens succeeded due to fatigue. This study contributed significantly to the novel specimen design to effectively replicated the serviceability of steel girder bridge loads. Additionally, to obtain the long-lasting reinforcement of corroded steel girder ends, CFRP guidelines and specifications should be adhered to.

Acknowledgment

Alhamdulillah hirobbil Alamin (all praise belongs to Allah)

After 3.5 years of living in Japan, learning fundamental knowledge of retrofitting corroded steel girder ends was a short time. I dedicated this dissertation to my beloved country Indonesia and my town Samarinda, which has many plans to develop a retrofit method for the bridge in the future. The correlation using new materials such as polymer and CFRP sheets to reinforce the damaged bridge structure becomes a bright idea for more development. Then, I hope this material's usability will be extended to collaborate with the main structure by following the necessity of an effective and efficient structure.

I sincerely thank MEXT for the financial support provided by the Japanese Government (MONBUKAGAKUSHO: Ministry of Education, Culture, Sport, Science, and Technology – MEXT). The scholarship has made this research possible, and it is greatly appreciated. Also, I am grateful to my family, who always give me advice and support, and then wait for me with calm and best hope. I apologize that I miss many moments during My study.

Acknowledgments and all gratitude are addressed, dedicated, and presented to Associate Professor. Hiroshi Tamura for his professional advice backed by a high level of generosity, patience, and wisdom in our active communication. Your contributions to this study are uncountable. May your goodness and kindness get the best reward.

Acknowledgments are also directed to the dissertation committee members: Professor. Hiroshi Katsuchi, Professor. Hitoshi Yamada, Professor. Koichi Maekawa, and Associate Professor. Chikako Fujiyama, for their comments and suggestions for any improvements in the present work. Furthermore, the author sincerely thanks the Nippon Expressway Research Institute manager, Yuya Hidekuma, for the CFRP reinforcement process work guidelines.

The members of the academic staff of the Bridge and Structural Engineering (Group I) Laboratory of Civil Engineering Department: Dr. Jiaqi Wang, Dr. Kensho Hirao, Miyuki Sakai, and all students are gently asked to receive the author's appreciation for their help in managing the problem involved by his presence between them.

Rusandi Noor

# Contents

# List of Figures

# List of Table

# Chapter 1

# Introduction

## 1.1 Background

Corrosion of steel plate girder bridges is one of the common damage phenomena. An aggressive attack on the environment and insufficient maintenance significantly intensify the situation and may influence the performance of steel bridge members. Corrosion of steel bridges is likely to progress due to flying sea salt particles and dust accumulation, so it is important to remove these [1]. In actual steel plate girder bridges, the outer surface of the exterior girder tends to corrode slower than the inner surface. It is presumed that one of the reasons for this is that sea salt particles and dust adhering to the outer surface of the exterior girder were washed away by rain. This condition is named wetting-drying-washing. Steel girder bridges were commonly located at the girder ends in corrosion cases. Data on damage in many steel bridges in Japan was inspected by Tamakoshi et al. [2] as a result of the ten-years (1994-2003) data collection period. They found the typical location of local corrosion damage at steel girder ends. They classified steel girder ends as 88.4% of the total steel bridge corrosion case. Figure 1.1 displays the result of wetting-drying-washing with field characteristic of local corrosion damage at steel plate girder ends. Especially at the inner side of exterior girder ends, which is dominantly subjected to the reduction of steel bridge members carrying capacity. The consequence of this deterioration can vary from a continuing weakening of the steel girder ends over long periods (life-service). Then, corrosion damages have to be carefully assessed and calculated. Hence, immediate repair is necessary, while the conditions generated by surface corrosion cannot be tolerated in many cases.

The effective life cycle of highway steel bridges differs in several aspects, including the fatigue strength and durability of the structural component. As the fatigue life of bridge parts depends on their service loading history, the frequency distribution of traffic stress range and their relationship with the traffic pattern are expected. Also, the influence of self-weight load plays a significant role in determining total (cumulative) stresses that could be experienced in the long-life expectancy. Consequently, the microstructure durability strength level determines the girder ends part resistance to the elastic-stress amplitude. John W. Fisher et al. [3] measured the maximum out-of-plane displacement at the bearing stiffener of Poplar Street Bridge. They found the displacement range is about 0.013-0.025 mm, with the highest web stress from random trucks recorded at 89.6 MPa and the lowest at 6.9 MPa. Moreover, this numerical and experimental study obtained the effect of extensive actual load conditions in the CFRP-strengthened steel girder end specimens. The retrofitted part's performance should count on the adverse service stress range ($\Delta\sigma$) and survive under repeated high-cyclic fatigue ($N>10^6$) loading. In structural bridges application, I-girders are exposed to eccentric traffic loading, eventhough a slight eccentricity of the service load was relative to undeniable. The eccentric bending loads occur as vehicles pass over

the bridge, each causing a fluctuational load cycle, triggering fatigue stresses over time. In this way, it is possible to imitate the eccentricity phenomena at the girder ends to generate the actual stress direction in the small-scale targeted region part, as shown in Figure 1.2. An issue caused by the traffic pattern load effect on CFRP retrofitted steel girder ends bridges depends on accurately understanding traffic load distribution. The critical region in CFRP retrofit should be identified as the location with the maximum equivalent of local stress representing the fatigue damage initiation parameter. And then, the type of visual damage initiation could be observed in this study to provide convincing evidence that the contribution of the development of local elastic stress ($\sigma_{local}$) under high-cyclic fatigue durability criteria. Finally, even the magnitude of the stress at the girder ends might be relatively below the allowed stress design $(\sigma_{Comp.} = 140\ MPa)$ [4], the large number of loading cycles caused by life traffic may result in potential damage regions in high-cycle fatigue conditions.

High-cycle fatigue is produced by small-scale elastic strain under high load cycles before damage initiation. In bridge cases, high-cycle fatigue contains two main factors: self-weight and live load. Thus, HCF is governed by elastic deformation and is usually characterized by a stress-life method. Dead load (self-weight) is also identified as permanent static load. Dead load comprises the weight of the bridge structure or other fixed elements before any live load is considered. Live load (traffic) is included in the dead load to provide the total (cumulative) loading applied to the bridge structure. Therefore, various local stress fluctuations must be idealized to study the high-cycle fatigue behavior of components subjected to constant-amplitude load fluctuation (CALF) traffic loading to represent the most severe condition. Besides, calculating the correct service load (dead-live) is necessary to ensure the engineer's structural assessment of the target part. A schematic diagram demonstrates the general relation between the actual self-weight and traffic load at the bridge girder support structure shown in Figure 1.3. Perform an excellent high-cycle fatigue experiment requiring accurate service load (dead-live) configurations in load-range conditions at the girder ends section. In addition, this investigation is currently being conducted to develop a simple method to predict CFRP-strengthened part durability against fatigue.

Moreover, to determine stress distribution based on the load service approach on the elastic state. One can establish the influence of more than one loading category on the girder ends regions by linearly adding the vertical or compressive stress due to each loading mode. Combining stress distribution based on service load for identical geometry is occasionally referred to as the stress principle of superposition, including corroded and retrofitted geometry. Finally, a single value of the highest local stress from service stress distribution data can define the maximum and minimum specimen loading conditions within load cycle numbers. The relationship between load range $\Delta P$

and frequency (Hz) are the essential parameters for controlling and monitoring the location of fatigue initiation damage life of CFRP retrofit components.

Cleaning, repainting, and attaching additional steel plates are standard methods to repair corroding steel bridge members. However, this method is insufficient to restore a cross-section loss with advanced corrosion, which requires another form of countermeasure for recovery of section modulus (Z). However, countermeasures generally require extensive equipment, facilities, and special skills, often inefficient when the applied area is relatively small. Then, carbon fiber reinforced polymer (CFRP) reinforcement is used to upgrade the load capacity of corroded steel bridge members due to its high elasticity and strength characteristics.

## 1.2 Related Research

This study targets the damage initiation of CFRP retrofit parts with high-cycle fatigue assessment parameters that are difficult to find or detect from actual conditions. Hence, the parameters affecting the structural performance of steel girder ends repaired by CFRP were clarified. These parameters were assessed and analyzed quantitively. In practice, the specimen could have experienced a slight deterioration in a high-cycle loading case. For this reason, the use of strain gauge measurement was proposed. In addition, the application of signal processing was considered to extract the irregularity stress or stress variant detection from cyclic static loading to evaluate the uncertain damage. The sinusoidal waveform data extracted by the signal contains an evolution of material strength. So, it should be visualized and identified by a simple assessment approach. The degree of an experiment to reproduce an actual condition was required. Based on these procedures, original assessment methods were constructed.

### 1.2.1 CFRP Mechanics and Its Modelling

Carbon fiber reinforced plastics (CFRP) have achieved general use as structural components in civil engineering due to excellent structural properties, such as high strength, high modulus, lightweight, and corrosion resistance [5]. The hardening (curing) process transformed the mechanical properties between fiber sheets and matrix (resin). Then, the mechanical property of CFRP is described as comprehensive implementation through a good mix proportion of several carbon fiber sheets (< 20 sheets) and resin (matrix). The typical method for calculating the mechanical properties of CFRP by the classical laminated theory. Under the conditions that the fiber sheets are uniformly distributed in the matrix. Typical calculation formulae of the mechanical properties of CFRP have been proposed based on the experiment result with the theory of elastic mechanics [6].

Also, many studies have conducted a deep analysis of the strength and stiffness of the CFRP part using finite element simulation software. Alfano et al. [7] found that the sensitivity of modeling laminated composite can be determined based on the constraint approach and the input mechanical parameter. For these reasons, the researcher should develop strategies for modeling mechanical behavior based on damage mechanics. Nirbhay et al. [8] simulated CFRP using an Abaqus S4R shell element rather than a solid element to save computational costs. The accurate result is preserved in their simulation due to the actual behavior of CFRP in the tensile test. The modeling of the rehabilitation of steel beams with CFRP was conducted by Bagale et al. [9]. The study showed the nonlinear finite element analysis under static and fatigue loads. As a conservative method, the fatigue life analysis for CFRP-strengthened members can be predicted based on localized points with high-stress concentration. The study also proposed the fatigue life formula for a simply beam strengthened by aramid fiber-reinforced polymer with an ultimate strain of more than 1.86 % and elastic modulus (E = 128.5 GPa). The study is also relevant to the linear elastic fracture mechanics fracture method (LEFM). The condition could be categorized as the maximum local stress level cannot exceed 50% of the material yield stress. Thus, the SN-curves generated between 31 and 200 MPa stress range level.

### 1.2.2 Severe Structural Response of Steel-CFRP Reinforcement

The structural fatigue assessment of the retrofitted steel-CFRP (corroded girder-ends cases) has not been established, considering the complexity of the evaluation parameters. Hence, to evaluate the fatigue performance of CFRP steel reinforcement. So many studies have been reported that affect the retrofitted steel-CFRP fatigue resistance to severe loads and conditions. In the following, some of the related studies will be announced.

Many investigators (Shenoy et al., Colombi et al., Liu et al., Zhang et al., Deng et al.) [10-14] adopted tensile-fatigue cyclic loading as the analytical method, leading to the rapid failure of the reinforced specimens. However, most studies focused on the CFRP steel reinforcement of fatigue behavior response due to single/double lap joints. Which contributed less to the actual retrofit condition of the girder ends. Hosseini et al. [15] significantly involved the Prestressed Unbonded (PU) CFRP tensile fatigue test, which finds the prestress level for applied fatigue crack arrest conditions. Still, Anbang et al. [16-18] considerably investigated the influence of the corrosion degree of steel plates specimen with CFRP strengthened on fatigue life. Also, from their result, it is important to consider surface loss design as a representation of corrosion. The surface characteristics have a significant effect on CFRP bond properties. Their specimen is made of an actual corroded plate. Ensuring the surface preparation cleaning up properly from a small corroded

pit is challenging. Even though their purpose is to determine the influence of corrosion duration of CFRP strengthened. As a comparison, Islam et al. [19] explored the degree of pitting (DOP) in steel plates due to bending load, which showed that the bending strength result was decreased following the increase of DOP. The possibilities of local stress-higher originating from pitting could be undetectable.

Then, the effect of fatigue damage of the corroded steel plate strengthened CFRP initiated at the bottom of the rust pits on the steel surface. Also, they found that the failure mode depended on the adhesive thickness rather than corrosion depth, which means they did not refer to any specification of CFRP reinforcement. The actual procedure of CFRP plates strengthened of corroded steel case should be followed to give a satisfactory result practically. Therefore, they recognized that the end anchorage successfully delayed the initiation process of the CFRP bonding interface and improved the fatigue-strengthening stiffness. In the finite element model (FEM), Anbang et al. considered the concept of elastic stress concentration to determine the corroded pit's peak stress. The elastic peak stress of a corroded steel plate can be decreased under the stress level of a healthy steel plate in the same load condition through CFRP strengthened. Then, their parameters have followed by the author due to generate the complete elastic condition during the CFRP reinforcement fatigue experiment.

Next, few studies have addressed compressive application. The CFRP was used to retrofit steel members dominated by compressive conditions. Ekiz et al. [20] experimentally studied the local buckling and post-buckling behavior. They utilized double channel members warped with CFRP and subjected them to compressive cyclic loading. Again, Liu et al. reported that using CFRP strip plates on damaged steel plates was more efficient using a higher elastic modulus. The high modulus CFRP reflects high stiffness. When the same loads were introduced in the damaged steel target, high-stiffness CFRP can hold more loads without increasing the stress level in the steel plate.

Another study by Khuram et al. [21] clarified the sensitivity of various girder ends corroded damage conditions. The uniform rectangular corrosion height based on those parameters is expected to provide an incredibly moderate or conservative analysis of the stiffness reduction at the inner web ends. They found that the load-displacement buckling mode will be seen with the height of corrosion of more than 60 mm at the girder web ends regions. After that, Wakabayashi et al. [22] also investigated the behavior of corroded steel girder ends with CFRP reinforcement. They carried out the uniaxial compression experiment, whose thickness reduction was replicated in the real corroded girder ends, with 100 mm corrosion height and 50% surface loss on both sides of the web. They also follow the retrofit CFRP specification to convert the steel surface loss using the

elastic modulus of CFRP. Then, the amount of CFRP sheet layer is agreed to be more than the reduced thickness by artificial corrosion. The load capacity was increased by 121 kN due to the strengthening CFRP. However, the location of damage initiation (buckling mode) between unrepaired and repaired is almost identical. Then, this study realized that this damage mode behavior should explore more. The influence of reinforcement unsatisfied to shift the location of stress concentration of the repaired target in actual conditions of bridge life service (elastic condition fatigue). The damage mode should be designed carefully to control the CFRP part that experienced more dominant damage than the damaged steel. Finally, the severe structural response for CFRP reinforcement should be laid on two parameters:

1) Design of artificial uniform corroded parts for specific structure applications is mandatory,
2) Determine the representative structural parameters to characterize local stress and deformation under fatigue conditions.

### 1.2.3 Eccentricity Load-Induced Fatigue

Maintaining the durability of CFRP reinforcement parts in a long life-service period is a critical issue directly related to the safety of the entire steel bridge structure. However, the deterioration of CFRP stiffness is difficult to assess and detect. Therefore, developing a convenient approach to monitoring the integrity of CFRP parts using vehicle eccentricity characteristics could be one option for safe maintenance post-retrofit. Many studies have been conducted to evaluate vehicle eccentricity problem-induced fatigue [23-28]. However, several studies will be pointed out due to the priority.

The eccentric load of a large vehicle group can cause the out-of-plane condition of the steel bridge components. The practical evidence was delivered from Kasra et al. [29] experiment, which assessed the FRP-repaired welded joints of the bridge due to distortion-induced fatigue. The study was conducted under constant-amplitude cyclic loading with 21, 28, and 35 kN load ranges. The specimen loading configuration rotated the specimen $90^{o}$, and the cyclic load was applied vertically at the stiffener. They also set the pin-rolled support at both flanges. This loading-unloading direction is coupled with in-service loading history, which was complicated to assess. Because the actual loading distributes from the slab to the flanges-web, not directly placed in the reclined stiffener. Consequently, the actual loading should be modified with a reduction factor. To apply this approach or use the stress superposition method (SSM) with finite element analysis to determine the load value in the experiment.

Next, Al-Salih et al. [30] investigated distortion-induced fatigue on bridge web gaps. They conducted a novel repair method by attaching the FRP part to reduce localized stresses in the web gap region. The out-of-plane fatigue test was established to investigate the performance of the CFRP part due to its durability. There was no debonding between CFRP and steel, suggesting excellent durability under demanding fatigue load. Even the stress range is almost 200 MPa at the bottom web. The load range in their experiment was three times that would be produced by AASHTO fatigue truck in a full-scale steel girder bridge. The reason was selected to ensure the sensible experiment time duration. This study also prioritized the load control as high-cycle fatigue (stress approach) with a maximum load of 25.5 kN and a minimum load of 2.2 kN with 0.5 Hz frequency fatigue cycles. Also, the result indicated that the residual strength of the damaged steel part plays an essential role in supporting the CFRP retrofit part to prevent crack propagation. The observation used a strain gauge to compute the abnormal stresses to indicate damage initiation and propagation. The damage initiation was observed at 6500 cycles on the interior girder web. Then, they continued the fatigue loading with CFRP retrofit sequence with crack length as a limitation. The last cumulative number of cycles was 10.405.000 million cycles with 161.3 mm crack length at web-flange weld crack. The comparison of maximum out-of-plane displacement results between unrepaired and repaired specimens was decreased due to CFRP reduction stress capability. These findings support the benefit of combining steel-CFRP to repair eccentricity-induced fatigue damage. The result shows that the steel girder was deformed linearly until the damage was initiated. The deformed web changed from a linear pattern before cracking, associated primarily with bending at the girder web. This condition should be avoided in this present study. After all, Al-Salih et al.'s study laid a significant foundation for field implementation. The CFRP retrofit has become a prevention method for eccentricity load problem-induced fatigue in steel bridges. This finding supports the present study in the manner of fatigue experiment testing approach.

Also, Hartman et al. [31] investigate the out-of-plane rotation-induced fatigue at the steel girder. Similar to Al-Salih et al., this study conducted large specimens. This study provides a 2.8 m long girder segment with cross-frame bracing type as a component-level test. Then, they also provided that the scaled bridge test included 9.1 m long girders spaced at 1.5 m with cross-frame bracing. A significant result from the two setups was that the scaled bridge test included the strong-axis bending effect, which the component-level test did not. The result is accepted because the component-level test was entirely subjected to out-of-plane loading. Comparing the crack pattern and length between the two setups was critical. Therefore, the crack pattern was placed in almost the exact location, and the crack length of the scale bridge test was small.

Based on the above research, reproducing the eccentric load of the bridge at a small-scaled test experiment level is promising. Developing a practical experimental instrument that can accurately predict the compressive out-of-plane behavior at the girder ends subjected to high-cycle fatigue. Also, it was further to understand the significance of eccentricity vehicle in-service loading variables. This study provided a distinctive prospect to recognize and analyze the durability of CFRP reinforcement parts of scaled corroded steel bridge web ends components in laboratory environments. The behavior of CFRP retrofitted parts can be sensitive to post-control of maintenance when members behave unexpectedly. Moreover, the lack of guidelines for post-retrofit construction of CFRP material is required to refine or improve the available design recommendation.

### 1.2.4 Damage Initiation of CFRP Reinforcement

An engineering classification for fatigue damage initiation is "the time required developing a damage of visible size." The damage initiation phase of CFRP under high-cycle fatigue has not been investigated intensively. Instead, damage initiation has always been described in a more predictive way without clear physical evidence. However, a few studies discussed the damage initiation of CFRP reinforcement [32-34]. In the next paragraph, some of the studies will be announced.

Magi et al. [35] defined CFRP damage initiation as the first nucleation in the off-axis of layers. It was observed that initiation corresponded to the actual separation of a different material. Thus, damage initiation shall be characterized as a critical condition that changes the rate of structural degradation for given actual loads. Further, O'Brien et al. [36] investigated the cyclic bending test of fiber-reinforced polymer. Under bending, damage initiates at the tensile bending surface. The physical evidence was generated that damage initiates coincide with the samples' final broke. Then, we can conclude that the damage propagation phase of CFRP-only is very short under cyclic loading.

Marco et al. [37] studied the relation of compressive strength properties. They found that in the unidirectional CFRP-only, it was often less than 60% of their tensile strength. A strong impact of the fiber alignment on the damage initiation has been discovered. Localized compressive stress develops simultaneously with damage initiation, three times lower than the tension stress limit. Damage initiation of CFRP-only has been assessed from the stress induced at the interface. Also, their study assumed that compressive strength is severely affected by the transverse behavior where micro buckling of the fibers can lead to damaged nucleation. Therefore, we have argued about it. The main problem occurs when the matrix or resin cannot hold together of fiber (material

characteristics). The resin's low modulus elasticity and flexibility make them more brittle than fiber. When micro buckling occurs of fiber, the resin cannot resist the micro displacement of fiber, resulting in the opening/crack.

Further, the matrix initiation damage was found by Skinner et al. [38]. The initiation damage at resin was the primary damage, including the transition stage 1 and stage 2 of fatigue life at about 10%. The initial damage at the matrix begins to merge, forming the macrocrack at the damage region. After all, the damage initiation of CFRP-only was dominated by the shear stress of components and initiated at matrix/resin material.

Deng et al. [39] pointed out that in the fatigue load of CFRP-strengthened steel beam, the damage initiation was observed firstly at the notch tip (pure bending zone). This result was also verified by Anbang et al. studied. Both studies reveal the exact characteristics of damage initiation. The initiation damage with the tension-tension test first appeared at the bottom of the rust pit on the surface of the corroded plate. The damage zone was the weakest and most profound in the initiation zone, caused by fluctuating opening and closing for a certain period. Especially in Anbang et al. studied, they have evidence for coloring damage initiation criteria darker than the propagation zone due to cumulative stress concentration. Another study by Panella et al. [40] successfully monitored fatigue initiation damage under fatigue endurance prediction. The study applied a complex thermoelastic stress analysis for the non-contact method during cyclic loading. Early fatigue damage was identified through the method. Next, Ammar et al. [41] found the typical damage initiation followed by a sudden stress drop. It occurred for many reasons, including the effect of significant change in the boundary of material. The investigation also mentioned the preexisted voids in the specimens under microscopic conditions. Then, the present study should avoid those situations and control the specimen before and after fatigue loading to ensure the retrofit work is satisfied. Further, the comparison should be maintained to validate the fatigue experiment result.

Finally, the fatigue damage initiation life of CFRP retrofit structural components is probably influenced by indications as follows:

1) Surface regularities
2) Existing defects or low-performance work
3) Reduce volumetric components that increase stress.

This research adopts an area-risk method parameter that can represent the fatigue damage initiation in retrofit components with proper actual loading, e.g., eccentric load in compression-compression (C-C)

## 1.3 Purpose and Objective

This study proposed the analysis process stage, which recognizes technical evidence under elastic conditions to generate the visual damage initiation characteristic in the CFRP retrofit girder ends specimen. Each damage indication in this mechanism should satisfy the fatigue damage criteria. The main task was to identify the "turning points" of constant load cycle counting to recognize the contributions of cumulative damage on girder ends structural reinforcement geometry. Based on these ideas, detecting damage initiation characteristics is suitable to describe CFRP retrofit high-cycle fatigue damage evolution. For this purpose, numerical simulations were conducted to find the severe element of the CFRP part by varying the type of steel bridge structures. Understanding the typical loading mode was intended to clarify these severe conditions. The assumption of the girder end conditions was followed in this stage. The finding of the identification stage was a basis for conducting the next stage. Second, a proposed novel design of compact specimen and bending fixture was designed following a previous result. To reproduce the CFRP retrofit girder end conditions, which significantly affect the bridge structural performance due to eccentric loading, was proposed. Here, it is shown that the proposed method can be applied to conduct the axial compressive load and bending mode together. Third, to evaluate the fatigue durability, which indicates low durability. The durability fatigue performance of the CFRP-steel retrofitted part was mainly prepared. A constant cyclic elastic loading experiment was proposed to observe and evaluate the damage initiation phenomena. The complementary experiment was included, i.e., constant creep loading and temperature experiments. In addition, the possibility of visual assessment evaluating fatigue damage was demonstrated. It was recommended to answer each objective sequentially. The specific objective of the research presented in this thesis are:

1. To identify the characteristics of high-local stress and displacement at steel girder ends CFRP retrofit considering fatigue damage.
2. To develop a novel experimental method reproducing eccentric cyclic loading at steel girder ends.
3. To observe cyclic loading conditions due to its lowest durability location on the retrofitted specimen.

## 1.4 Dissertation Outline

This study used a combination of both numerical and experimental methods. To address the research objectives are discussed in three main chapters, Chapters 2 to 4, respectively. The flow of this research is illustrated in Figure 1.5.

Chapter 1: Introduction

Background, related research, purpose, and research objective have been described.

Chapter 2: Identification of Severe Structural Parameters of CFRP Retrofit Girder Ends

An analysis of numerical to find the representative structural parameter of CFRP retrofitted steel girder ends is described in this section. The out-of-plane problem caused by vehicle eccentricity is analyzed and classified into two cases load. The determination of the target considering fatigue damage, e.g., severe, moderate, and mild, was pointed out. The development of CFRP modeling is essentially in the present study with validation of field measurement. Finally, the stress distribution of the healthy-corroded-retrofit (HCR) target girder was constructed to support the identification of fatigue assumed stated.

Chapter 3: Reproduction of Load Conditions on Fatigue Experiment

The compact design specimen, which reproduces local deformation of retrofitted girder ends under actual service loading, is created, and clarified in this chapter. First, the design requirement by the specification of fatigue testing to reproduce eccentric axial load (designed fixture). Then, following the CFRP manual specification for corroded steel girder ends, consider the compact specimen shape and dimension. Also, the form of elastic stress distribution should be agreed with each other (retrofit girder ends sub-model and retrofit specimen) to determine the value of cyclic loading. Furthermore, by the design of eccentric load specimens for fatigue conditions, experiment evaluation of steel-CFRP strengthened became possible.

Chapter 4: Fatigue Durability Observation of Steel Girder Ends CFRP Reinforcement Specimen

The present experimental study was constructed to give adequate data to determine the dependence of CFRP fatigue durability by observing the damage initiation type. This objective can be explained based on elastic response over cycles. Thus, this research proposed a new parameter related to the practical definition of CFRP damage initiation as "the period required to produce a damage into visible size". The following experimental setup is intended to observe CFRP reinforcement-steel girder ends degradation through damage initiation.

This study proposes a different approach in the retrofitted specimen material application of polyurea putty (FU-Z), considering the degree of field application. Also, to perform a

durability experiment in fatigue, uncertain parameters, e.g., temperature and creep, have been clarified in this study. Then, to apply the cyclic load of more than 1 million cycles is required 2 days or more at the shortest. The cyclic loading decided to stop at 3.5 million cycles that spent 10 days long. Moreover, the strain measurement was performed intermittently so that the deformation of the retrofit specimen could be grasped in units of 10.000 cycles.

From the experiment specimen without putty, the detection of damage initiation is possible by using shifted local stress $\sigma_{SLS}$ that indicated the change of micromechanics due to fatigue. Since the $\sigma_{SLS}$ is achieved by the separation of joint bonds perpendicular to the stress direction. The modulus elasticity of CFRP held a constant local stress level for an extended cyclic load. Also, it immediately dissipated a shifted local stress. It returned to the initiation stress level, while the modulus elastic of joint material transformed with time. However, the contribution of putty material was noticed to control the internal detachment and delamination in the CFRP reinforcement structure. The polyurea putty's ability to elongate helped the specimen matrix (resin) sustain long eccentric cyclic loading. Finally, by analyzing the characteristics of signal waves of fatigue loading, it was shown that it is possible to evaluate the CFRP retrofit of steel girder ends experimentally.

Chapter 5: Conclusion and Recommendation

The main conclusion of this work is discussed in this section, along with the author's proposed CFRP reinforcement treatment method to control the durability under service life.

## 1.5 References


[1.1] Tamaki, Y., Shimozato, T., Tai, M., Fuchiwaki, H., & Taira, H. (2019). A Study on Washing Effect of Steel Girder Bridges Under Airborne Salt Environment in Subtropical Okinawa Areas. *Steel Construction Engineering*. 26(102), 102_43-102_55. (In Japanese)

[1.2] Tamakoshi, T., Yoshida, Y., Sakai, Y., & Fukunaga, S. (2006, October). Analysis of damage occurring in steel plate girder bridges on national roads in Japan. *In Proceedings of the 22nd US–Japan Bridge Engineering Workshop*, Seattle, WA, USA (pp. 23-28).

[1.3] Fisher, J. W., Yen, B. T., & Wagner, D. C. (1987). Review of field measurements for distortion-induced fatigue cracking in steel bridges. *Transportation Research Record*, (1118).

[1.4] Japan Road Association. (JRA) (2012). Specifications for Highway Bridge (Part II Steel Bridges). ISBN978-4-88950-717-1 C2051

[1.5] Nippon Expressway Research Institute (NERI). 2015. Design and Installation Manual for Upgrading Steel Structure with The Use of Carbon Fiber Sheet. Tokyo

[1.6] Pham, N. V., Miyashita, T., Ohgaki, K., Hidekuma, Y., & Harada, T. (2021). Repair Method and Finite Element Analysis for Corroded Gusset Plate Connections Bonded to CFRP Sheets. *Journal of Structural Engineering*, 147(1). 04020310

[1.7] Alfano, G., & Crisfield, M. (2001). Finite Element Interface Models for The Delamination Analysis of Laminated Composites: Mechanical and Computational Issues. *International Journal for Numerical Methods in Engineering*, 50(7), 1701-1736.

[1.8] Nirbhay, M., Dixit, A., Misra, R. K., & Mali, H. S. (2014). Tensile test simulation of CFRP test specimen using finite elements. *Procedia Materials Science*, 5, 267-273.

[1.9] Bagale, B. R., & Parvin, A. (2021). Fiber-Reinforced Polymer Strengthening of Steel Beams under Static and Fatigue Loadings. *Practice Periodical on Structural Design and Construction*, 26(1), 04020046.

[1.10] M. Shenoy, J. Zhang, and D. L. McDowell. (2007). Estimating fatigue sensitivity to polycrystalline Ni-base superalloy microstructures using a computational approach. *Fatigue Fract. Eng. Mater. Struct.*, vol. 30, no. 10, pp. 889–904.

[1.11] P. Colombi and G. Fava. (2012). Fatigue behavior of tensile steel/CFRP joints. *Compos. Struct.*, vol. 94, no. 8, pp. 2407–2417.

[1.12] H. Liu, X. L. Zhao, and R. Al-Mahaidi. (2020). Fatigue crack growth simulation for CFRP bonded steel plates using boundary element method. *Compos. Civ. Eng. CICE 2006*. vol. 4, no. Cice, pp. 425–428.

[1.13] D. Zhang, W. Huang, J. Zhang, W. Jin, and Y. Dong. (2021). Prediction of fatigue damage in ribbed steel bars under cyclic loading with a magneto-mechanical coupling model. *J. Magn. Magn. Mater.*, vol. 530, no. January, p. 167943.

[1.14] J. Deng, J. Li, and M. Zhu. (2022). Fatigue behavior of notched steel beams strengthened by a prestressed CFRP plate subjected to wetting/drying cycles. *Compos. Part B Eng.*, vol. 230, no. July 2021, p. 109491.

[1.15] A. Hosseini, J. Michels, M. Izadi, and E. Ghafoori. (2019). A comparative study between Fe-SMA and CFRP reinforcements for prestressed strengthening of metallic structures," Constr. Build. Mater., vol. 226, pp. 976–992.

[1.16] A. Li, S. Xu, H. Wang, H. Zhang, and Y. Wang. (2019). Bond behavior between CFRP plates and corroded steel plates. *Compos. Struct.*, vol. 220, pp. 221–235.

[1.17] A. Li, S. Xu, Y. Wang, C. Wu, and B. Nie. (2022). Fatigue behavior of corroded steel plates strengthened with CFRP plates. *Constr. Build. Mater.*, vol. 314, no-PB, p. 125707.

[1.18] A. Li, H. Wang, H. Li, D. Kong, and S. Xu. (2022). Stress Concentration Analysis of the Corroded Steel Plate Strengthened with Carbon Fiber Reinforced Polymer (CFRP) Plates. *Polymers (Basel).*, vol. 14, no. 18, p. 3845.

[1.19] M. R. Islam and Y. Sumi. (2011). Corroded Steel Plates Subjected to Uniform Bending : Experimental and Corroded Steel Plates Subjected to Uniform Bending : Experimental and Nonlinear Finite Element Studies.

[1.20] E. Ekiz and S. El-Tawil. (2008). Restraining Steel Brace Buckling Using a Carbon Fiber-Reinforced Polymer Composite System: Experiments and Computational Simulation. *J. Compos. Constr.*, vol. 12, no. 5, pp. 562–569.

[1.21] N. Khurram, E. Sasaki, H. Kihira, H. Katsuchi, and H. Yamada. (2014). Analytical demonstrations to assess residual bearing capacities of steel plate girder ends with stiffeners damaged by corrosion. *Struct. Infrastruct. Eng.*, vol. 10, no. 1, pp. 69–79.

[1.22] D. Wakabayashi, T. Miyashita, Y. Okuyama, and N. Koide. Study on Repair Method using CFRP for Corroded Steel Girder Ends.

[1.23] C. Zhao, Y. Zhou, X. Zhong, G. Wang, Q. Yang, and X. Hu. (2022). A beam-type element for analyzing the eccentric load effect of box girder bridges. *Structures*, vol. 36, no. December 2021, pp. 1–12.

[1.24] M. Lei, Z. Linyun, L. Shuqin, and W. Shui. (2012). Eccentric Load Coefficient of Live Load Normal Stress of Continuous Composite Box-girder Bridge with Corrugated Steel Webs. *Procedia Earth Planet. Sci.*, vol. 5, pp. 335–340.

[1.25] L. M. Gil-Martín, B. Šćepanović, E. Hernández-Montes, M. A. Aschheim, and D. Lučić, . (2010). Eccentrically patch-loaded steel I-girders: The influence of patch load length on the ultimate strength," *J. Constr. Steel Res.*, vol. 66, no. 5, pp. 716–722.

[1.26] C. Graciano and A. F. Uribe-Henao. (2014)Strength of steel I-girders subjected to eccentric patch loading," *Eng. Struct.*, vol. 79, pp. 401–406.

[1.27] M. K. Razzaq, K. Sennah, and F. Ghrib. (2021). Live load distribution factors for simply-supported composite steel I-girder bridges. *J. Constr. Steel Res.*, vol. 181, p. 106612, 2021.

[1.28] S. W. Tabsh and M. Tabatabai. (2001). Live Load Distribution in Girder Bridges Subject to Oversized Trucks. *J. Bridg. Eng.*, vol. 6, no. 1, pp. 9–16.

[1.29] K. Ghahremani, S. Walbridge, and T. Topper. (2015). Inhibiting Distortion-Induced Fatigue Damage in Steel Girders by Using FRP Angles. *J. Bridg. Eng.*, vol. 20, no. 6, pp. 1–10.

[1.30] H. Al-Salih, C. Bennett, and A. Matamoros. (2021). Evaluation of novel combined CFRP-steel retrofit for repairing distortion-induced fatigue. *J. Constr. Steel Res.*, vol. 182, p. 106642.

[1.31] A. Hartman, C. Bennett, A. Matamoros, and S. Rolfe. (2013). Innovative retrofit technique for distortion-induced fatigue cracks in steel girder web gaps. *Bridg. Struct.*, vol. 9, no. 2–3, pp. 57–71.

[1.32] B. Bhattacharya and B. Ellingwood. (1998). Continuum damage mechanics analysis of fatigue crack initiation. *Int. J. Fatigue*, vol. 20, no. 9, pp. 631–639.

[1.33] M. Quaresimin and M. Ricotta. (2006). Fatigue behavior and damage evolution of single lap bonded joints in composite material. *Compos. Sci. Technol.*, vol. 66, no. 2, pp. 176–187.

[1.34] M. May and S. R. Hallett. (2010) An assessment of through-thickness shear tests for initiation of fatigue failure. *Compos. Part A Appl. Sci. Manuf.*, vol. 41, no. 11, pp. 1570–1578.

[1.35] F. Magi, D. Di Maio, and I. Sever. (2016). Damage initiation and structural degradation through resonance vibration: Application to composite laminates in fatigue. *Compos. Sci. Technol.*, vol. 132, pp. 47–56.

[1.36] T. K. O'Brien, A. D. Chawan, R. Krueger, and I. L. Paris. (2002). Transverse tension fatigue life characterization through flexure testing of composite materials. *Int. J. Fatigue*, vol. 24, no. 2–4, pp. 127–145.

[1.37] M. Marco, E. Giner, M. H. Miguélez, and D. González. (2021). On the effect of geometrical fiber arrangement on damage initiation in CFRPs under transverse tension and compression. *Compos. Struct.*, vol. 274, no. July, p. 114360.

[1.38] T. Skinner, S. Datta, A. Chattopadhyay, and A. Hall. (2019). Fatigue damage behavior in carbon fiber polymer composites under biaxial loading. *Compos. Part B Eng.*, vol. 174, no. May, p. 106942.

[1.39] J. Deng and M. M. K. Lee. (2007). Fatigue performance of metallic beam strengthened with a bonded CFRP plate. *Compos. Struct.*, vol. 78, no. 2, pp. 222–231.

[1.40] F. W. Panella and A. Pirinu. (2020). Thermal and ultrasonic analysis of fatigue-damaged CFRP samples under traction and bending load. Procedia Struct. Integr., vol. 28, no. 2019, pp. 1709–1718.

[1.41] M. M. A. Ammar, B. Shirinzadeh, P. Zhao, and Y. Shi. (2021). An approach for damage initiation and propagation in metal and carbon fiber hybrid composites manufactured by robotic fiber placement," Compos. Struct., vol. 268, no. February, p. 113976.

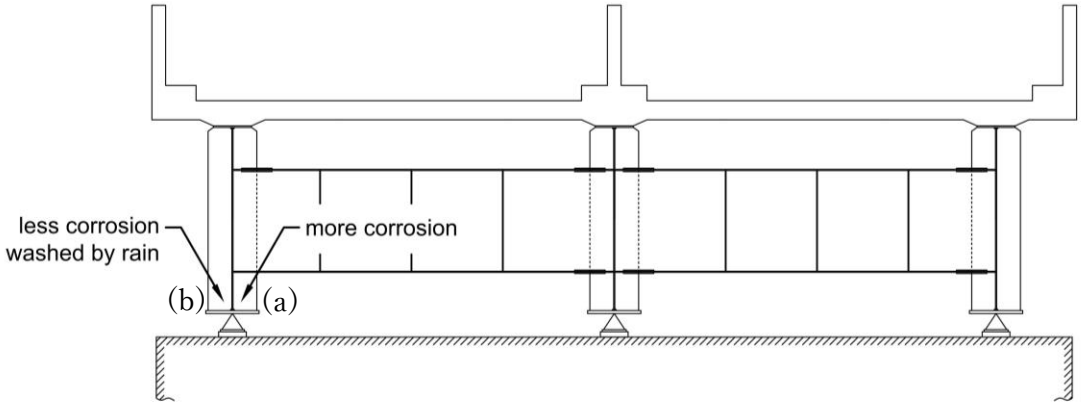


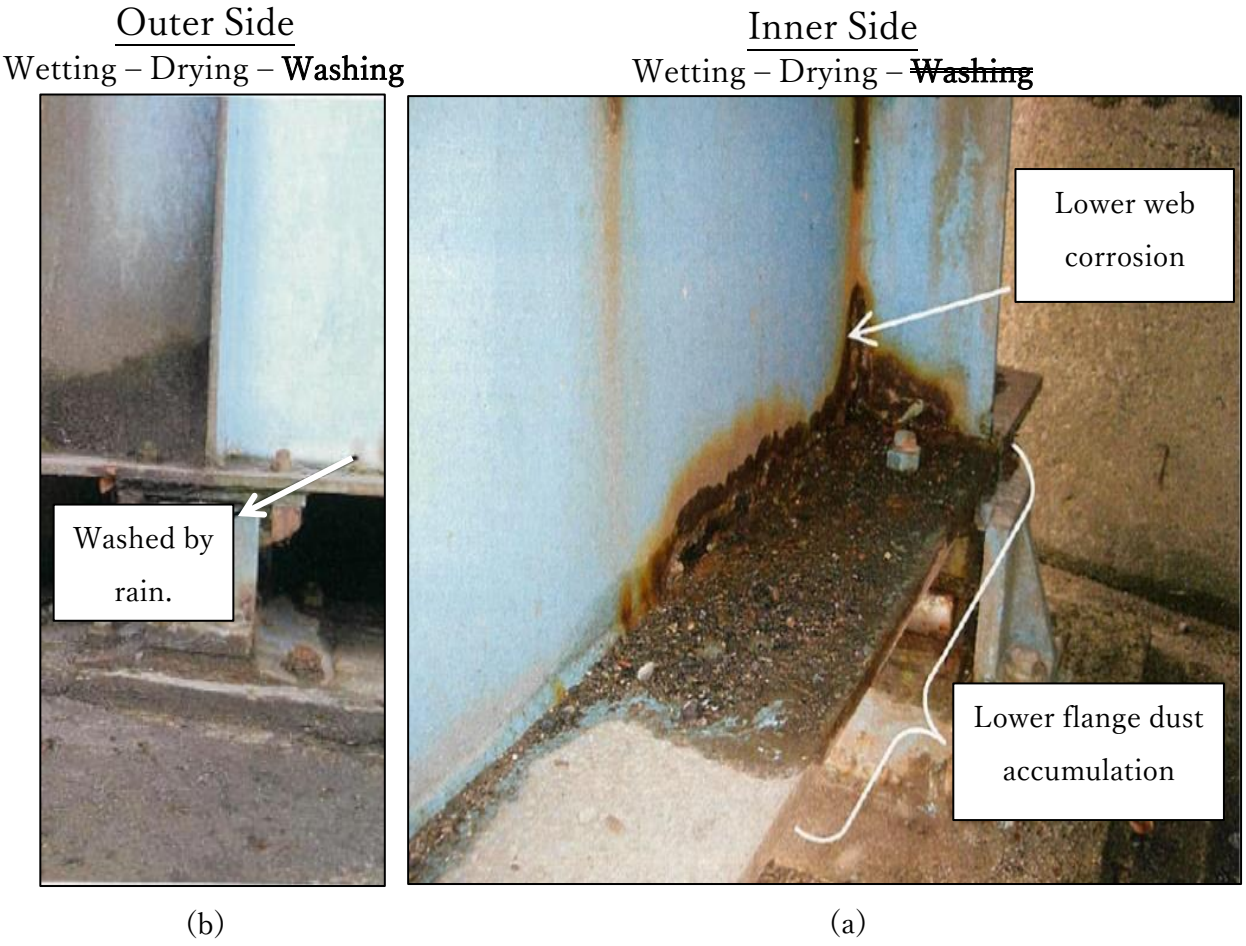


**Figure 1.1** Particles and dust accumulation at the exterior steel plate girder. a) inner side with corrosion at lower web; b) clean outer side washed by rain. (Source: Japan Public Works Research Institute, March. 2010, Research on Corrosion Countermeasures at Steel Bridge Girder End, ISSN 0386-5878 – In Japanese)

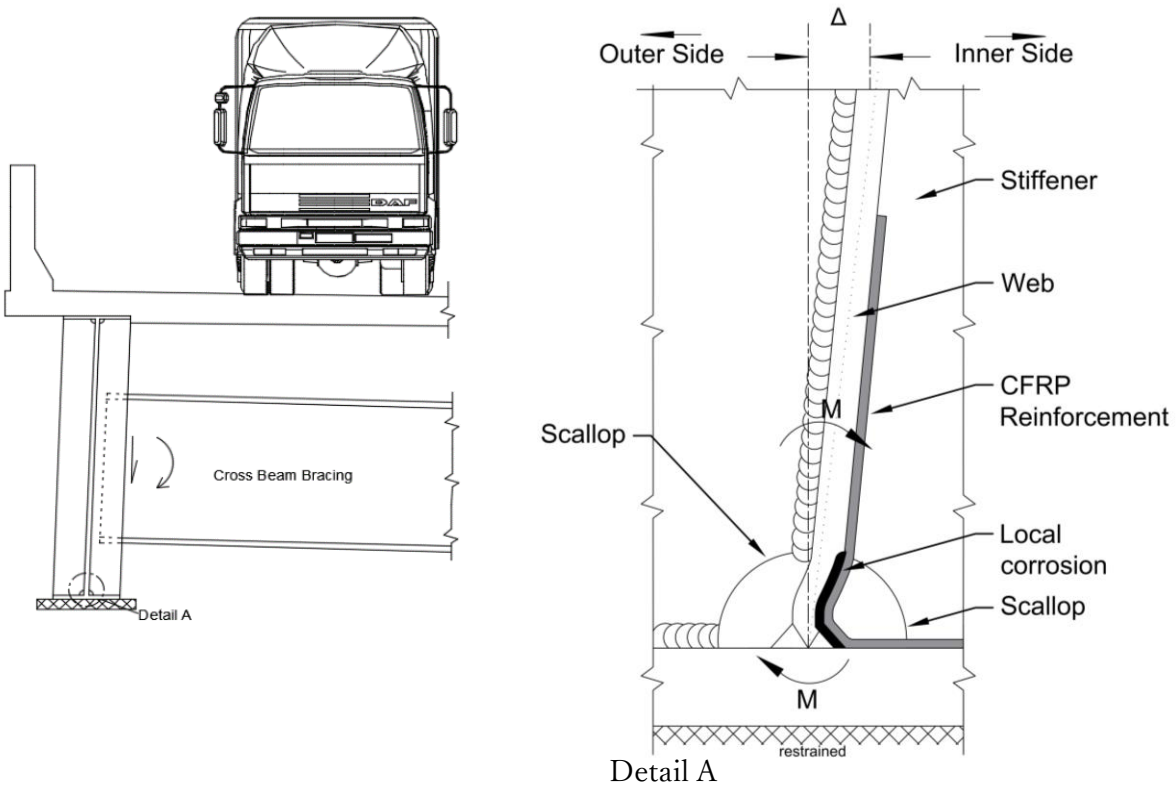


**Figure 1.2** Schematic out-of-plane deformation in the CFRP retrofitted exterior girder web scallop at the girder end on the transverse stiffener plate.

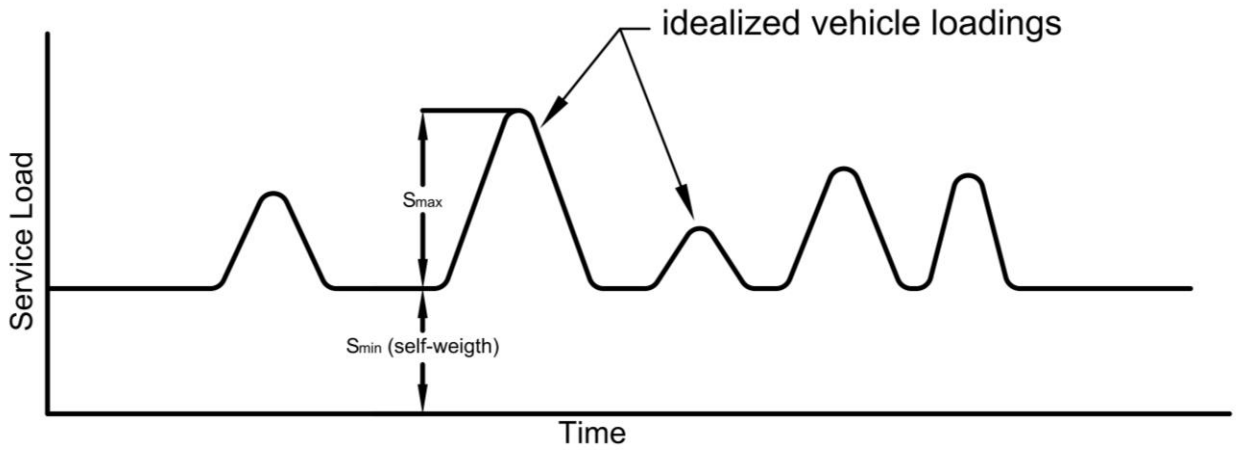


**Figure 1.3** Schematic of load history in the bridge structure subjected to variable load fluctuation.

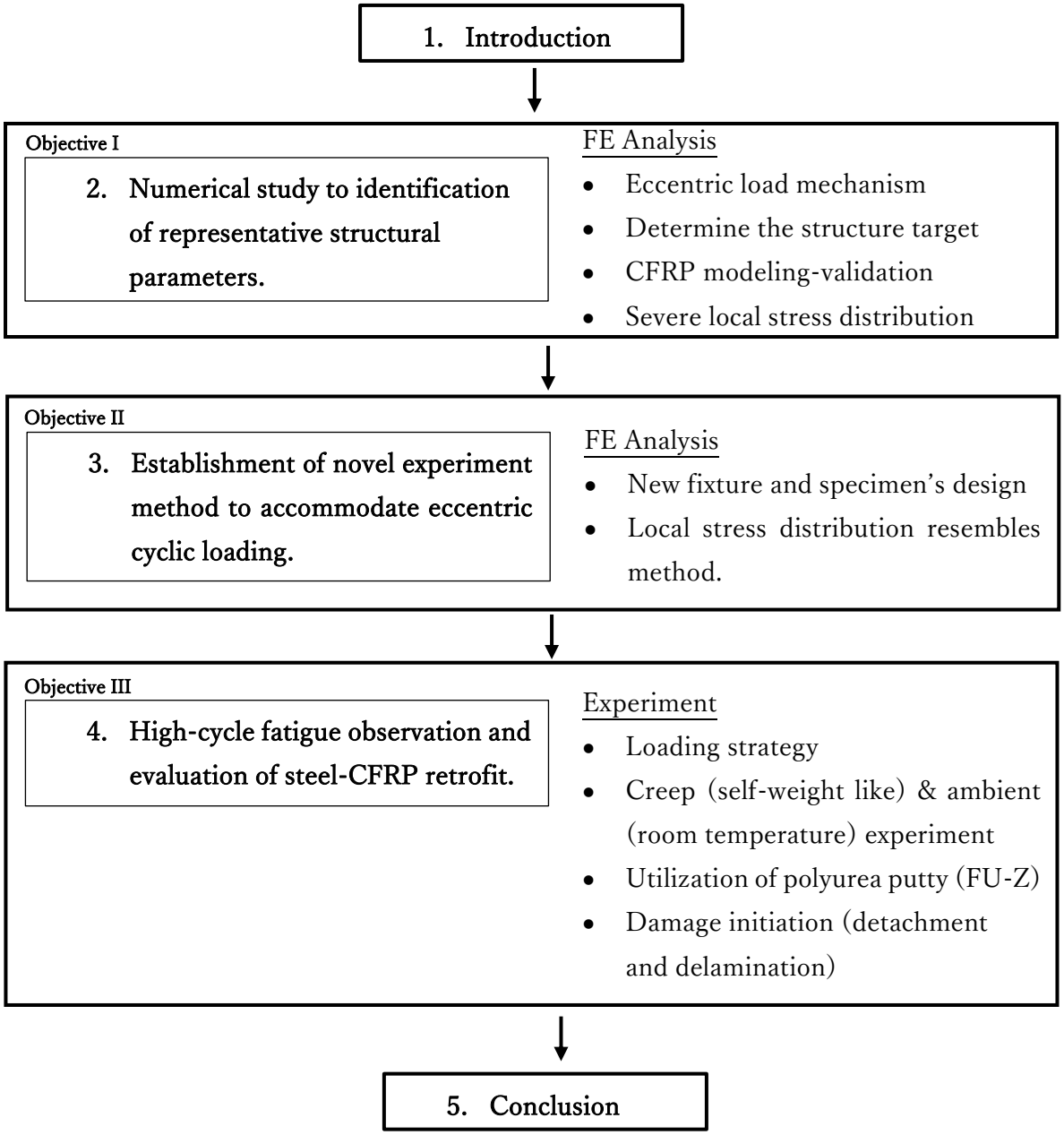


**Figure 1.4** Research flow of study

# Chapter 2

# Identification of Severe Structural Parameters of CFRP Retrofit Girder Ends

## 2.1 Overview

The cyclic bending stresses of out-of-plane at the girder end always occur during the service life of the bridges. The stress range within tolerable limits is determined by the web thickness and the magnitude of the load to overcome the possibility of out-of-plane deformation at the girder ends. Then, reducing the thickness of girder web ends due to corrosion should be considered more.

Healthy-corroded-retrofit conditions potentially transform the local stress because of different strength element behavior combinations. The prediction of local stress redistribution of the corroded part under CFRP retrofit has been a general challenge because of the need to identify the potentially damaged region in terms of localization of the high stress in the corroded part.

Using finite element simulation, observing the physical phenomena of CFRP compressive stress has essential significance. Comparing the compressive stress distribution on each CFRP sheet is necessary to determine the value of in-plane stress transferred from the girder ends section. At this point, the high compressive stress concentration location is essential in determining the durability of the CFRP retrofit structure. It must be ensured that to measure a local compressive stress value in the CFRP parts should be under structural strength limit.

Asao et al. observed the thickness reduction of the steel web. They found that local corrosion significantly affects maximum capacity more than other girder end sections [1]. The corrosion depth has a linear relationship with the moment inertia of the girder end cross-section. Matsumoto et al. defined the weakest section of the corroded area by the average corrosion depth. Their research developed the concept of the triggered value of local corrosion in the steel bridge with a mean value of 0.7 mm, and the variation coefficient is 0.15 [2].

Further, Yosri et al. found a correlation between the minimum thickness loss location and stress concentration for damage identification. The spreading of high-stress concentration may propagate to thicker sections or adjacent welded joints, affecting severe structure damage [3]. Al-Salih et al. recently evaluated the CFRP retrofit for steel girder end due to out-of-plane deformation. They provided the scallop between the web and the stiffener in detail. All specimen configurations identify the potential damage in the scallop region over the girder height [4].

The compressive stress of the unidirectional CFRP was almost the same as its tensile strength, found by Ueda et al. They studied the compressive stress of CFRP in the epoxy matrix based on the prediction of elastic conditions in which fiber misalignment and fiber bending are considered [5]. Baumann et al. discovered that the non-retrofit CFRP layup for compressive stress in the matrix material is more important to assist respectable CFRP performance than tensile loading. The matrix material has to prevent the high stress of the CFRP during the loading condition [6].

Due to the thickness reduction approach, this numerical investigation will predict the girder web end's local stress distribution and displacement characteristics. Thus, a predictive method is described as when the originally linear-elastic girder ends structure remains linear-elastic in healthy-corroded-retrofit conditions. To further understand CFRP retrofit effects at the corroded steel girder ends, the potential damage identification of the CFRP must be relatively assessed. Analyzing stress transformation behavior will inform the novel local stress redistribution post-retrofit method and identify dominant critical retrofit geometry constraints. The contribution of multi-layers of CFRP reinforcement could be shifted to the local compressive stress distribution of steel corroded parts.

The author states that artificial corrosion can be simulated by reducing the thickness of the girder web ends. Adjusting the surface thickness area can use to detect severe corrosion depth. The regular topography of web ends thickness reduction refers to the surface loss, the deepest corroded surface in the thickness direction. This research is generally repeated for three types of bracing simple supported steel bridge configuration as a three-dimensional global model. Next, the applicability of steel girder ends sub-model retrofit with CFRP sheets was investigated. To clarify the local stress distribution transformation, which was subjected to the interaction of various live loads and the constant dead load conditions. The local stress redistribution of those external forces is considered independently to demonstrate the recovery contribution with a detailed corroded model.

To identify the potential damage region in the retrofit structure, the simulation of the CFRP strengthening to the target part heavily relies on adequate bonding modeling. This research proposed a full-scale CFRP finite element model based on the actual retrofit specification (NERI) [7] to analyze the transfer of stress and displacement from the girder ends corroded region to the CFRP. The reproduction of high local stress at the retrofit girder ends should be considered with a group of vehicles running where they will cause the most adverse stress. The author designed a numerical simulation that would mimic the corroded edge's stress concentration on the web ends to produce a "jump" stress behavior associated with the stress distribution of corroded depth surfaces under CFRP retrofit conditions. The stress jump phenomena describe an elastic local stress instability occurring in the corroded part during a loading. Consider local corrosion under elastic loading. The local stress will be concentrated where the force distribution is forced together by smaller sections, e.g., at the transition curve (TC) or corrosion edge. The transition curve is the transition part between the healthy and corroded regions. The corrosion edges are designed considering the following fillet with a certain radius. The following sub-chapter, 2.7.1 (Corrosion Approach Design), explains the detailed design approach.

Because of the structure modeling complexity, simplifying the compressive stress of CFRP layer-by-layer was a conventional method. This study modeled a non-uniform shape in the retrofit

CFRP sheet with a curve (R = 50 mm) as the anchoring part. In this modeling, anchoring length and shift are set at 100 mm and 25 mm, respectively. By anchoring the CFRP on the lower flanges, the direction of the compressive stress can be oriented in the direction of the webs, further enhancing reinforcement. The aligned CFRP sheets are embedded in a matrix (primer-epoxy-putty) modeling while maintaining the local fraction and buckling for the CFRP retrofit part. CFRP modeling should be oriented so that fibers are aligned vertically in the same direction of local distribution stress in the web subjected to reaction force at the supporting point. It generalized the specification of in-plane stress distribution at the CFRP layer interface.

## 2.2 Description of Target Bridges

Bracing in steel bridges serves the dual aims of requiring overall stability of the girders and immediately increasing the stiffness and strength of the system of the steel bridge structure. This study selected steel bridge girders with various bracing types (cross-beam, cross-frame type V, and cross-frame type X). The steel I girder bridge's selected structure is a good representation of the simply supported bridge. It corresponded to a composite roadway bridge with a span length of 40 m and lane width of 12.5 m, respectively. In a selected bridge where the ratio of girder spacing (S) to girder depth (D) is more than 1.5, cross-frame type V or cross-frame type X may be implemented. However, keeping the angle of 45° of the cross-frame diagonals helps attach the cross-frame member to the girder connection plate.

The purpose of this study is to consider the role of bracing variation with the retrofit specification of reference to the prevention of the general durability of the retrofit part. In this context, a difference is described between the type of bracing requirement when retrofit parts are used-for reinforcement activity. When considering bracing type, it is essential to be sure that the stability of web ends under vertical load is restricted. Then, the various bridge was selected under the Japan code of steel bridge design.

It should be noted that the girder ends under consideration will be a simple span subject to uniform axial loading. In principle, the girder slenderness parameter $(\bar{\lambda})$ depends on the elastic critical moment $(M_E)$ for the loading design and restraint, as provided by $(\bar{\lambda} = \sqrt{M_P/M_E})$ [8]. Thus, if $(M_P)$ plastic moment capacity leading to higher and reduced slenderness value than the lateral stability should be considered more. The selected bridge bracing in this study must satisfy at least two requirements:

(1) Adequate strength to avoid the force induces as a result of restricting the deformations of the main parts.
(2) Sufficient stiffness changes the main parts' buckled modes, thus increasing its load-carrying capacity conditions.

In modeling, providing that functions acted as if they were rigid characteristics. The full 3D steel bridges with composite deck modeling were provided between the main steel bridge members in continuous span. Various bracings imply that fatigue conditions must be considered because service-life loads mainly induce the local stresses in the bracing systems. Consequently, it may be advisable to use such arrangements (bracing type). The cross members are assumed to consist of width concrete slab to lesser of $(L_u/2)$, where $L_u$ is the distance between bracings.

Cross-frame bracings are required at all support of a straight (simple span) I-girder bridge to transfer lateral loads due to vehicle loads from the superstructure to the support bearing. To provide no-twist (sway) condition for lateral buckling and transfer torsional uplift forces to the foundations. For the specification of intermediate and support, cross-frames be spaced no more than 7 meters [9]. Typically, cross-frames (type V & X) play an essential role in curved steel girder bridges compared to straight steel bridges because the skew bridges are subjected to combined bending and torsion. Generally, a cross-frame allows plate girders to work together effectively to resist the uniform external force compared to cross-beam bracing. Therefore, the investigations only consider the comparison of straight steel girder bridges with different bracing types.

The end bracing was developed from a capacity design perspective. Battistini et al. [10] found that the elastic range of cross-frame type V in compression force was slightly higher than in cross-frame type X. Then, they suggested that type X could be delivered as the best alternative to reduce the external forces in the individual part members while offering excellent stiffness. Also, in the vehicle load test, the X frame was most flexible when subjected to a vertical force acting at the cross-frame location. However, the out-of-plane web mode should be considered with the attached brace stiffness ($\beta_b$) design.

Therefore, the out-of-plane mode of web ends essentially shall not occur for the cross-frame type or entire diaphragm (cross-beam). The bending deformation is controlled with a connection plate and amount of girders installed. Based on the formula, the capacity inertia of the cross-beam at the web ends plays a vital role in stabilizing the distortion impact. The web distortional stiffness could significantly influence the behavior of the plate girder under long fatigue conditions. Even the out-of-plane value of displacement could be modest (small).

Based on that, the number of girders of each structure is considered different, which makes more sense from a geometrical perspective. The main steel girder section and cross beam (CB) section considered are welded wide flanges made with SM400 ($f_y$ = 235 MPa; $f_u$= 400 MPa) and cross-frame (CF type V & X) are designed with SS400 ($f_y$ = 235 MPa; $f_u$ = 400 MPa), all the steel sections adopted the 2.10x$10^5$ MPa Young's modulus with 0.3 Poisson's ratio and 7850 kg/$m^3$ material density. The concrete slab model possesses 2400 kg/$m^3$ density, $f_c$ = 25 MPa, and E = 2.4 x$10^5$ MPa of the Young Modulus, with 0.2 Poisson's ratio. The general view and detailed target

section (G1) members of the exterior steel I girder bridge are presented in Figure 2.1 and Figure 2.2.

## 2.3 Implementation of Loading Condition

This study adopted the service loading conditions designated by Japan Road Association (Specification for Highway Bridges-2012) [11]. The traffic load model of the main girders is that the bridge should be loaded with a sequence of large vehicles moving where they will induce the most adverse stress. To observe the uncertain possibility of the traffic situation to adverse stress at the steel girder end, as shown in Figure 2.3 (a), the middle (case 1) and the edge (case 2) position of the p1+ p2 placement is applied. In the transverse bridge structure direction, the reaction's influence line in the main girder (G1) is fully considered the target, as shown in Figure 2.3 (b).

It is stipulated to impose the L-load on the roadway portion so that the loading will cause the most adverse stress at the point for the structural members. That is, the live load on the main lanes should be imposed over a width of up to 5.5 m. The live load on secondary lanes should be imposed on the other part of the roadway portion. Therefore the live load on the main lanes and the live load on the secondary lanes will be loaded in the following area. Their influence line has the same positive or negative sign in both bridge's longitudinal and transverse directions.

## 2.4 Modeling Approach for Steel Girder Ends

The study described that steel girders are generally represented by the term "plate girder", which included all girder structures of full web type. However, it was difficult to establish detailed requirements considering the specific properties of each type of steel girder ends. Thus, the study here was prepared for the basic girder types, meaning girder of I-section. The healthy girder was dedicated to determining the effective longitudinal width ($12t_{web}$). The effective cross-sectional area as a column shall be the cross-section of the stiffener plus the web portion on both sides up to 12 times the web thickness from the stiffener attaching point. However, the effective cross-sectional area shall not exceed 1.7 times the cross-sectional area of the stiffener. This condition is established considering that the above-stated longitudinal effective width of the web does not work yet at the place closest to a bearing. So the reaction must be endured almost with the cross-sectional area of the stiffener. When a standard scallop is installed at the bottom end of the stiffener, the bearing stress shall be verified against the allowable stress design ($\sigma_{140}$). Then, the design of artificial corrosion should be based on the effectiveness of the girder ends. The location of the maximum section loss is defined as a location where the total area of section loss is the largest.

A finite element analysis with the linear elastic steel material model was much simpler and more accurate. The linear steel bridge model caused the bridge model to maintain their initial stiffness. The realistic local stress values prove that the full-scale steel bridges model was suitable

for simulating the support part's sub-scaled. The global-local modeling approach's main idea was to correctly assess specific target parts of the structure on various scales. It was developing an accurate, realistic result of each part of the bridge structure, including information concerning the potential damage of reinforcement condition. For this reason, shell-solid modeling is employed, as shown in Figure 2.4.

The global model was applied to repeated traffic load (case 1; case 2) and gravity load. An advanced transformation from healthy condition modeling was assigned to the corroded surface loss and retrofit condition. The refinement mesh of the sub-model element was carried out to reach a higher level of accuracy in calculating the sub-model, as shown in Figure 2,5. Abaqus version 2018 was utilized in this research to simulate the complete assessment process [12]. The standard shell element (S4R) was not proficient in calculating the thickness difference, nor can they calculate the corresponding behavior when adding the new component on the surface of the shell element. Then, the solid element (C3D8R) tends to be not stiff enough in bending. The result of stresses and displacement accurately reduced the girder ends dimension.

### 2.7.1 Corrosion Approach Design

The surface preparation method was conducted in this simulation to obtain optimal performance from CFRP sheets. Khuram et al. assumed that the corrosion height based on those parameters gives a very conservative prediction of the stiffness reduction at the inner web. They found that the load-displacement buckling mode will appear with the height of corrosion greater than 60 mm at the girder ends regions [13]. The detailed corrosion model consists of a curve (R=3mm) at the top of end corrosion that replicated the uncertain shape of corrosion that induced the stress transition from corroded to healthy region. It was decided that the curve shape corrosion was primarily located on the top edge since the result could be higher to reduce the stress concentration, as shown in Figure 6. This study has decided to set the height of distribution to be considered 100 mm.

This study achieved global shape optimization of artificial corrosion design at steel girder ends. Although optimum surface loss design of girder ends was considered by many researchers before [14-23]. The improved design was obtained in this investigation by applying a transition curve of the corroded part to a healthy region. As for the optimum shape design of the corroded part, the numerical result obtained in this study was acceptable under severe elastic conditions. The optimum stress level refers to allowable axial compressive stress $\sigma_{140}$. When a member between fixing point of a compression web containing a surface loss section in which the local stress was to be checked. The vertical bending mode is varied, and the allowable stress may be increased and exceed the upper limit.

It defined the boundary of corrosion dimension using various local corrosion to increase the target precision under severe elastic conditions. A numerical method was proposed to select a proper surface loss deep. In this way, local stress concentration was obtained by comparing numerical results. The accuracy of severe shifted local elastic stress was ensured, which was susceptible to local fatigue damage. To intensely observe the contribution of surface loss on the allowable stress design, the depth of surface loss varied from 1 mm, 2 mm, and 3 mm. Three key points obtain the optimal corrosion shape: corroded weld bead, web surface loss (SL), and corroded web edge. Those parameters were designed to experience severe local elastic stress simultaneously increasing together when loading was applied, so the corrosion depth was designed continuously. The variations of those parameters were not considered according to the influence of transition corrosion depth that could be independently shifted of lower local elastic stress at the target parts.

In this study, The corroded web edge and corroded weld bead joint experienced the redistributed local stress from low to high value at the surface loss where the cross-sectional area changes. The design of the corroded web edge was to get the local stress so that the local stress gets sufficient space to have redistributed evenly. The fillet curve was adopted in this approach. However, if the fillet radius is improper, the local stress change could be more abrupt. The design of the transition curve or corrosion edge in this study also brings a new approach to a sudden change in the geometric form of corrosion. Because local stress concentration increases mechanical stress, a better design of corrosion is to attempt to reduce the stress concentration effect at uncertain corrosion shape form.

The finite element analysis's accuracy affected the resulting optimized corrosion shape significantly. The depth of the SL and corroded web edge significantly affected the level of local elastic stress. When the surface loss depth was 1 mm, the local vertical stress at the pick point of SL and corroded web edge part was less than the allowable stress design. The local stress on the transition curve region was 94.61 MPa, 60% of design stress. Then the surface loss experienced lower vertical stress (45.39 MPa). Based on this result, the depth of surface loss increased twice to 2 mm. In this condition, the local stress increase around 30 MPa (TC = 127.53 MPa; SL = 93.16 MPa). This analysis aimed to treat the corroded girder ends part that experienced severe local stress without initiating the buckling mode under applied loading. Then, the depth of the corrosion model was increased to 3 mm. The simulation revealed that the parameter target exceeded the allowable stress is reached. The local vertical stress increased around two times. The local vertical stress at the corroded web edge reached 156.96 MPa, and the local elastic stress at the surface loss (SL) part reached 142.52 MPa. Because of the sensitivity of fatigue initiation damage behavior to stress ratio, the local stress should be maintained in elastic condition, at least far enough from yield stress condition at 235 MPa from design specification. In the design specification, the standard yield point was multiplied by a safety factor of about 1.68 for materials SS400, SM400, and SMA400W. Also, the local stress at a surface loss with 3 mm depth was selected to prevent local

buckling. The stress ratio of SL reached 1.018, and the corroded web edge reached 1.121, respectively. From this result, the corrosion shape design optimization was satisfied. The detail of the local stress contour from surface thickness loss can be seen in Figure 2.7.

## 2.5 Retrofit Process Modeling

Three-dimensional model analysis simulated the corroded web end part with the designed CFRP sheets layer using sub-model boundary conditions, as shown in Figure 2.8 (a). The element type used for this simulation is shown in Figure 2.8 (c), with the meshing size (rectangular) detailed in 1 x 1. The web end part, polyurea putty, epoxy putty, and adhesive were modeled using a brick element (C3D8R). This study also conducted the standard CFRP retrofit construction order is shown in Figure 2.8 (c). The adhesive prevents corrosion and upgrades the bonding ability between steel and epoxy putty. Even the elastic properties of polyurea putty maintained the flexibilities that prevent damage (peeling, debonding, delamination, detachment) under high stress (about 1/3000 of that steel). The element connection was modeled as a monolith with different material properties to support a simple connecting element section between adhesive-epoxy-polyurea. The CFRP sheet layer with a curve-shaped (50mm) was modeled using a shell element (S4R) 0.5 x 0.5 size of the mesh. The tie constraint approach was generated to tie separate CFRP sheet surfaces together to prevent relative motion. Joining the CFRP sheets together using the tie constraint option allows modeling the CFRP sheet retrofit structure to be more realistic. The material properties description of the sub-model of CFRP retrofit is summarized in Table 2.1. In this study, the CFRP sheet number had to be established as a numerical basis for retrofit. Then, the local stress at surface loss thickness was recovered, which could be close to healthy local stress distribution. Therefore, the amount of CFRP layers for the main direction (regarding compression behavior) was designed. The layers sheet bonded were thicker than the thickness reduced by the corrosion damage. It was calculated by the steel web end part equivalent thickness of the CFRP sheet deriving using Equation. 2.1 [24], as follows:

$$E_{cf} \times t_{cf} \times n \geq E_s \times t_{sd} \tag{2.1}$$

where CFRP sheet thickness ($t_{cf}$), the required number of CFRP sheets ($n$), Young's modulus of the steel ($E_s$), the thickness of the cross-section corrosion part ($t_{sd}$), Young's modulus of the CFRP sheet ($E_{cf}$). In this case, having a surface loss of 16% of the web endplate thickness with, $t_{sd} = 3\ \text{mm}$, the required number of the CFRP sheet layers for the main direction (vertical direction $90^\circ$) was 7 layers for the inner-side bonding arrangement, as shown in Figure 2.8 (d). Based on the past evaluation test, the shift length between CFRP sheets is 100 mm and 25 mm, respectively. The upper end of the carbon fibers sheet should be bonded by shifting each layer down 25 mm vertically. The length of the carbon fibers sheet should be determined to satisfy the Equation. 2.2 [24]as follows:

$$L_{cf} \geq L_{sl} + 100 \quad (2.2)$$

Where $L_{cf}$ is the length of the outermost layer of carbon fiber sheets (mm). $L_{sl}$ is the length of sectional loss (mm). The general layup orientation of the CFRP sheets should meet the $90^\circ$ (fiber in the vertical direction) criteria at all topologies, especially the arch-like shape part. To perform this condition, the CFRP sheet model was modeled by a discrete orientation option in Abaqus to represent changing orientation at the centroid of each mesh element. The variation of layup orientation contributed to simulating the CFRP's proper behavior at the steel girder end. The orientation of the elements of the CFRP sheets between seven-layer is identical, and it allows for the description of a consequence of continually varying orientation. However, the change (twist) of fiber orientation modeling probably influences the compressive strength of the curve shape section. The modeling of material orientation is demonstrated by the arch-like shape shown in Figure 2.8 (b).

## 2.6 CFRP Model Validation

In this validation, the target bridge as a highway steel I girder bridge (L=23.42 m; w=7.6 m) was constructed with complete 3d modeling. The loading characteristic in Abaqus was different. The static condition of the front (68 kN) axial load and the rear truck wheel (156.5 kN) was transformed to a pressure load equal to 0.283 MPa and 0.414 MPa. The loading condition is considered separately at the middle and edge of the bridge to reproduce the maximum and minimum CFRP stress distribution, which was the purpose of this validation phase. The measurement target in modeling was decided following four vertical strain gauges near the column part, as shown in Figure 2.9 (a). The part of the bridge, such as the stiffener, bracing, support condition, actual surface loss, and material property, were generated considering Jin-Hee Ahn study [25]. The FE model developed in Abaqus as a validation reveals the contribution of vehicle positions. The vehicle's position in the middle of the bridge could trigger CFRP behavior at the steel girder end to obtain the vertical stress (S22) on the tension side, as shown in Figure 2.9 (b).

However, compressive stress will produce when the vehicle is placed at the edge of the bridge. This validation also provides strong evidence to confirm CFRP's various stress results from different live load conditions. The curve shape CFRP modeling part experienced the high-density resultant stress due to vehicle movement on the bridge. The validation of CFRP modeling and loading test reached 88%. The vehicle's speed was not considered in the field test. Then the static loading of validation was agreed upon static numerical simulation. The strain gauge captured the strain from the moving truck. Even the condition is not similar to the validation.

The CFRP modeling and loading test result reached 88% and was accepted. In Figure 2.9 (b), the stress result differences might have occurred under the construction work process. The amount of resin (FR-E9P) attached to the CFRP sheet was not the same along the CFRP part.

Then, the result was that the effect of the thickness of the resin on the CFRP itself became different. Thicker resin probably slightly reduced the CFRP local stress due to local thickening. Therefore, the thickness of the CFRP and model was maintained to be constant.

## 2.7 Numerical Result Discussion

### 2.7.1 Deformation Characteristics

The evolution of deformation of the modeling steel girder end is highly dependent on the applied load during bridge service. However, it was deformed elastically, returning to the initial shape. The deformation analysis is predicted based on the evolution of the out-of-plane deformation, followed by complete or partial recovery of the damaged part. This finding revealed that the displacement distribution at the girder end was proportional to the steel bridge bracing type. Figure 2.10 presents the dominant distribution of transversal displacement at the steel girder end in all cases. This result indicates that a higher stiffener can effectively reduce out-of-plane deformation, as shown in detail in Table 2.2.

The former parameter of corrosion surface loss was developed as artificial damage for the end of the steel girder section. Consequently, the structure's stiffness decreased dramatically when applied surface loss. Essential observations were made regarding the influence of surface loss at the steel girder end. First, surface loss at the bottom weld bead of the web significantly affects the deformed configuration of the steel girder end. As expected, the part of the bottom weld that closes to the bottom flange experienced the more significant displacement. However, the upper part of the bottom weld gave a more substantial displacement. This numerical study showed that the correct modeling weld part is sufficient to consider severe corrosion based on the sensitivity to girder end deformation.

Additionally, the surface loss length increased the distortion at the section part. Second, the residual displacement in the corroded steel girder end part plays an essential role in the magnitude of deformation and a higher stress range during bridge service, as seen in Figure 2.10. The general result indicates that the retrofitted sub-models are susceptible to corrosion damage at the steel girder end. The size and shape of the curve part play a crucial role, especially in the inner side or corner. In this study, we are using R=50 mm. This geometric parameter will have a decreased fiber waviness generated by the curvature of the CFRP sheet. The change in part of the CFRP sheet transitions from the straight-up (vertical) to parallel (horizontal) direction can constantly distribute the bending stiffness and displacement. Thus, it could be established that the deformation behavior of the retrofit model was related to the shape design of the CFRP sheet retrofit. The visualization of the transversal displacement contour of a steel bridge with cross-beam (CB) bracing is shown in Figure 2.11.

### 2.7.2 Local Stress Distribution Characteristics

The steel bridge with cross-beam bracing receives a high-stress concentration at the weld bead compared to other bridges, which means the configuration is less stiffened. Figure 2.12 presents a significant distribution of transformation of local vertical stress in traffic case 2 combined with gravity load. As shown in Figure 2.12, the analysis was performed separately to understand the behavior of each condition. However, the traffic load in each case should be added to the gravity load to represent the permanent load situation, as summarized in Table 2.3. Moreover, the higher local compressive stress generated at the scallop region was reduced along with the height of the girder. The result would be influenced by the eccentricity of the design traffic load associated with the scallop structure. This observation was related to the loading configuration that the author applied. It can lead us to the statement that when a configuration of traffic load acts away from the axis of the steel I girder end column. The traffic load will be termed eccentric load. Therefore, arranging the available vehicle's position during the bridge's service life is challenging. It is proven that all healthy structure modeling succeeds as it does not experience overstress against the allowable stress of design manual specification. In the healthy model, the weld bead at the scallop region part experienced higher stresses than the other section at the web end section. This stress characteristic involved the surface loss simulation analysis. The stress concentration effect could justify this trend. When subjected to the load, the uniform surface loss area would lose the internal elastic modulus that will cause stiffness degradation as dramatically. Next, the high concentration of residual stress was increased at the nearest undamaged part of the region based on the equilibrium state. It is shown that the stress distribution of the upper tip of the corroded part approaches zero stress and then continues to the compression sign at the healthy part of the web end. This phenomenon occurred by shifting geometrical features of the local corrosion model, as shown in Figure 2.13 for all cases. The local compressive stress distribution of all steel girder end in HCR (healthy-corroded-retrofit) became typical. Even though the value of local compressive stress was variated, the residual corroded compressive stress was still reformed after the retrofit condition. It cannot recover from an initial state of stress. However, the residual stress was under allowable stress design. The steel girder end with cross-beam bracing was an example of the detailed compressive stress for complete loading conditions (gravity + traffic).

The local stress ratio indicates that the stress on the corroded case exceeds the allowable stress. However, allowable stress is the maximum local stress that can be safely applied to a bridge structure. From Table 2.3, the local stress from gravity load was influenced by 40% for complete compressive stress at the steel girder end in all cases. The donation of permanent load as a dead load was an instance considering elastic stress's contribution due to the allowable stress ratio. For

3 mm surface loss at the steel girder end, the dead load was increased by approximately 50% of initial compressive stress. The retrofit condition reduced stress by 50 % from corroded compressive stress. The characteristic of traffic load was slightly different. The local compressive stress from case 1 and case 2 contributed linearly. Then, the transformation of local compressive stress should correspond to service loading as better as possible.

Consequently, we obtain a 30% higher compressive stress at the edge than at the middle. Furthermore, the steel girder ends experience a double transformation related to the p1+p2 and p2 movement. That leads to some standardized load conditions parameters. The potential damage will occur when the retrofit stress is more significant than healthy stress. The proportion of this condition is relatively small compared to all retrofit regions due to CFRP reinforcement. This result was found in the relationship of vehicle position to post-retrofit stress. In all cases 1 + gravity, the retrofit stress is tight to the initial stress of a healthy condition due to more considerable bending in the middle of the bridge structure. However, in the cross frame type V, the retrofit stress is larger than the initial stress, about 11.46 MPa. The bending moment of case 1 contains the implication of shear stress in the girder ends. Then the deviation of retrofit stress is narrow due to healthy stress. Compared to case 2 + gravity, the deviation of healthy and retrofit stress is in good agreement. Then the stress of the retrofit part is reduced. This condition may be related to the orientation of CFRP that is more preserved for the vertical axial force at the girder ends regions. This type of stress occurred when the CFRP reinforcement body was under equivalent vertical stress in all directions and might be known as isotropic normal. This result also confirmed that the shear buckling did not appear, considering the corrosion area height is less than 10% of the girder height.

The steel girder end and the CFRP sheets for the composite restore system mainly conduct the local compressive stress. At the same time, the infill (epoxy or primer) material was used as a barrier between CFRP sheets and the corroded web end. To prevent debonding and detachment of CFRP while benefiting from the high modulus of carbon fiber. Therefore, the infill material's modulus elasticity could influence the restore system's load transfer mechanism as a transitional layer between the steel girder end and the CFRP sheet. A linear trend was observed for the maximum local compressive stress at the CFRP sheet. This result indicates that with the accurate modeling of putty interaction, the corroded web end carries the lower stress.

In comparison, the CFRP sheets take the higher local stress. The primary reason for this trend is that the young's modulus of a putty layer is (1/12) smaller than that of CFRP sheets and (1/4) smaller than the steel girder end. This putty layer could not bear immense stress in this

simulation. So the local compressive stress from the steel girder end could effectively be transferred to the CFRP sheet with high modulus elasticity. This result indicates that the CFRP transferred the local compressive stress perfectly in a vertical direction following the layup orientation of CFRP. The section (bottom part) that obtained the thickened portion of putty will significantly decrease the local compressive stress. However, the upper corroded section loss experienced higher compressive stress in all cases, as shown in Figure 2.13. This characteristic parameter showed us that every CFRP sheet layer performed together during the loading condition. The critical part of CFRP sheets attached to the steel girder has been discovered. All conditions of the sub-models indicated the higher stress distance of CFRP sheets is 50 mm from the column part of the web end and decreased following the CFRP geometry. This observation conducts the visualization of stress in-plane characteristics to analyze the stress distribution in the CFRP sheet, as shown in Figure 2.14. By modeling a surface loss, web ends thickness bonded to CFRP sheets under service loading, indicating that it was possible to accurately evaluate CFRP reinforcement's strength.

## 2.8 Summary

The stress distribution transformation in the healthy-corroded-retrofit (HCR) steel girder end was clarified through the simulation, and the conclusions are drawn as follows:

1. It is discovered that when the web-ends thickness reduction is subjected to the compression-compression conditions due to service (traffic-gravity) loading. The assumption of stiffness degradation in compressive load still can hold against the web-ends elastic strength limit. The local compressive stress was increased by around 30% from case 1 to case 2 based on p1+p2 configuration. Therefore, the transformation of local compressive stress case 1 and case 2 at the steel girder ends occurred linearly according to vehicle movement over the bridge. Then, the proposed approach was successfully used to estimate the variance of the corroded model. Thus, the assumed severe corrosion model of steel girder ends can be considered realistic. The proposed method provides a general method for determining traffic control for corroded steel girder ends safety prediction. An adequate distance of bracing was to reduce the high local compressive stress. The stress redistribution of retrofit web-ends has been discovered to determine the local stress shape characteristics of the damaged area under CFRP reinforcement. In addition, local out-of-plane deformation was observed at the CFRP retrofit of exterior girder ends. Due to the girder's height, the small eccentric deformation was undeniable in the local retrofit area.
2. Potential damage regions of the CFRP retrofit were discovered with the theoretical basis of structural geometric changes effect of retrofit girder ends. The stress redistribution on the retrofit part is influenced by the surface topography of different thickness web plates and

external three-dimensional constraints of reinforcement. This coupling effect makes the potential damage of stress concentration at the edge corroded part higher than that midplane. The curve part (R = 50 mm) plays an essential role in shifting the distribution peak of stress. High compressive stresses were mainly initiated at the beginning of the curve part. The stress distribution of the corroded and retrofit cases revealed that the transition zone has a jump in stress phenomena. Because the surface loss modeling on the girder ends will generate the stiffness decline, which could explain why being under the material strength threshold still has a residual impact. However, the out-of-plane deformation of the girder ends was prevented completely.

3. Based on the result of this study, the maximum in-plane stress of CFRP sheets (1st-7th layers) is established almost consistently (108 – 123 MPa). It was discovered that the maximum compressive stress was placed on the curve part top edge, close to the cruciform corner edge of the column girder end. The contribution of the Epoxy-Putty model was significant as a basis of curve shape in the retrofit method.

4. The numerical result of local stress distribution (S22 – vertical direction) and eccentric bending deformation (U1 – out-of-plane displacement) of various steel girder end bridges became the basis of this study. The reproduction of those results shall be generalized and contributed to the durability fatigue experiment compact specimen design (Chapter 3).

## 2.9 References


[2.1] Asao, N., & Fujii, K. (2018). Remaining Strength Evaluations of Steel Girders with Corrosion near Supports and their Reinforcements. *KSCE Journal of Civil Engineering*, *22*(10), 4047-4055.

[2.2] Matsumoto, M., Shiraishi, N., Rungthongbaisuree, S., & KIKUTA, T. (1989). Corrosion of steel bridges-its long-term prediction and effect on safety. *Doboku Gakkai Ronbunshu*, *1989*(410), 59-67.

[2.3] Yosri, A., Zayed, A., Saad-Eldeen, S., & Leheta, H. (2021). Influence of stress concentration on fatigue life of corroded specimens under uniaxial cyclic loading. *Alexandria Engineering Journal*, *60*(6), 5205-5216.

[2.4] Al-Salih, H., Bennett, C., & Matamoros, A. (2021). Evaluation of novel combined CFRP-steel retrofit for repairing distortion-induced fatigue. *Journal of Constructional Steel Research*, *182*, 106642.

[2.5] UEDA, Masahito, Atsuhito HIRAGA, and Tetsu NISHIMURA. "Compressive strength of a carbon fiber in matrix." *Journal of the Japan Society for Composite Materials* 37.3 (2011): 103-110.

[2.6] Baumann, A., & Hausmann, J. (2021). Compression Fatigue Testing Setups for Composites—A Review. *Advanced Engineering Materials*, *23*(2), 2000646.

[2.7] Nippon Expressway Research Institute (NERI). (2015). Design and Installation Manual for Upgrading Steel Structure with The Use of Carbon Fiber Sheet. Tokyo

[2.8] Japan Road Association. (JRA). (2012). Specifications for Highway Bridge (Part II Steel Bridges). ISBN978-4-88950-717-1 C2051

[2.9] Helwig, T., & Yura, J. A. (2012). Steel bridge design handbook: Bracing system design (No. FHWA-IF-12-052). United States. Federal Highway Administration. Office of Bridge Technology.

[2.10] Battistini, A. D., Donahue, S., Wang, W. H., Helwig, T. A., Engelhardt, M. D., & Frank, K. H. (2013). Brace Stiffness and Forces of X Type, K-Type, and Z-Type Cross Frames in Steel I-Girder Bridge System. *In Proceedings of Structural Stability Research Council/North American Steel Construction Conference*, St. Louis, MO, April 16 (Vol. 20)

[2.11] Japan Road Association. (JRA). (2012). Specifications for Highway Bridge (Part I Common). ISBN978-4-88950-714-0 C2051

[2.12] Abaqus Analysis User's Guide Version 2018; Dassault Systèmes Simulia Corp.: Providence, RI, USA

[2.13] Khurram, N., Sasaki, E., Kihira, H., Katsuchi, H., & Yamada, H. (2014). Analytical demonstrations to assess residual bearing capacities of steel plate girder ends with stiffeners damaged by corrosion. *Structure and Infrastructure Engineering*, *10*(1), 69-79.

[2.14] Fujikubo, M., & Yao, T. (1999). Elastic local buckling strength of stiffened plate considering the plate/stiffener interaction and welding residual stress. *Marine Structures*, 12, 543–564.

[2.15] Hung, V.T., Nagaswa, H., Sasaki, E., Ichikawa, A., & Natori, T. (2002). An experimental and analytical study on bearing capacity of supporting point in corroded steel bridges, *Journal of Structural Mechanics and Earthquake Engineering*, 710/I–60, 141–151.

[2.16] Tamagawa, S., & Kim, Y.C. (2010). Effect of welding residual stress on compressive behavior and ultimate strengths of corroded plate. *International Journal of Steel Structures*, 10 (2), 147–155.

[2.17] Kayser, J. R., and A. S. Nowak. (1989). Capacity loss due to corrosion in steel-girder bridges. *J. Struct. Eng*. 115 (6): 1525–1537

[2.18] Shi, X., L. Fay, Z. Yang, T. A. Nguyen, and Y. Liu. (2009). Corrosion of deicers to metals in transportation infrastructure: Introduction and recent developments. *Corros. Rev*. 27 (1–2): 23–52

[2.19] Wu, B., J.-L. Cao, and L. Kang. (2017). Influence of local corrosion on behavior of steel I-beams subjected to end patch loading: Experiments. *J. Constr. Steel Res*. 135 (Aug): 150–161

[2.20] Khurram, N., Akmal, U., Azhar, F., Salmi, A., Hameed, A., Tamura, H., & Mohamed, A. (2022). Spatial Numerical Simulation of Locally Corroded Steel Plate Girder with Various End Panels. *Advances in Civil Engineering*.

[2.21] N. Khurram, E. Sasaki, H. Katsuchi, and H. Yamada. (2013). Finite element investigation of shear capacity of locally corroded end panel of steel plate girder. *Int. J. Steel Struct.,* , vol. 13, no. 4, pp. 623–633.

[2.22] N. Khurram, E. Sasaki, H. Katsuchi, and H. Yamada. (2013). Finite element investigation of shear capacity of locally corroded end panel of steel plate girder. *Int. J. Steel Struct.,* , vol. 13, no. 4, pp. 623–633,

[2.23] N. Khurram, E. Sasaki, U. Akmal, M. U. Saleem, and M. N. Amin. (2016). A comparative study in utilizing the shell and solid elements formulation for local corrosion simulation at bearing stiffener," *Arabian Journal for Science and Engineering*, vol. 41, no. 10, pp. 3897–3909,

[2.24] Pham, N. V., Miyashita, T., Ohgaki, K., Hidekuma, Y., & Harada, T. (2021). Repair Method and Finite Element Analysis for Corroded Gusset Plate Connections Bonded to CFRP Sheets. *Journal of Structural Engineering*, *147*(1), 04020310.

[2.25] Ahn, J. H., Kainuma, S., Yasuo, F., & Takehiro, I. (2013). Repair method and residual bearing strength evaluation of a locally corroded plate girder at support. *Engineering Failure Analysis*, *33*, 398-418.

**Table 2.1** Material properties of element for retrofit sub-model simulation [7,24]

| Parameter | Unit | CFRP sheet | | Polyurea Putty | Epoxy Putty | Adhesive | Steel |
|---|---|---|---|---|---|---|---|
| Young's modulus | MPa | Transversal direction | 2533 | 65 | 4021 | 2533 | 210000 |
| | | Vertical direction | 640000 | | | | |
| | | Longitudinal direction | 2533 | | | | |
| Poisson's ratio | - | 0.3 | | 0.38 | 0.38 | 0.38 | 0.3 |
| Design thickness | mm | 0.143 | | 1 | - | 0.5 | - |
| Density | g/cm$^3$ | 2.1 | | 1.25 | 1.53 | 1.17 | 7.86 |

Note: vertical (Y) direction was the main direction of the CFRP sheet

**Table 2.2** Transversal displacement characteristic of various girder ends at 50 mm of height.

| Condition | | Healthy (mm) | | Corroded (mm) | | Retrofit (mm) | |
|---|---|---|---|---|---|---|---|
| | | outer | inner | outer | inner | outer | inner |
| CB | Case 1 + G | | 0.00144 | 0.0122 | | | 0.00275 |
| | Case 2 + G | 0.0101 | | 0.0204 | | 0.0191 | |
| CF-V | Case 1 + G | | 0.0044 | | 0.00805 | 0.00192 | |
| | Case 2 + G | | 0.00162 | | 0.00458 | 0.00171 | |
| CF-X | Case 1 + G | 0.00188 | | 0.00669 | | | 0.00638 |
| | Case 2 + G | 0.0079 | | 0.00934 | | 0.0015 | |

Note: outer (transverse displacement direction to outside the bridge); inner (transverse displacement direction to inside the bridge)

**Table 2.3** Local vertical stress characteristic of various steel girder ends.

| Condition | $\sigma_c$ (MPa) | | Ratio ( $\sigma_c$ / $\sigma_{140}$) | | $\sigma_c$ (MPa) | | Ratio ( $\sigma_c$ / $\sigma_{140}$) | |
|---|---|---|---|---|---|---|---|---|
| | GL | LL C 1 | Y | N | GL | LL C 2 | Y | N |
| Healthy CB | 42.25 | 62.65 | 0.75 | | 42.25 | 91.58 | 0.95 | |
| Healthy CF-V | 38.97 | 48.16 | 0.62 | | 38.97 | 67.32 | 0.76 | |
| Healthy CF-X | 40.37 | 47.77 | 0.63 | | 40.37 | 65.31 | 0.75 | |
| Corroded CB | 62.17 | 99.01 | | 1.15 | 62.17 | 129.16 | | 1.36 |
| Corroded CF-V | 67.62 | 89.82 | | 1.12 | 67.62 | 108.88 | | 1.26 |
| Corroded CF-X | 67.23 | 87.13 | | 1.1 | 67.23 | 111.06 | | 1.27 |
| Retrofit CB | 36.04 | 50.88 | 0.62 | | 36.04 | 61.11 | 0.69 | |
| Retrofit CF-V | 37.11 | 44.47 | 0.58 | | 37.11 | 58.04 | 0.67 | |
| Retrofit CF-X | 36.86 | 46.83 | 0.59 | | 36.86 | 57.72 | 0.67 | |

Note : $\sigma_c$ = maximum compressive stress; $\sigma_{140}$ = allowable stress in Japan Steel Specification (140 MPa); GL= Gravity load; LL C1= Live load case 1; LL C2=Live load case 2

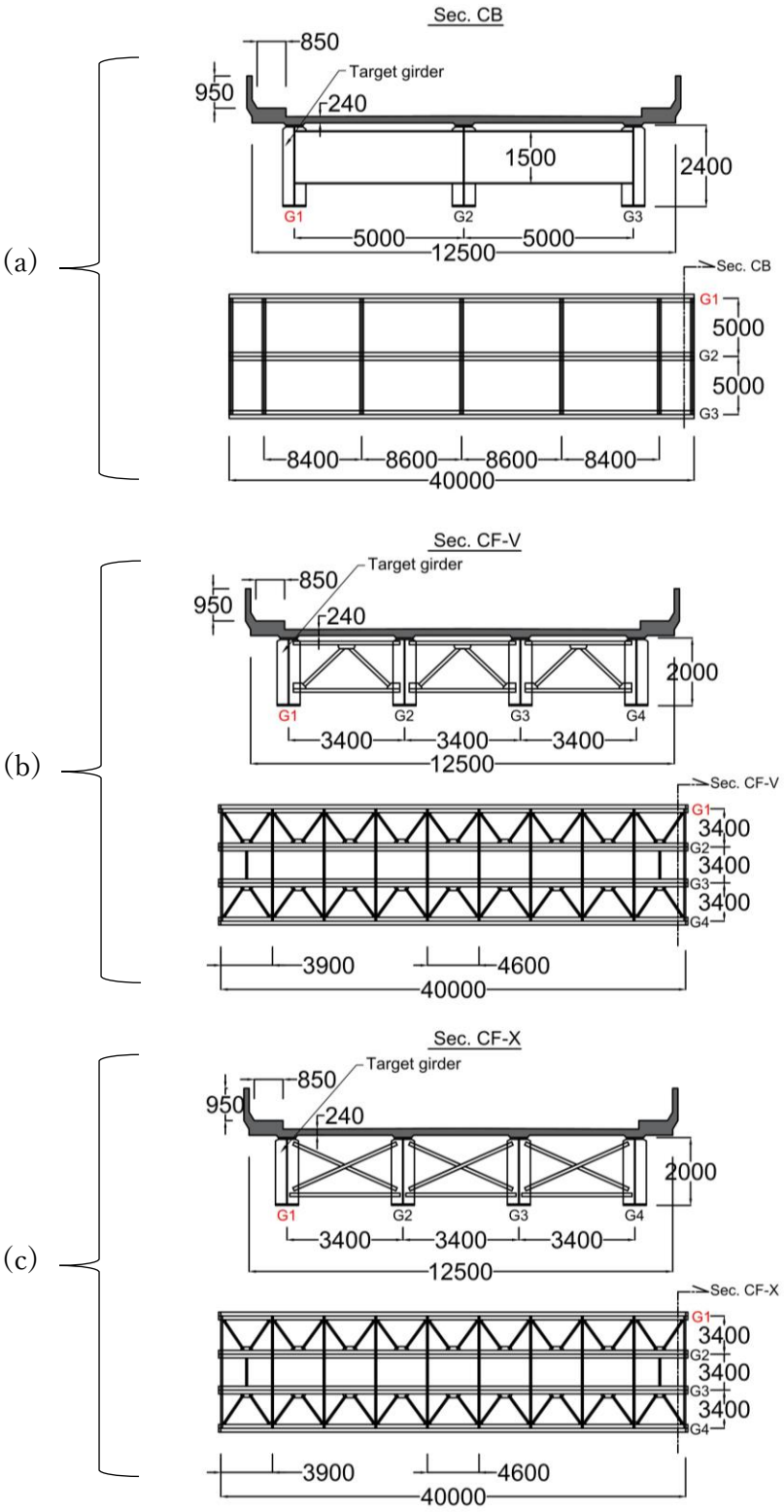


**Figure 2.1** Various of simply supported steel I girder roadway bridge overall view. (a) steel bridge with cross beam (CB) bracing; (b) steel bridge with cross frame V bracing (CF-V); (c) steel bridge with cross frame X bracing (CF-X). (Unit: mm)

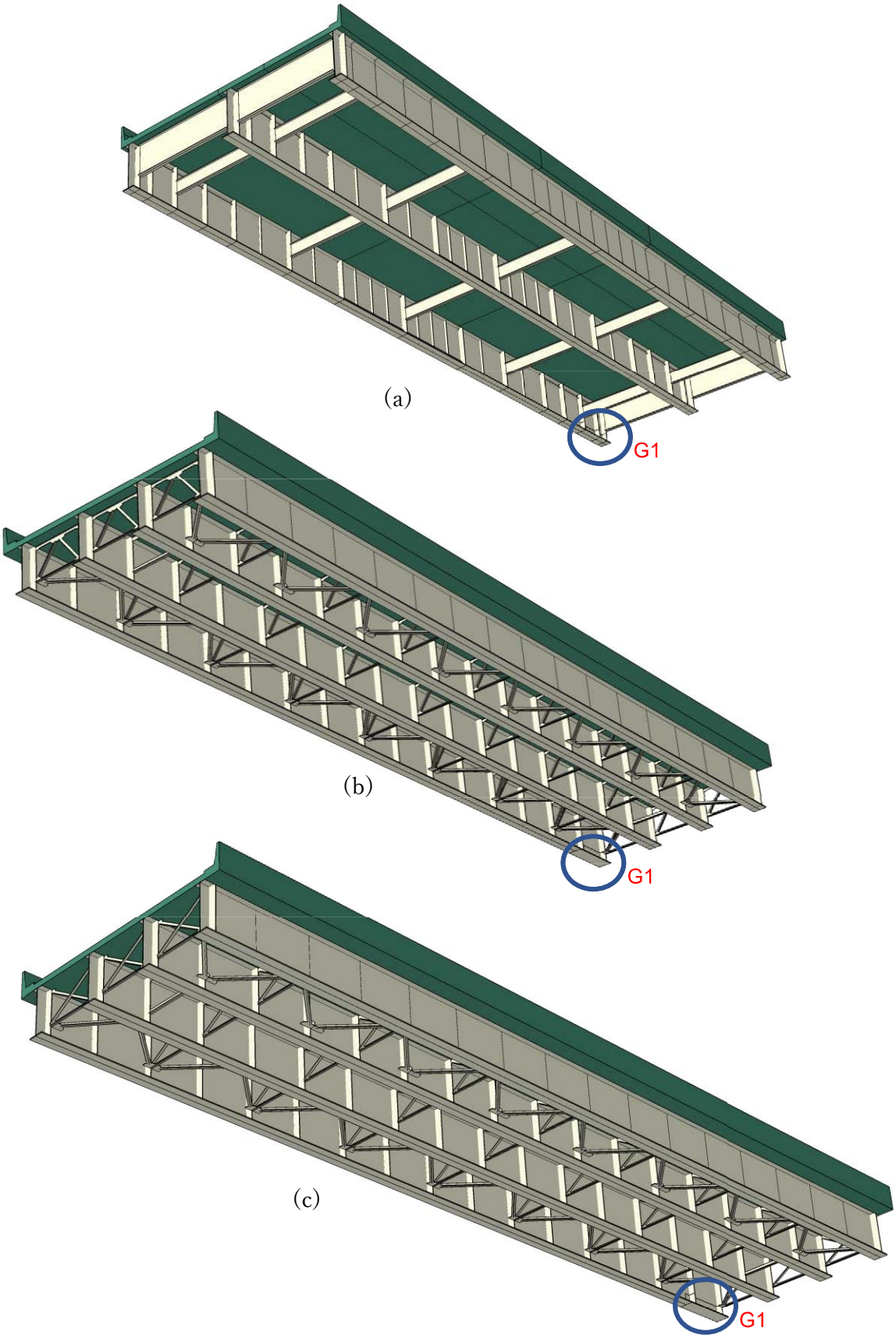


**Figure 2.2** Three-dimension modeling of various bridge. (a)CB; (b) CF-V; (c) CF-X.

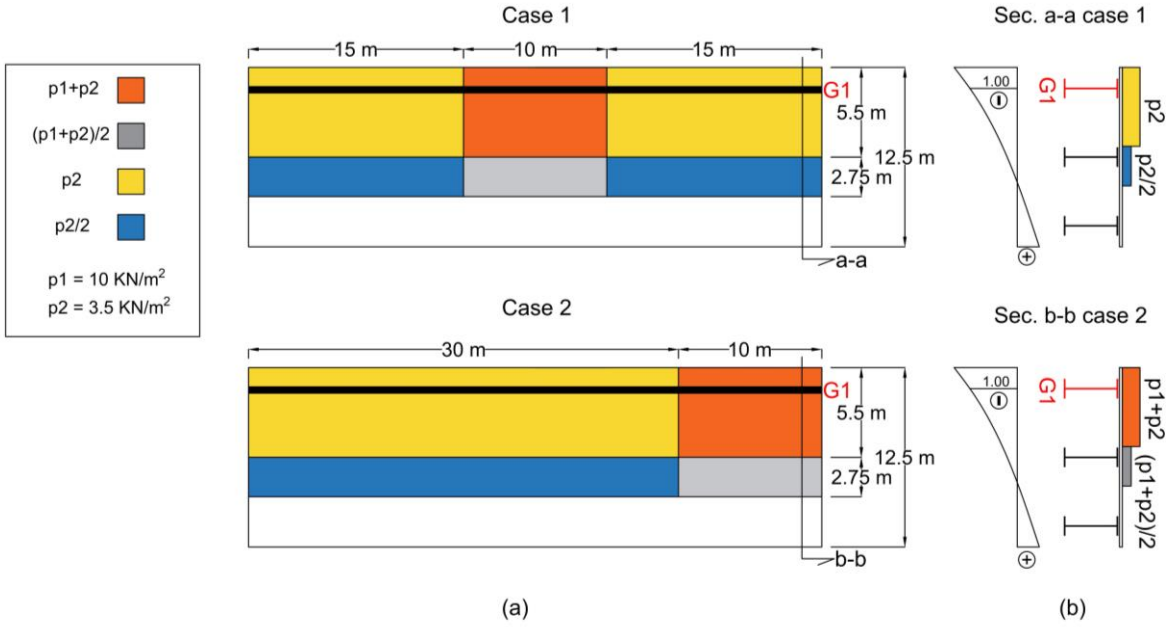


**Figure 2.3** (a) Various loading method at the middle (Case 1) and the edge (Case 2); (b) Influence line reaction in the target girder under various cases.

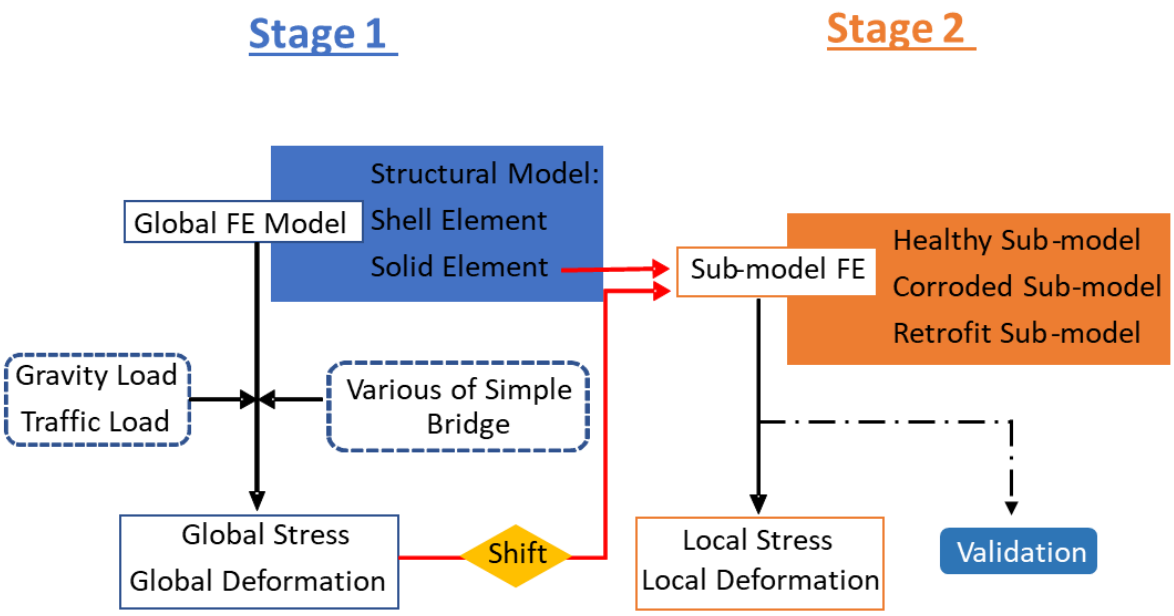


**Figure 2.4** The strategy of global-local modeling approach of steel girder end bridges

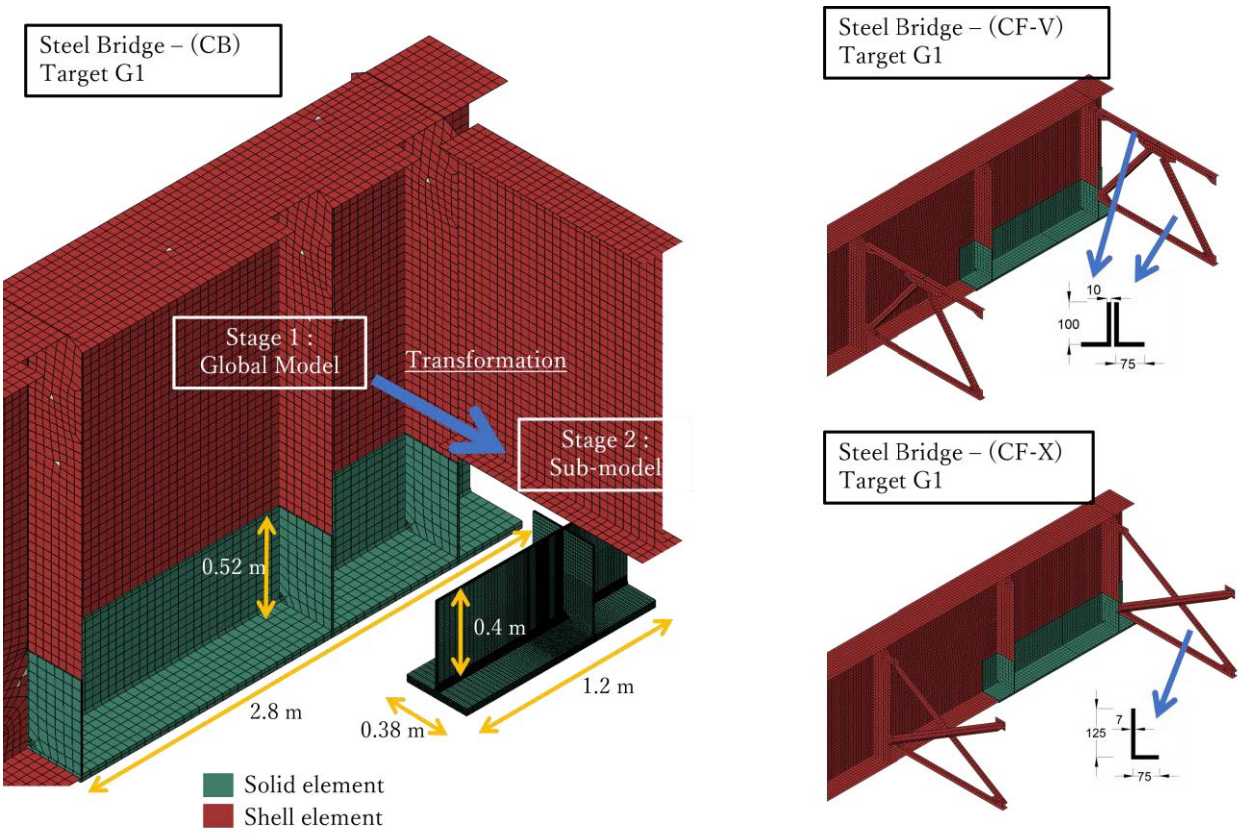


**Figure 2.5** Idealization of steel bridge modeling in Abaqus 2018

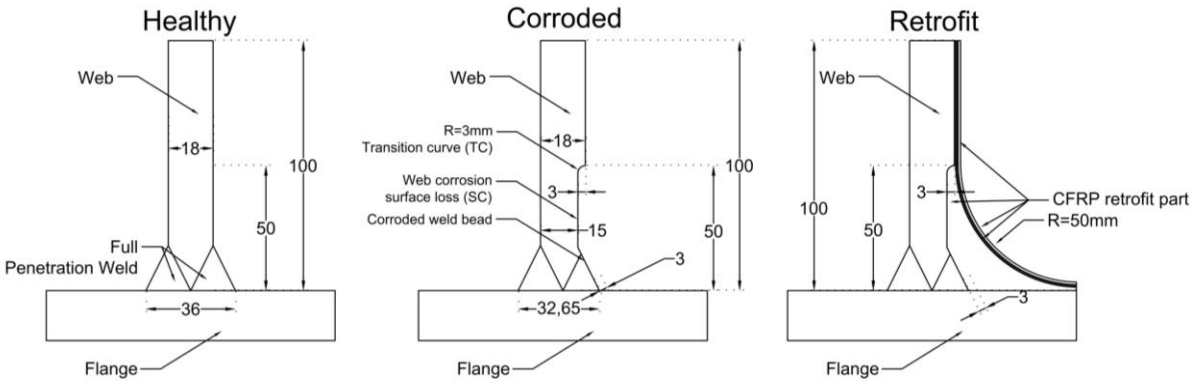


**Figure 2.6** Assumed state condition healthy-corroded-retrofit (HCR) of girder ends modeling. (Unit: mm)

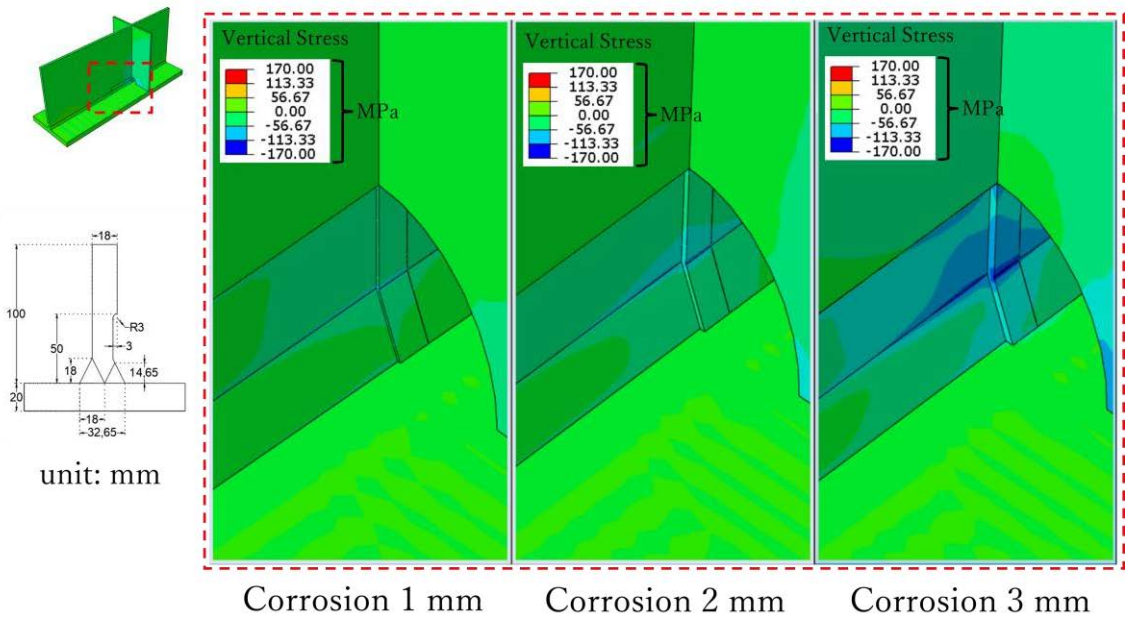


**Figure 2.7** Vertical local stress contour due to variation of corrosion depths

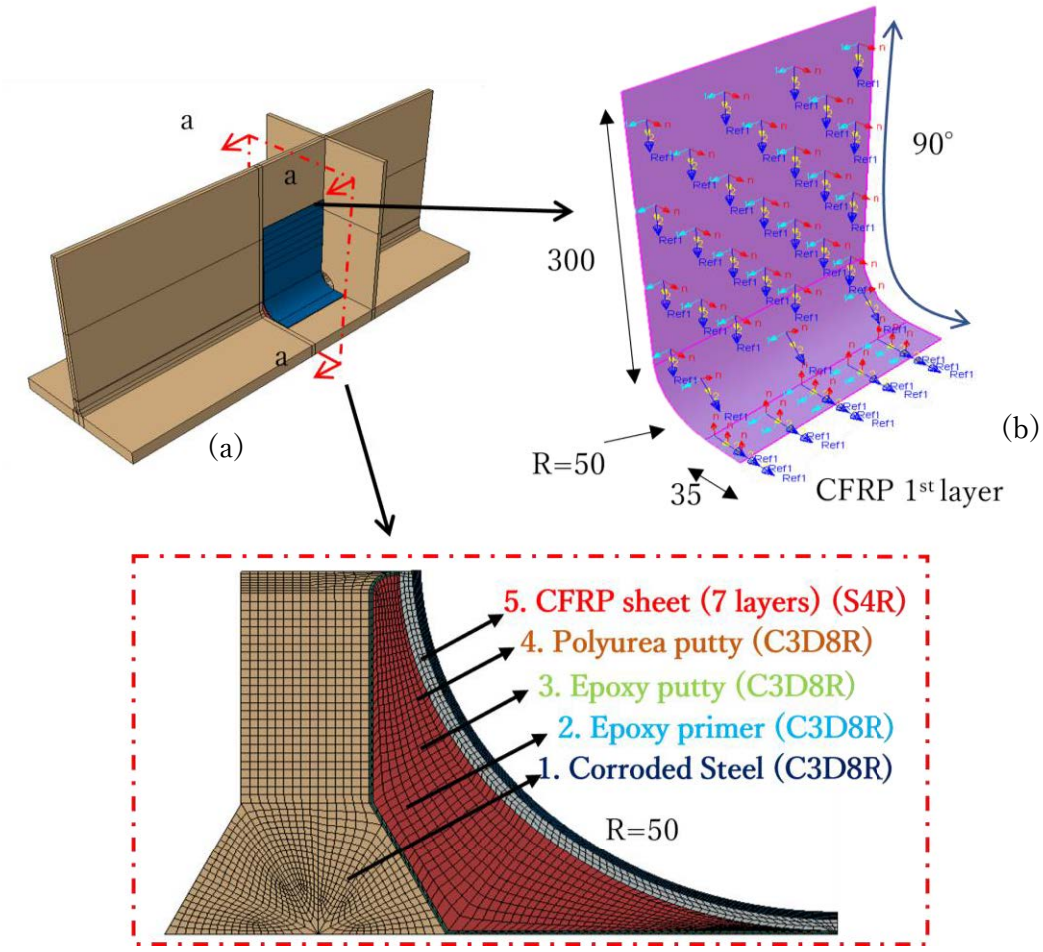


(c)

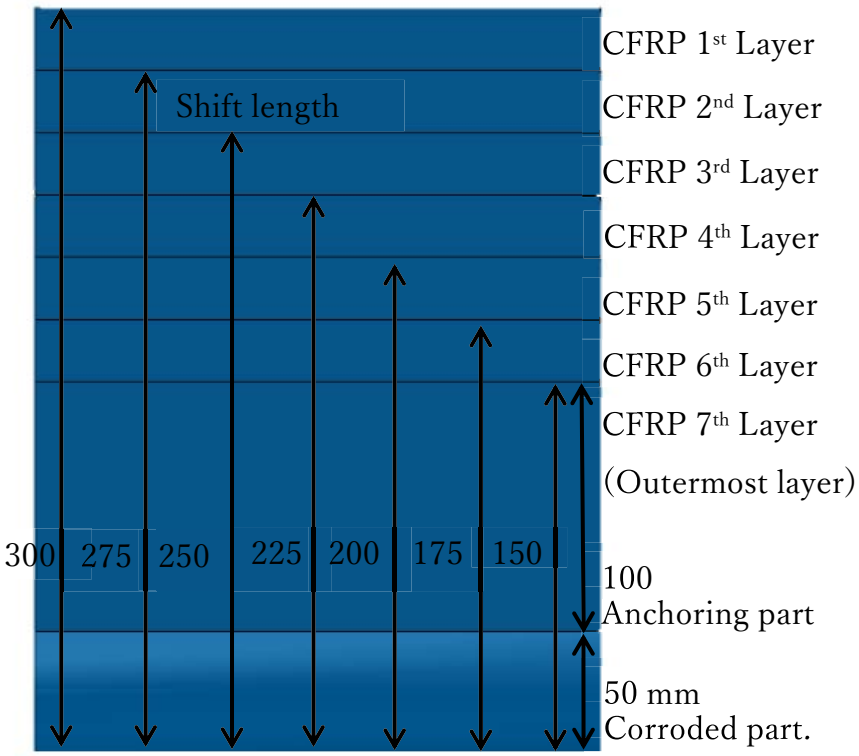


(d)

**Figure 2.8** (a) General view of CFRP retrofit sub-model cross section; (b) layup orientation of 1st layer of CFRP modeling; (c) cross section of retrofit part; (d) arrangement of CFRP sheet modeling by following NERI specification.

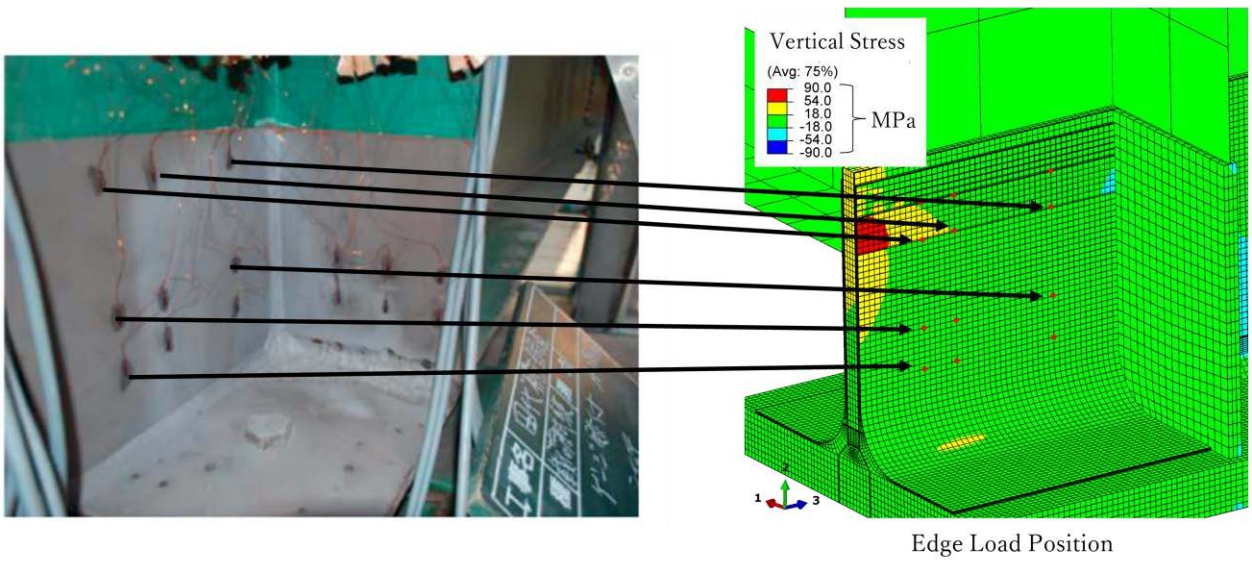


(a)

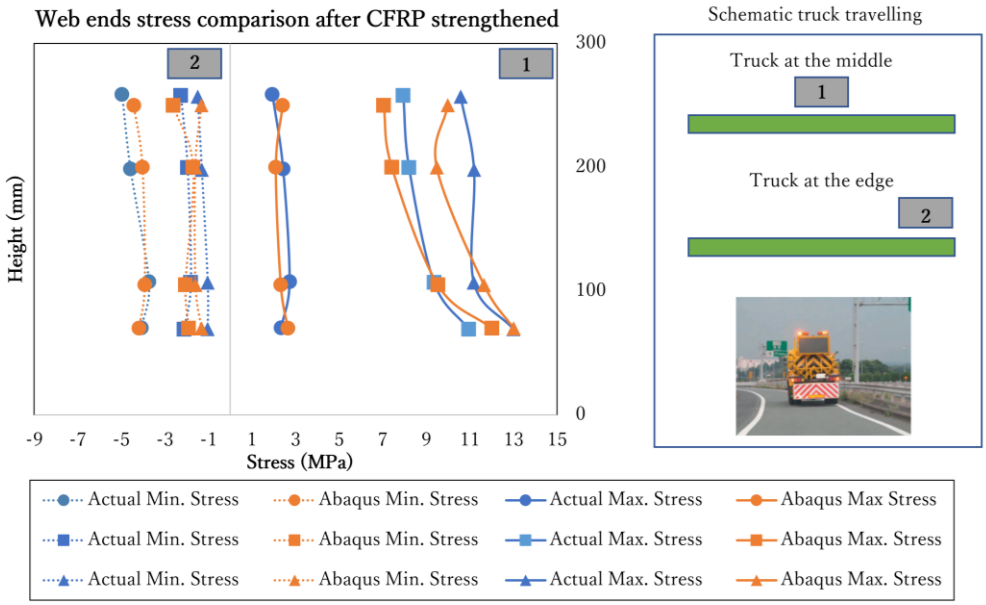


(b)

**Figure 2.9** (a) Reproduction of actual conditions with target location; (b) validation of CFRP modeling and loading test

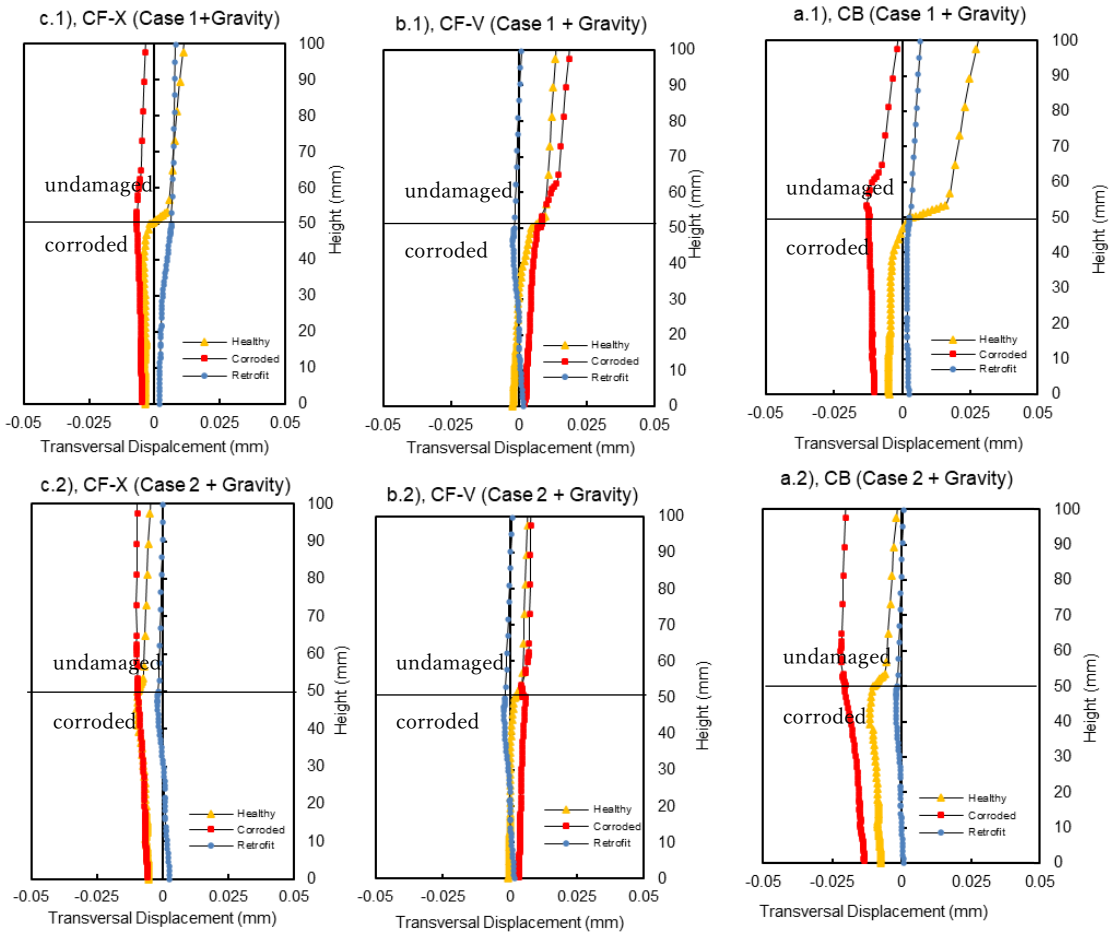


**Figure 2.10** Distribution of transversal displacement characteristic of all girders ends.

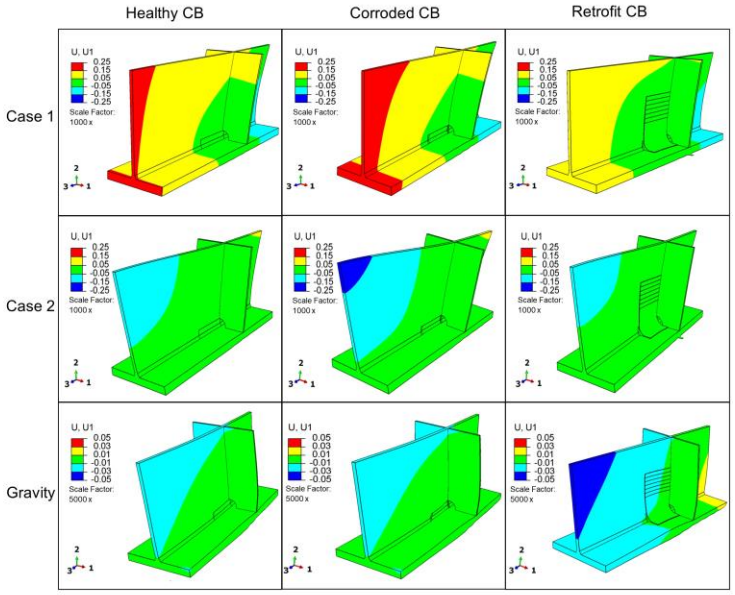


**Figure 2.11** The contour of transversal (U1) displacement transformation of steel girder ends. (a) CB; (b) CF-V; (c) CF-X

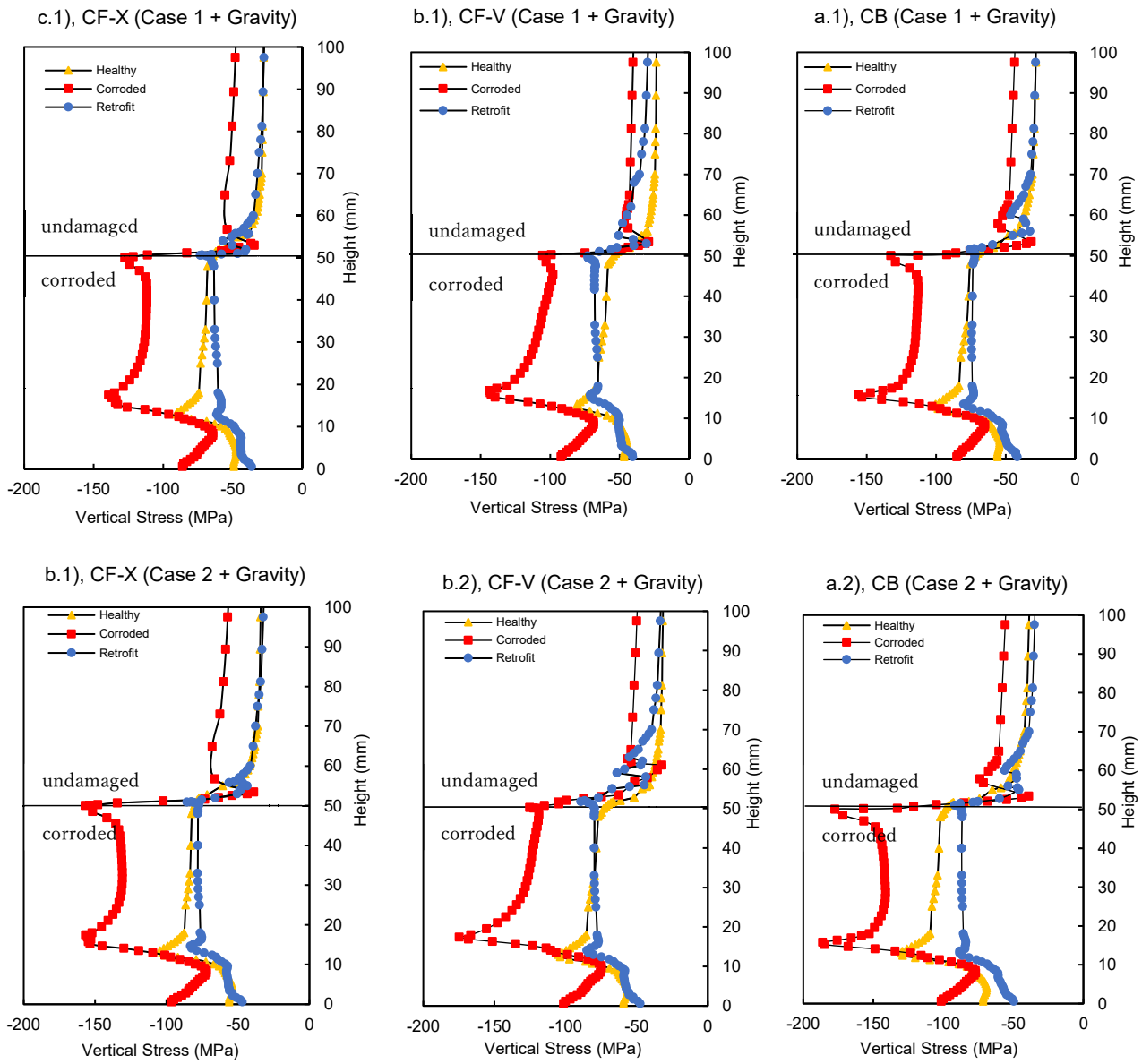


**Figure 2.12** Local vertical stress distribution of girder ends all cases.

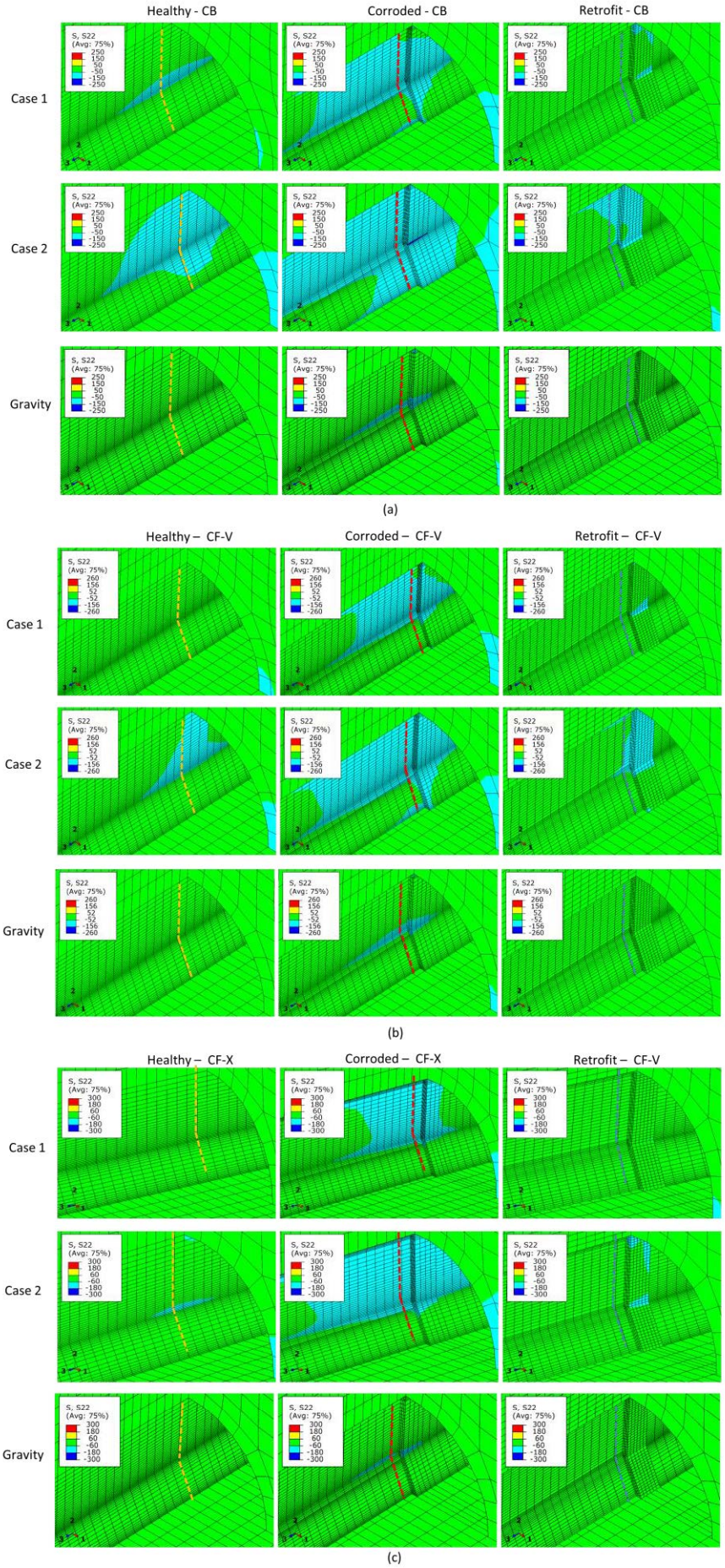


**Figure 2.13** The contour of local vertical stress (S22). (a) CB; (b) CF-V; (c) CF-X.

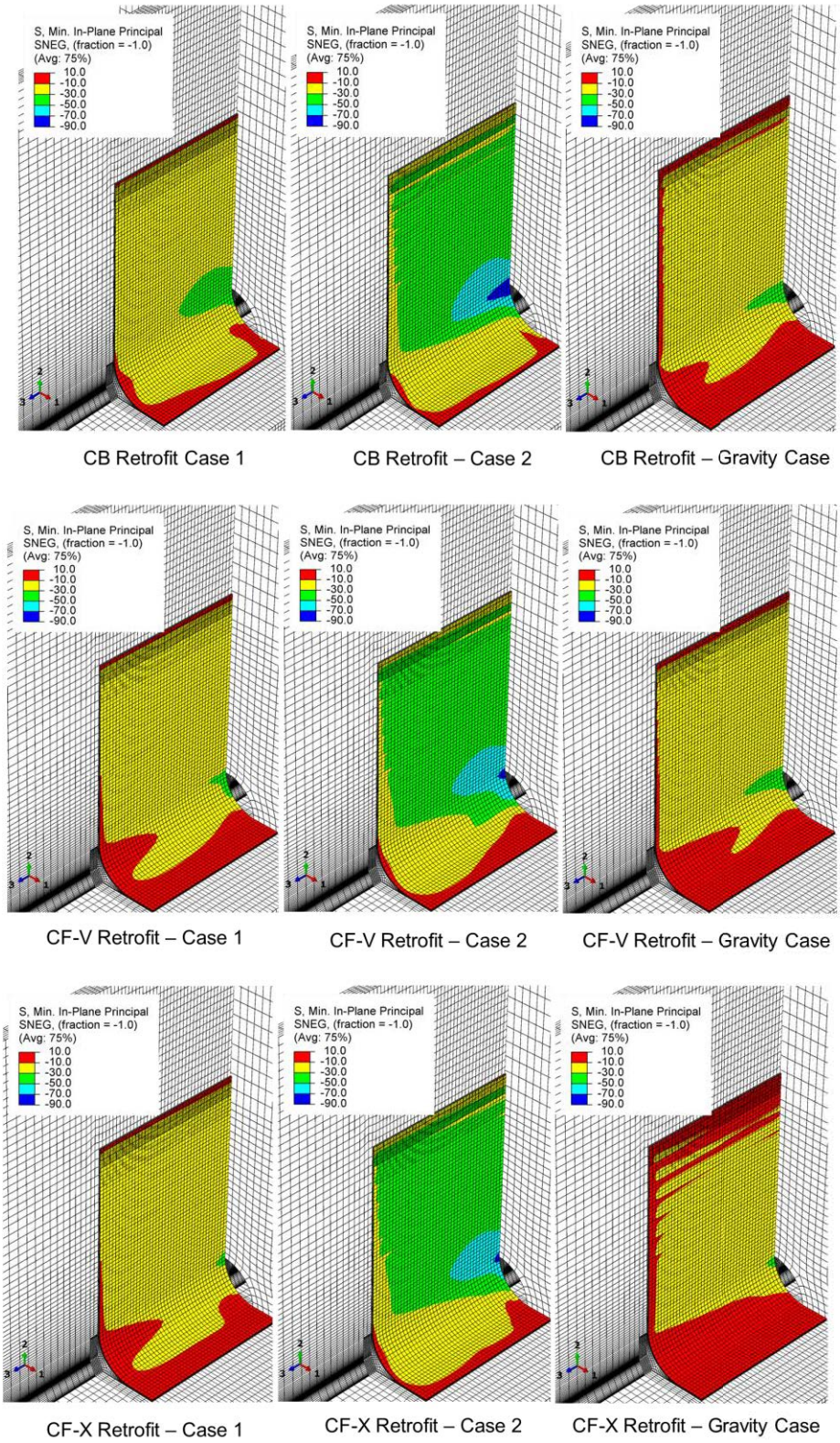


**Figure 2.14** Visualization of In-plane stress principal of all girders ends CFRP reinforcement.

# Chapter 3

# Reproduction of Load Conditions on Fatigue Experiment

## 3.1 Overview

Steel girders bridges are efficient structural systems from the point of view of load-bearing capacity and economical design. However, the bridge structures are still more susceptible to out-of-plane displacement under eccentric load, especially for one-lane traffic jams. Even though the bracing is utilized to limit the adverse out-of-plane distortion [1], many studies have been reported to investigate the eccentricity of vehicle-induced fatigue problems [2-8]. Therefore, as a maintenance technology to guarantee the structure's safety, it is required to determine a method for accurately evaluating the eccentricity effect of the steel girder end retrofitted part. Most of them use steel bottom web-flange gaps as an out-of-plane problem indication. However, Ahn et al. [9] evaluated the residual bearing strength capacity of the CFRP retrofit corroded steel girder end with the one-lane vehicle loading test (out-of-plane). In the method using actual load, there is a high correlation between reproducing the target load and live service time condition. The dominant compressive eccentric load effect of steel girder ends was determined and recognized in Chapter 2. Combining compression load and eccentricity in cyclic loading was necessary to reproduce the fatigue conditions scheme. In addition, consideration must be provided to target part of the specimen design that follows the design of finite element analysis of retrofit girder ends. The consistency should be maintained to perform the accurate compressive-compressive (C-C) eccentric fatigue load experiment, primarily to design the assumed corroded part.

In this way, previous studies that attempt to evaluate the fatigue durability of CFRP have a problem with the reproducibility, applicability, and workability of existing retrofit steel girder ends, and there is space for development. Therefore, in this assessment, the proposed method with adequate evaluation accuracy follows the requirement parameter design of existing specifications (NERI) [10]. Since the target structure is web ends, the CFRP alignment vertically ($90^{o}$) is applied. It is condition based on the following same direction of principal stress in the web plate subjected to reaction force as supporting points. First is the realization of a compact specimen design structure by following the specifications of the fatigue testing machine (Shimadzu Servopulser EHF-E200 kN) [11] must determine. The compact specimen's dimension should follow the fatigue machine's maximum opening. Next, the material properties of specimens and fixtures shall be appropriately decided after fully understanding the design condition of the mechanical properties of rolled steel for the general structure (SS400 or SM400). Then, the loading conditions should be controlled by axial force and using the additional bending fixture to reproduce eccentric axial load and local stress. Second, the anchoring and shift length specification was set to 100 mm and 25 mm, respectively. In this case, mold the smoothing agent in an arc-like shape, R=50 mm, at the joint between the bottom flange and the web. Also, the CFRP curved part was expected to act as a

countermeasure against corrosion. Third is narrowing the width of the compact specimen to produce a localization of deformation. The following load conditions have been adopted based on numerical analysis to generate outer girder ends under severe local stress conditions. It considered the shift/transformation characteristics of the narrowing area due to local high-stress concentration in the retrofit specimen.

Furthermore, the primary key is determining the load value of traffic and dead with the stress-fitted method. The elastic stress distribution should be close or fitted enough between the selected target of the retrofit steel girder end and the retrofit specimen. The tolerance of target points should be less than 15 %.

## 3.2 Specimen Design Configuration

The specimen preparation included cutting, welding, and piercing with steel-grade SM400. For a steel material whose plate thickness is less than 40 mm, it is guaranteed that the compressive cyclic load does not consider local buckling. The allowable axial compressive stress of structural specimens shall be the value determined by 140 N/mm$^2$ [12]. First, it is assumed that the specimen is supported at both ends by pin supports and that the loads act on it with eccentricity. This assumption was made when a specimen between fixing points of the compression side contains a target section in which the stresses are to be controlled. The bending moment differed between two ends of the specimen and changed linearly between two ends. The allowable stress may never be reached under a long fatigue cycle. Moreover, applying SM400 represents the material structure application of steel girder bridges, particularly in Japan.

The study invention was made in consideration of the high-cycle fatigue problem. It aims to make it possible to assess the location of fatigue fracture initiation more accurately than ever before. With low durability section in long life region of the retrofit specimen, as shown in Figure 3.1. During the cutting process, a target area of the specimen was established with artificial uniform corrosion on one side. This area proposes concentrating the elastic stress in the retrofit region during cyclic loading. Then, as mentioned earlier, from the result of the numerical simulation of girder ends, the elastic local stress concentration was located at the bottom weld bead. This finding is similar to Tohidi et al. [13] investigation on corroded steel plate girder ends. The corroded bottom flange does not influence the crucial elastic buckling of corroded plate girder ends, but the locally corroded web does. However, Sharifi et al. [14] claimed that the uniform thickness of surface loss of corrosion could be appropriate for evaluating corroded steel girder ends, especially at the bottom part of the structure. Next, the issue with this type of eccentric compressive test was that buckling failure could probably become dominant at the center of the specimen, not at the ends.

This study to solve the current issue adopted the simple narrowing-area method inspired by dog bone specimen geometry [15,16]. Shifting dimension configuration at the specimen body is essential in preventing local buckling. It was shown that the narrowing area of the target part makes it possible to determine the initiation damage fatigue behavior in the presence of the experiment.

To further understand the significance of eccentricity vehicle in-service loading variables. Developing a practical experimental instrument that can accurately predict the compressive out-of-plane behavior at the girder ends subjected to high-cycle fatigue. The characteristics of the specimen were decided to replicate the severe out-of-plane displacement from selected outer steel girder ends. The fixture design became a key to avoiding damage at the load cell and actuator due to eccentric load. The out-of-plane displacement value should be small enough during the cyclic process. This study assumed that the transversal (U1) displacement should be less than 0.01 mm, which was monitored by numerical analysis. Then, the effective local elastic stress was determined in only one side direction of the retrofit specimen. Also, the fixed variables in specimen design should be considered first, e.g., maximum capacity load (200 kN), the fatigue machine's vertical opening, and the chuck grip's dimension. An understanding of fatigue machine specification could be led to the accurate result of the long run of high-cycle fatigue. Out-of-plane eccentricity approaches may occur in some conditions. Still, they can be complicated because of an inability to visualize the displacement of the component's bridge structure, especially the web ends girder. Cyclic axial compressive-compressive (C-C) load ($P_{DL} \leftrightarrow P_{DL+LL}$) associated with elastic bending moment were utilized (eccentric load) to the fatigue specimen resulting in a local stress concentration gradient at the target part. Ideally, the axial loads ($P$) were designed by integrating the specimen local stresses over the sub-model local stress. Here, the load ($P$) was the elastic load capacity as first order-moment (linear dependence) was achieved by combining the load ($P$) by initial load eccentricity $(e_{xy})$, whereas in target part cross-sections, the high-stress concentration will achieve based on inertia ($I$) changed. The target part was the representative scallop part at the girder ends. The first bending mode that reproduces as an eccentric load ($P$) should be estimated as the final bending moment, i.e., $M_{xy} = P(e_{xy} + y_0)$

### 3.2.1 Material Parameter

The steel grade shall be selected appropriately according to the:

1) The stress state of the member,
2) Fabrication method, strength, elongation, ductility,
3) Geometrical dimension.

According to the current JIS Z 2214 (Method of tensile test for metallic material), the proof stress of steel decreased by increasing plate thickness. On the other hand, it has become possible to fabricate steel whose proof stress does not change by the plate thickness. When the specimen thickness is small compared to the width, sustaining the specimen's lateral deflection or out-of-plane bending is difficult. This study used 12 mm in thickness for a healthy specimen body, 9 mm for a corroded part, 10 mm for the griping plate, and 24 mm for the fixture. Then, the thickness parts have allowable compressive stress at 140 N/mm$^2$. In order for the results obtained by this experiment to be valid, it is required that the material behavior be predominantly linear elastic at all values of applied loads.

Also, specimen design must be performed in such a manner that the detail category specified in Specification for Highway Bridges, Japan Road Association. The detailed category was difficult to determine. Even with precise finite element analysis, a universal method has not yet been established for indexing the appropriate setting of stress variations and determining the grades of fatigue strength corresponding to stress variation. This study used the range of stress ratio, $R > 1.00$, where compressive stress was predominant. Residual stress was released when fatigue damage was initiated. The dimension of the damage initiation due to brittleness exhibited the influence of the magnitude of the stress ratio when the growth of fatigue cracks was slowed down.

In verifying the stress fatigue durability of the specimen, it shall be confirmed by adequately applying a load that safety against fatigue for the joint. It shall be confirmed that the maximum value within the range of stresses exerted on joints was lower or equal to the stress range. The cut-off threshold for each joint corresponded to constant amplitude stress. This study described methods and procedures for estimating the stress range from finite element analysis based on Specifications for Highway Bridges Part I Common [17]. The detailed analysis is described in Chapter 2. Then, further finite element analysis has been carried out in this chapter to control whether the retrofit specimen's stress range is satisfied.

According to the finite element analysis result, verification shall be performed using maximum and minimum local stress subtraction. The calculated local stress range of the retrofitted specimen, $\Delta\sigma = \sigma_{max} - \sigma_{min}$, and the value is 49.89 MPa. It is confirmed that the normal stress range of the retrofitted specimen was lower than the allowable stress range for $2 \times 10^6$ cycles in detailed category D ($\Delta\sigma_f = 100$ MPa). Under constant amplitude loading, a stress range is designed almost half below of fatigue design limit. So fatigue life will be long for only slight changes in the stress range. The local and structural geometric stress range concentration significantly influenced

the fatigue strength for constant amplitude loading. It can be judged that the fatigue life durability of retrofitted specimens will be survived under the long-run fatigue experiment. This study maintained the elastic conditions as eccentric cyclic loading parameters that will apply to another steel grade.

### 3.2.2 Compact Specimen Design

When a new fatigue assessment method is developed, unsatisfactory fatigue machine specifications could be needed to make full-size retrofitted specimens. Due to the sub-model of CFRP retrofitted girder ends dimensions, only a small-scale practical part of the retrofitted section is initially constructed into the compact specimen. An essential challenge in fatigue compact specimen design depends on correlating how the actual service live load could be applied. A constant-amplitude fatigue cyclic test is imposed on a specimen under suitable test conditions (specimen stiffness, shape, and assumed corrosion shape). It caused a damage initiation to start from a low-durability location at the target part. The detailed dimension of the specimen and fixture design is shown in Figure 3.4(a-b), and the compact specimen manufacture result is shown in Figure 3.5(a-b). Then, the explanation follows the next section.

- Target Part Design

Numerical simulations have been conducted to assess the severe section in retrofitted girder ends. First, the most adverse region in various girder ends based on CFRP longitudinal stress distribution is covered by 50 mm length, as shown in Figure 3.2(a). In the analysis, s. min in-plane principal stress of steel bridge with cross-bracing (CB) at the longitudinal distribution is higher than other steel bridge types (CF-V and CF-X). In the length of 50 mm, the local longitudinal stress is reduced following the direction in all cases. Therefore, the finding of the severe section at the retrofitted girder ends was clear according to the bracing type. The distribution of local stress itself shall influence more stiffening of the steel bridge structure. In Figure 3.2(b) shown, the determination of specimen height and width are visualized. This process should represent the severe region of the retrofit girder end. The lowest difference in local stress indicated that the high local stress distribution of the section part was uniformly distributed along 50 mm length. More specifically, the longitudinal local stress difference of all sub-models of retrofit steel girder ends was confirmed (CB = 18 MPa; CF-V=21 MPa; CF-X=30MPa). Then, the local longitudinal stress also reveals the high-stress position in the CFRP retrofit part. Compared to the length of the CFRP part at the girder ends, the high local stress occurred at 23 % of the total length based on the service life load in numerical application. Second, to adopt the complete vertical direction of the CFRP retrofit part, the 300 mm height of the specimen is considered. However, the specimen's height

should satisfy the fatigue machine's maximum opening gap. Then the 7th layers of CFRP could be attached perfectly. The complexity in interpreting CFRP retrofit simulation result to compact specimen design have generally received more attention in this study. Thus, the detailed process determines the specimen's width and height.

The result of local stress distribution in Chapter 2 shows that the corroded part sub-model on the undamaged parts slightly increased. The vertical local stress difference varies from 15 to 25 MPa, respectively (Figure 2.12). The detail of local stress distribution only showed at 100 mm of retrofit girder ends. However, the narrow of local stress distribution cannot represent the behavior of the entire girder end. Then, the local stress distribution is expanded to 1500 mm.

This study found that corrosion at girder ends will increase the local stress at the undamaged part of girder ends for 6 times of length. However, the parameter of severe condition was determined with the thickness of the cross-section part ($t_{sd} = 3\,mm$), and the length of sectional loss ($L_{sl} = 50\,mm$). As displayed in Figure 3.3, the local vertical stress distribution of the corroded girder end with cross beam (CB) bracing at the healthy part. It was increased to 250 mm from the corroded web edge. After that, the corroded local stress distribution was shown to resemble healthy and retrofit stress distribution. Also, as seen in Figure 3.3, due to the steel girder end height, the local stress concentration on the girder ends will be dissipated at a sufficient distance. This characteristic can be explained by following saint-venant's principle. The local stress distribution line parallel to the local plane stress (vertical) could be changed. Due to the relatively near distance from the corroded part in which the stiffness is changed. Applied loads on the corroded local region give rise to stress along a cross-section caused by discontinuity of cross-sectional shape. However, due to the girder height, the stress localized corroded effect on the girder ends will be dissipated at a sufficient distance. However, the concern of CFRP retrofit in the field could rely on these characteristics if the local stress was insignificant at the undamaged part of the corroded condition. Then, the changing of local stress should be more careful due to fatigue on the service life of steel bridge. Finally, the design parameter of the specimen was also considered due to these conditions.

The artificial surface loss or corroded damage is expected to represent severe, although potentially retrofittable, damage. Additionally, consideration was given to the capability to substantially corrosion scale for laboratory investigation. Produce artificial surface corrosion intended as the starting point of the high local stress under fatigue loading. In the compact specimen at the target area, the target area was required to maintain an elastic condition. The corroded part's local stress shall not be influenced by load fluctuation and high frequency.

Generally, in the case of uniform corrosion, the local stress can be easily estimated and calculated [18]. As mentioned before in Chapter 2, based on Khuram et al. [19] height of the practical corroded part has to be less than 60 mm due to prevent local buckling. Then, based on Noor et al. [20] investigation, the detailed corrosion model design consisted of a curve (R = 3 mm) at the top of the end corrosion. That replicated the uncertain shape of corrosion that induced the peak of stress transition from a corroded region to a healthy region. The parameter of corrosion depth, also related to the maximum number of laminated layers of the carbon fiber sheet, could be attached. It was specified as 20 because, with 20 layers of CFRP, the surface loss depth of steel that should be replaced is around 9 mm, and separate experiments should verify the applicability. Then, this study maintained the amount of carbon fiber sheet under 10 layers (7 layers – 3 mm surface loss depth with 3mm curved). It is convenient to make the depth of corrosion 25 % to the initial thickness of the specimen to maintain elastic stress in high-cyclic fatigue.

- Narrowing Specimen Design

There has been limited published research regarding a novel compact specimen design. However, this study tried to achieve the rational design with former selective research considering a simple dog bone geometry. Then, a new compact specimen may also need a side groove or narrowed shape with a fillet radius. To avoid the buckling deviating from the plane of the specimen. Narrowed width may also improve the specimen's stiffness due to extension width and the visibility of the target area when using visual methods for damage initiation assessment. The other essential purpose is to localize the stress at the target area by narrowing the width of the compact specimen, as shown in Figure 3.4(a). The direction of principal stresses (S22) was concentrated at the target area part, thanks to the narrowing shape. Also, it was analyzed deeply with the finite element, which indicated a local vertical stress of about 1.6 lower than the local vertical stress at the retrofit part at the same level. However, it is known that the narrowing-shaped specimen geometries often represent inhomogeneous stress distribution characteristics of the corroded part region.

If the local stress applied was too high outside the target part, detachment and debonding would be initiated unconditionally. It can be assumed that stress-dependent narrowing shaped under the single mode of cyclic loading played an essential role in maintaining overstress except for the target area. Narrowing the width of a compact specimen to produce a localization of deformation was produced. Therefore, limited published research has been on a novel compact specimen design. This study tried to achieve the rational design with former selective research considering a simple dog bone geometry [20-22]. Then, a new compact specimen may also need a side groove or narrowed shape with a fillet radius. To avoid the buckling deviating from the plane

of the specimen. Narrowed width may also improve the specimen's stiffness due to extension width and the visibility of the target area when using visual methods for damage initiation assessment. The other essential purpose is to localize the stress at the target area by narrowing the width of the compact specimen.

The direction of principal vertical stresses (S22) was concentrated at the target area part, thanks to the narrowing shape. Also, it was analyzed deeply with finite elements, which indicated a local vertical stress of about 1.6 lower than the local vertical stress at the retrofit part at the same level. It can be found that stress-dependent narrowing shaped under the single mode of cyclic loading plays an essential role in maintaining overstress except for the target area. Moreover, as displayed in Figure 3.4(a), the narrowing shape shall be equal in width to the target area and have a radius of 50 mm. The specimen design requirement should be considered due to fatigue compression load type.

- Corroded Weld Bead Design

In Chapter 2, the result of an assumed state of the corroded condition followed in this chapter, but the issue came up. The local stress distribution of both specimens does not resemble, especially the starting point of the retrofit specimen's local stress. So, the adjustment of weld bead size and dimension is applied. Compact specimen weld bead simplification was applied due to the limited reproduction of full CFRP retrofitted girder, e.g., stiffener and scallop part. The size of the specimen weld bead was decreased 1/4 from corroded steel girder end, as shown in Figure 3.5(b). The issue appeared when the corroded assumed state was fully implemented. The accuracy of comparison local stress distribution of weld bead did not resemble. Then, the specimen weld bead should modify to resemble the local stress of the retrofit girder end. The compatibility of starting value of local stress between the girder end and specimen shall be considered due to the reproduction of the actual condition. The Fatigue Load Determination section describes the details regarding this parameter.

### 3.2.3 New Fixture Design Fundamental

The primary purpose of this phase is to select the fixture elements. Fixture design contains various activities: fixture planning, layout strategy, and fixture element design. Therefore, the fixturing layout is essential to identify the technical parameter configuration in fatigue cyclic loading. The fixture design was developed in parallel and established with basic fixture concepts:

- The fixture layout shall accommodate the high-cycle fatigue in long-run loading, which was the configuration of the retrofit specimens following the limitation of the fatigue machine.
- The fixture element design was to reproduce actual compressive axial with bending mode in retrofit girder end specimens.
- The fixture design must be observed during the procedure of fixture design, which should be safe and easy to use.

The above criteria are particular in the assessment of steel bridge support. The fixture design is a new kind of fixture developed to adopt the eccentric load of the steel bridge, which was adjustable to create a particular value of eccentricity. The filler plate adjusted the eccentricity of the specimen. An out-of-plane containing the bending mode of the specimen was captured using an asymmetry fixture and filler plate concerning the cyclic elastic condition. Clearance or gap between the fixture and filler plates was not acceptable to permit the elastic bending mode. The accuracy of the fixture model approach was verified by finite element analysis. More importantly, the experimental performance analysis approach can guide to achieving more reasonable results.

The new fixture parts design is constructed from common fixturing elements such as grip plate, filler plate, and bolt joints, as shown in Figure 3.4(b). These parts can be assembled without the need for additional machining operations. The main improvements of using integrated fixtures are their assembly state, especially the bolt joint connection-based systems, due to the following physical characteristics:

- Easy to assembly and disassembly using manual tools
- Relatively simple applying combination loads design
- To produce sufficient eccentric axial force without causing any undesirable effect

These fixtures designed have not produced a CFRP retrofit specimen bearing failure. With this performance, the fixture design is appropriate for developing accuracy in various applications.

### 3.2.4 Element of Fixture

The load conditions were complicated. Generally, girder columns are designed to align the axial load with the part. However, the eccentric vehicle load situations that the live load will be off center and cause an out-of-plane in the column in the addition of compression. When steel girder end columns are a load of the center, bending can be a severe problem and may be more important than compression stress. Figure 3.5(a) shows the setting placement of the specimen on the fatigue machine. The members of each part are visualized well, and the explanation is as follows:

- Plate Grip

A plate grip is usually a component to transfer the axial load from the machine to the specimen. It was used to establish and maintain the compression-compression position of the specimen part in the fixture by constraining the part's movement. A plate grip design with a single bolt connection was also adjustable for workpieces of more constructible shape and assembly conditions. The plate grip was designed to be added and placed at a top and bottom specimen.

- Fixture

The experiment setup adopts proportional type loading to create compressive bending action. During a setup, it is necessary to restrict certain degrees of freedom. The fixture body was the primary structural element of the reproduction CFRP condition at the specimen. It maintains the spatial relationship between the specimen parts. Based on the finite element model analysis, fixture design was effectively established in elastic and maximum load conditions.

The lateral displacement at the top and bottom ends of the specimen was constrained at the support. To apply the eccentric force, the axial load $(P)$ direction $\left(U_x = 0;\ U_y = 1; U_z = 0\right)$ The load was released. The complete design of the novel compact specimen will be detailed in several figures in this chapter (in Figure 3.5(a)).

The fixture's reverse L shape design was a new fixture model. This geometry shape could maintain the target condition, such as compressive load and out-of-plane deformation. This degree of freedom $U_x$ was not perfectly restrained. However, there was a possibility that the movement reached the maximum displacement. So, this distinctive design aimed to generate eccentric conditions elastically.

Verification check that fixture design does not experience high-stress concentration during the loading scheme. Finally, a single value of the highest stress from service stress distribution data can define the maximum and minimum of specimen loading conditions within a specific load range. The relationship between $P_{LL}$ , $P_{DL}$ , load-range $\Delta P$, and frequency $(Hz)$ are the essential parameters for controlling and monitoring the location of fatigue initiation damage life of CFRP retrofit specimen components.

- Filler Plate

Filler plates were used in compact specimens to reproduce the eccentricity condition associated with the fixture. The thickness design of each filler plate was 10mm. The use of filler consisting of two plates to attach the specimen. The inside filler plate was designed to provide out-

of-plane bending deformation during the fatigue experiment. The inside filler's contribution also decreased the friction stress from each part during cyclic loading.

Moreover, the outside filler is made to avoid the bolt connections' concentration stress. Developed fillers can be achieved by cutting the plate and drilling for bolt connections. The objective of the filler plates was to quantify the effect of bending mode on fatigue performance in elastic conditions.

In this experiment, there is a fixed variable related to CFRP reinforcement. From this point of view, the CFRP repairment specification is hard to modify or improve. The option of modification should be considered in the former research. For example, in the Study on Repair Methods using CFRP for Corroded Steel Girder Ends, Dai Wakabayashi et al. They found that the bottom ends of CFRP were not necessarily anchored on the lower flange. The expected improvement effect is sufficiently obtained. However, the anchoring part prevented additional corrosion attacks in the same region.

This experiment tried to create the condition that imitated the out-of-plane behavior in the steel girder ends. The first experiment's corroded part or surface loss type adopted the severe damage condition. However, overall, the CFRP part survived under high-cycle fatigue loading (> 2 million cycles). The chance to observe the further durability effect of CFRP reinforcement increases the out-of-plane state in the specimen. The specimen's filler plate plays a vital role in realizing this condition. The elastic condition is still considered in this high cycle fatigue loading. In the following investigation, the out-of-plane behavior would induce the performance of retrofit members. The analysis of out-of-plane will support the rational layout of heavy vehicle position to evaluate the durability of reinforcement members through validation of numerical calculation. The higher natural frequency of the steel bridge could be combined in this experiment. The loss modulus of CFRP is proportional to the net energy dissipated per cycle and thus can provide valuable information about the initial damage failure.

The specimen with 1 filler has a high vertical (S22) stress concentration but smaller transversal displacement (U1). Then, the specimen with 2 filler indicated opposite conditions. The bending moment was increased significantly due to eccentricity, and the peak of stress was reduced. The consequences of this scenario could be dependent on the frequency applied in cyclic loading

With increasing bending moment, the maximum local stress on the CFRP components is affected by the rigidity of CFRP under compressive-compressive conditions. This condition expects that the higher the bending stress, the smaller the local stress. Then, the damage initiation

could have occurred in the bending stress dominant. Moreover, the maximum transversal displacement value was increased from 0.04989 mm to 0.088258 mm or 57 % under (DL+LL) case.

- Bolt Connection

It was required in the connection joint that could hold the specimen parts (fixtures, filler plates, and specimen) in their positioned location. It should not trigger any potential displacement or excessive distortion under the compressive axial force. Bolt connection should be addressed to support and locate elements on overhanging in the set-up machine loading conditions. In addition, the axial force should be transmitted to the rigid section of the body specimen (in Figure 3.5(a)).

The bolt connection elements within the elastic region were based on elastic local stress deformation. Next, the connection was assumed to have a constant amplitude load fluctuation value independent of elastic deformation at the contact surface. Both fixtures were conducted with the axial compressive load. This bolt connection force remains constant and would not lose over time.

## 3.3 Fatigue Load Reproduction

. Determining the fatigue load with the local stress distribution reproduction method was necessary. The application of stress distribution to maintain the elastic condition due to cyclic loading is part of this study; to optimally design load and control the compact specimen under elastic regions. It has been the focus of considerable former research [23-26]. Many studies can be found using finite element model analysis in the literature. The degree of precision of the solution depends on how close the vertical stress of the two components was. Estimating vertical local stresses at any point in structure due to external vertical loadings significantly predicted displacement and deformation of the element target part. According to elastic theory, the simulation was conducted to observe the local stress distribution that will be matched with the CFRP retrofit girder end local stress distribution.

The result of local vertical stress of the retrofit specimen and retrofit girder ends were compared. To find the close local stress distribution, which will be chosen for further cyclic loading experiments. As mentioned before, the local stress of the retrofit specimen did not reproduce the retrofit girder end when the corroded girder end model was fully implemented in the retrofit specimen. In the first attempt, the local stress at the weld bead specimen was 0.695 MPa. This result was too far from retrofit girder end local stress (49.788 MPa). The retrofit specimen was simulated with 55 kN compression load. So, the next attempt should consider the local stress of starting point was close enough.

As displayed in Figure 3.6, the comparison of the local stress distribution of the specimen with retrofit girder end corrosion model and specimen with weld bead adjustment was shown. The idea was to smaller the weld bead dimension to increase local stress. So that the retrofit specimen's local vertical stress could be aligned with the local vertical stress of the retrofit girder end. In this attempt, the local stress point was 49.879 MPa increased for 55 kN compression load. If the weld bead was not adjusted, the local stress condition would not represent the retrofit girder end. The corroded weld bead dimension reduction was 4 times smaller than the weld bead of retrofit girder ends. The area section of the weld bead at the steel girder end was 47.39 $mm^2$, and the adjusted weld bead of the retrofit specimen was 11.74 $mm^2$. The simplification of calculation, the line of stress distribution of the retrofitted specimen was decided in the middle surface of a cross-section of the retrofit specimen.

Moreover, the type of weld bead was full penetration weld (V-grooves). This type of joint was selected because it allows a filler weld material to fill the entire joint gap of the specimen. Then, the fatigue effect possibility could be reduced at the specimen web and flange joint.

The display of “local plane stress” is presented in Figure 3.7. The value of local stress distribution was almost identic with the weld bead of retrofit girder ends. With numerical simulation, the weld bead's size could properly be designed based on the reproduction of local stress distribution. Determining the resemblance between local stress distribution shapes is necessary for shape-based structure reproduction. The shape distribution matched relatively simple work when remodeling an object or surface was required. The shape distribution comparison shall describe the dissimilarity between the retrofit sub-model steel girder end with cross beam (CB) bracing (case 2+gravity) and the retrofit specimen. The local stress distributions are fitted simply by using the trial load of the retrofit specimen and specifying the value of the local stress of girder ends. The primary key was the shape of the elastic stress distribution shown in Figure 3.7. Local stress distribution should be close enough to each other (retrofit sub-model and retrofit specimen) to generate the typical conditions. The local stress distribution of selected CFRP retrofit steel girder ends with cross-beam bracing is referred to in Noor & Tamura [12] result. It is discovered that the reproduction of live load case 2 and gravity (LL+DL) on the retrofitted specimen is equal to 55 kN ($P_{LL+DL}$) and dead load (DL) equal to 15 kN ($P_{DL}$).

The difference in specimen shape and girder ends occurred due to simplifying the girder end. The stiffener cannot be built into the specimen, considering the limitation of the fatigue machine itself. The consideration was necessary to reproduce the practical part.

## 3.4 Summary

The reproduction of loading conditions has succeeded in this chapter, and the parameters have been recognized. The method of reproduction of local stress distribution shape is one option to determine the configuration of compact specimen parts. Then the conclusions are drawn as follows:

1. The numerical result of the local stress distribution of retrofit steel girder ends (Chapter 2) and the retrofit specimen (Chapter 3) was successful. It was to determine the service loading value of the experimental conditions. The requirement parameters and reinforcement specification were followed to construct a novel compact specimen and new eccentric fixture parts. The reproduction process should start with understanding the retrofit specimen's target area dimension. Because, it is related to the specification of the fatigue machine, CFRP retrofit specifications, and girder end-loading characteristics. This study recognized a small portion of retrofit girder ends of the target part that can represent the severe region of CFRP retrofit girder ends. This new assessment method is important because it is simpler to apply and more cost-efficient than existing retrofit measures or using a deep steel girder model. The implementation of the new strategy was investigated. The method experimentally designed 441 mm of CFRP retrofitted specimen height (1/6 actual size). It was a simplified steel girder end model that subassemblies subjected to long cyclic loading. Moreover, the corroded area part of the specimen was designed small portion of the corroded girder end (50 x 50 mm). Here, it is shown that the proposed method can be applied to conduct the axial compressive load and bending mode simultaneously.

2. The influence of local stress distribution of corroded area was found in this study with certain parameter ($t_{sd} = 3\,mm;\ L_{sl} = 50\,mm$). Corroded length could increase the local stress at the undamaged part of the girder until 250 mm from the corroded web edge. Next, due to the girder height, the localized corroded effect on the girder ends will be dissipated at a sufficient distance.

3. The fixture parts contain several separate elements. Those elements are connected with a bolt to maintain the “pin” joint, which allows small out-of-plane displacement. The finite element analysis shows the local stress of fixture design below the allowable stress design $\sigma_{140} = 140\,\text{MPa}$. This method succeeds in using the resemble local stress method to determine the maximum load to represent the traffic load + self-weight (55 kN) and self-weight (15 kN). Both loads represent the compressive-compressive (C-C) condition at the girder ends. These compact specimen design parts have not produced a CFRP retrofit specimen bearing failure to date (elastic condition).

4. It can observe the consistency of local stress concentration at the corrosion web edge or transition curved (TC) from the retrofit steel girder end, and retrofit specimens are made. The change of weld bead dimension between them was also solved by adjusting the weld bead size. It was necessary to perform the relative stress value on the steel girder end. The starting point of local stress is necessary for this experiment. When the weld bead is not adjusted, each starting point's vertical local stress has a different experience value. The method of adjusting was to decrease the dimension of the weld bead specimen to gain higher local stress close to the girder end local stress. The reproduction of local stress for the fatigue experiment of this study became the main parameter to treat the specimen close to service conditions of the girder end.

## 3.5 References


[3.1] Nethercot, D. A. (1989). The design of bracing systems for plate girder bridges. Doboku Gakkai Ronbunshu, 1989(404), 23-34.

[3.2] Zhao, C., Zhou, Y., Zhong, X., Wang, G., Yang, Q., & Hu, X. (2022, February). A beam-type element for analyzing the eccentric load effect of box girder bridges. In Structures (Vol. 36, pp. 1-12). Elsevier.

[3.3] Lei, M. A., Linyun, Z., Shuqin, L., & Shui, W. A. N. (2012). Eccentric load coefficient of live load normal stress of continuous composite box-girder bridge with corrugated steel webs. Procedia Earth and Planetary Science, 5, 335-340.

[3.4] Gil-Martín, L. M., Šćepanović, B., Hernández-Montes, E., Aschheim, M. A., & Lučić, D. (2010). Eccentrically patch-loaded steel I-girders: The influence of patch load length on the ultimate strength. Journal of Constructional Steel Research, 66(5), 716-722.

[3.5] Graciano, C., & Uribe-Henao, A. F. (2014). Strength of steel I-girders subjected to eccentric patch loading. Engineering structures, 79, 401-406.

[3.6] Ghahremani, K., Walbridge, S., & Topper, T. (2015). Inhibiting distortion-induced fatigue damage in steel girders by using FRP angles. Journal of Bridge Engineering, 20(6), 04014085.

[3.7] Razzaq, M. K., Sennah, K., & Ghrib, F. (2021). Live load distribution factors for simply-supported composite steel I-girder bridges. Journal of Constructional Steel Research, 181, 106612.

[3.8] Tabsh, S. W., & Tabatabai, M. (2001). Live load distribution in girder bridges subject to oversized trucks. Journal of Bridge Engineering, 6(1), 9-16.

[3.9] Ahn, J. H., Kainuma, S., Yasuo, F., & Takehiro, I. (2013). Repair method and residual bearing strength evaluation of a locally corroded plate girder at support. Engineering Failure Analysis, 33, 398-418.

[3.10] NERI (Nippon Expressway Research Institute). 2015. Design and installation manual for upgrading of steel structure with the use of carbon fiber sheet. Tokyo : NERI

[3.11] Shimadzu Instruction Manual. Shimadzu Servopulser EHF-E Series. 2021.pdf

[3.12] Specifications For Highway Bridges Part II Steel Bridges Japan Road Association March 2012.pdf.

[3.13] Tohidi, S., & Sharifi, Y. (2016). Load-carrying capacity of locally corroded steel plate girder ends using artificial neural network. Thin-Walled Structures, 100, 48-61.

[3.14] Sharifi, Y., & Tohidi, S. (2014). Ultimate capacity assessment of web plate beams with pitting corrosion subjected to patch loading by artificial neural networks. Advanced Steel Construction, 10(3), 325-350.

[3.15] Nip, K. H., Gardner, L., Davies, C. M., & Elghazouli, A. Y. (2010). Extremely low cycle fatigue tests on structural carbon steel and stainless steel. Journal of constructional steel research, 66(1), 96-110.

[3.16] Khan, R., Khan, Z., Al-Sulaiman, F., & Merah, N. (2002). Fatigue life estimates in woven carbon fabric/epoxy composites at non-ambient temperatures. Journal of composite materials, 36(22), 2517-2535.

[3.17] Specification for Highway Bridge Part I Common Japan Road Association March 2012.pdf

[3.18] Ok, D., Pu, Y., & Incecik, A. (2007). Computation of ultimate strength of locally corroded unstiffened plates under uniaxial compression. Marine structures, 20(1-2), 100-114.

[3.19] Khurram, N., Sasaki, E., Kihira, H., Katsuchi, H., & Yamada, H. (2014). Analytical demonstrations to assess residual bearing capacities of steel plate girder ends with stiffeners damaged by corrosion. Structure and Infrastructure Engineering, 10(1), 69-79.

[3.20] Baumann, A., & Hausmann, J. (2021). Compression fatigue testing setups for composites—a review. Advanced Engineering Materials, 23(2), 2000646.

[3.21] Brunnhofer, P., Buzzi, C., Pertoll, T., Leitner, M., & Mössler, W. (2022). Fatigue strength assessment of TIG-dressed high-strength steel cruciform joints by nominal and local approaches. Welding in the World, 1-10.

[3.22] Chandran, S., Verleysen, P., Lian, J., Liu, W., & Münstermann, S. (2017). Design of an experimental program to assess the dynamic fracture properties of a dual phase automotive steel. Procedia engineering, 197, 204-213.

[3.23] Liu, Z., Guo, T., Huang, L., & Pan, Z. (2017). Fatigue life evaluation on short suspenders of long-span suspension bridge with central clamps. Journal of Bridge Engineering, 22(10), 04017074.

[3.24] Peyrac, C., Jollivet, T., Leray, N., Lefebvre, F., Westphal, O., & Gornet, L. (2015). Self-heating method for fatigue limit determination on thermoplastic composites. Procedia Engineering, 133, 129-135.

[3.25] Khalili, S. M. R., Shokuhfar, A., Hoseini, S. D., Bidkhori, M., Khalili, S., & Mittal, R. K. (2008). Experimental study of the influence of adhesive reinforcement in lap joints for composite structures subjected to mechanical loads. International Journal of Adhesion and Adhesives, 28(8), 436-444.

[3.26] Vassilopoulos, A. P. (Ed.). (2019). Fatigue life prediction of composites and composite structures.

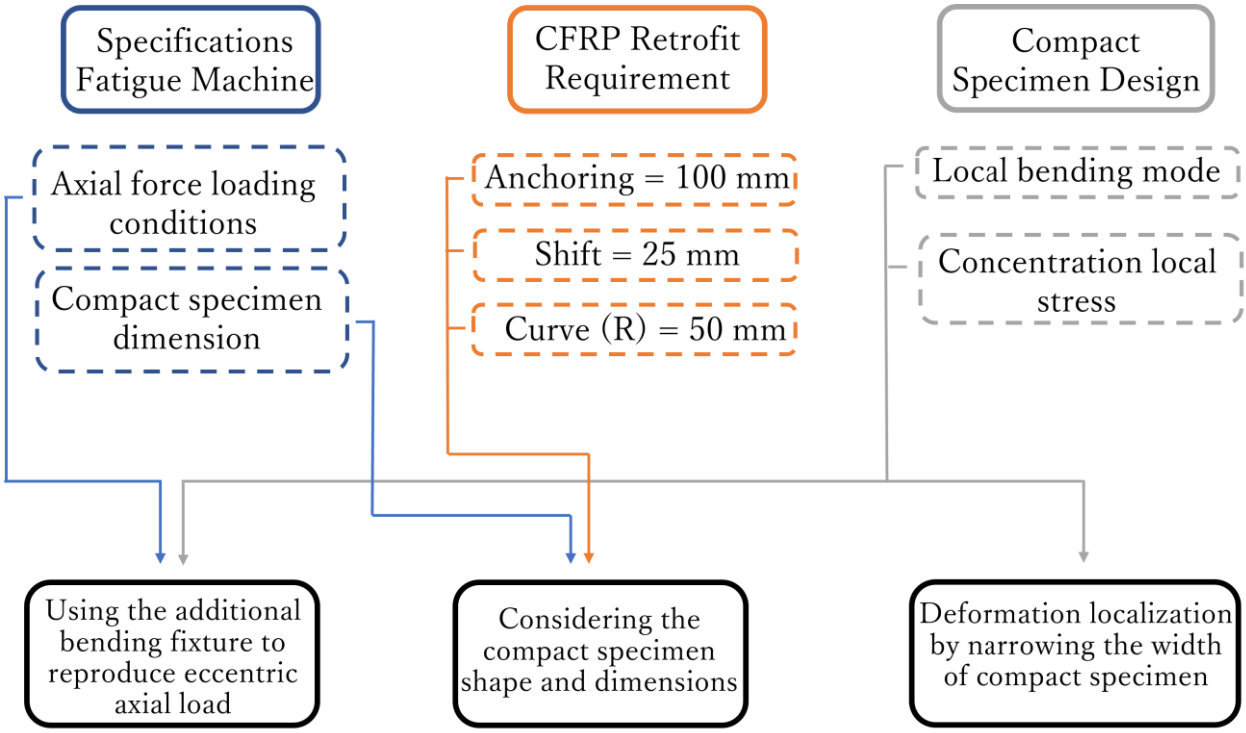


**Figure 3.1** Schematic figure process of specimen idealization

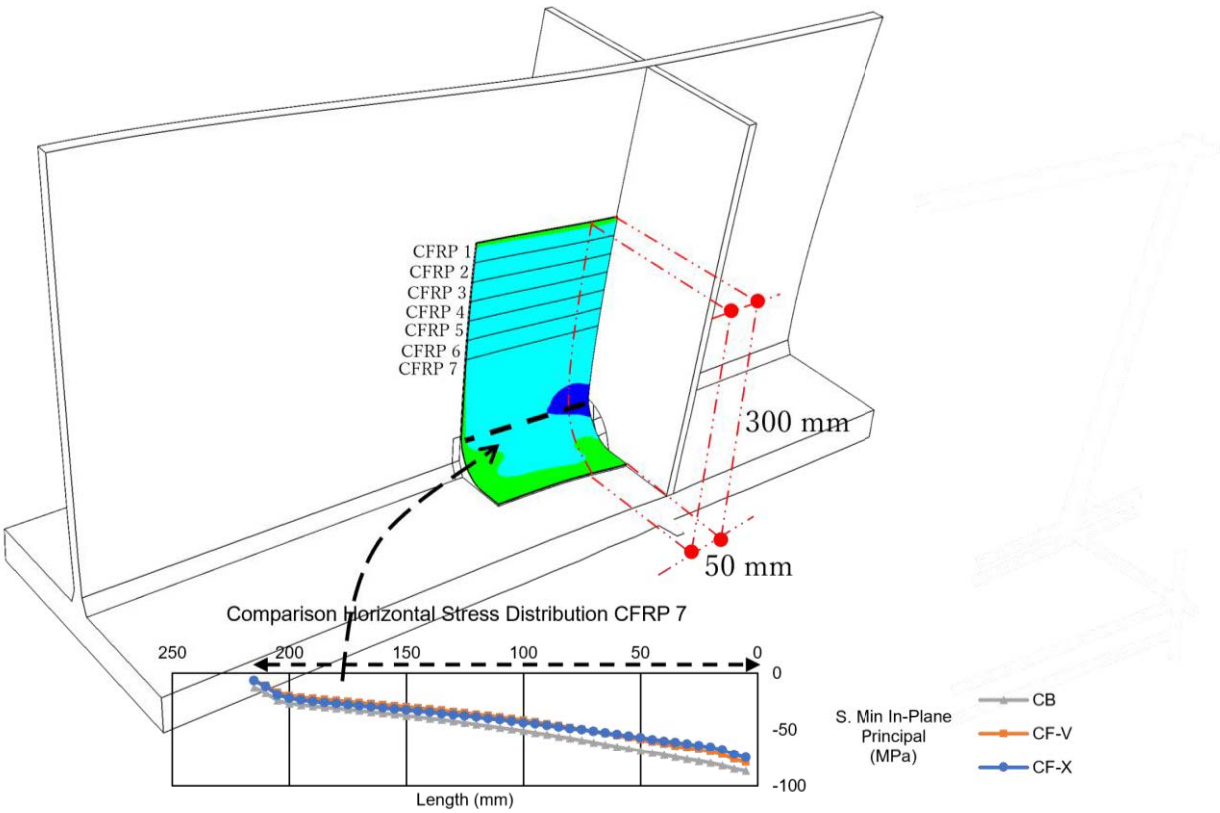


(a)

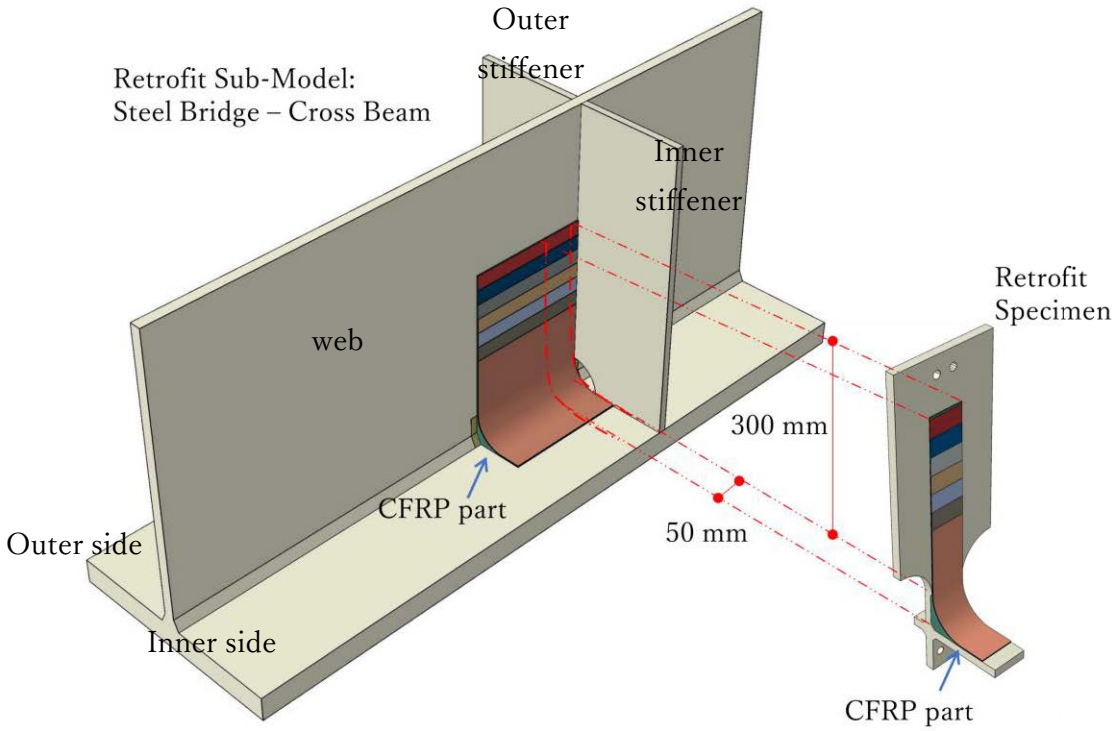


(b)

**Figure 3.2** Idealization of compact specimen dimension. (a) comparison of local horizontal stress of S. Min In-Plane Principal of CFRP 7th layer; (b) Specimen dimension determination from retrofit sub-model girder end.

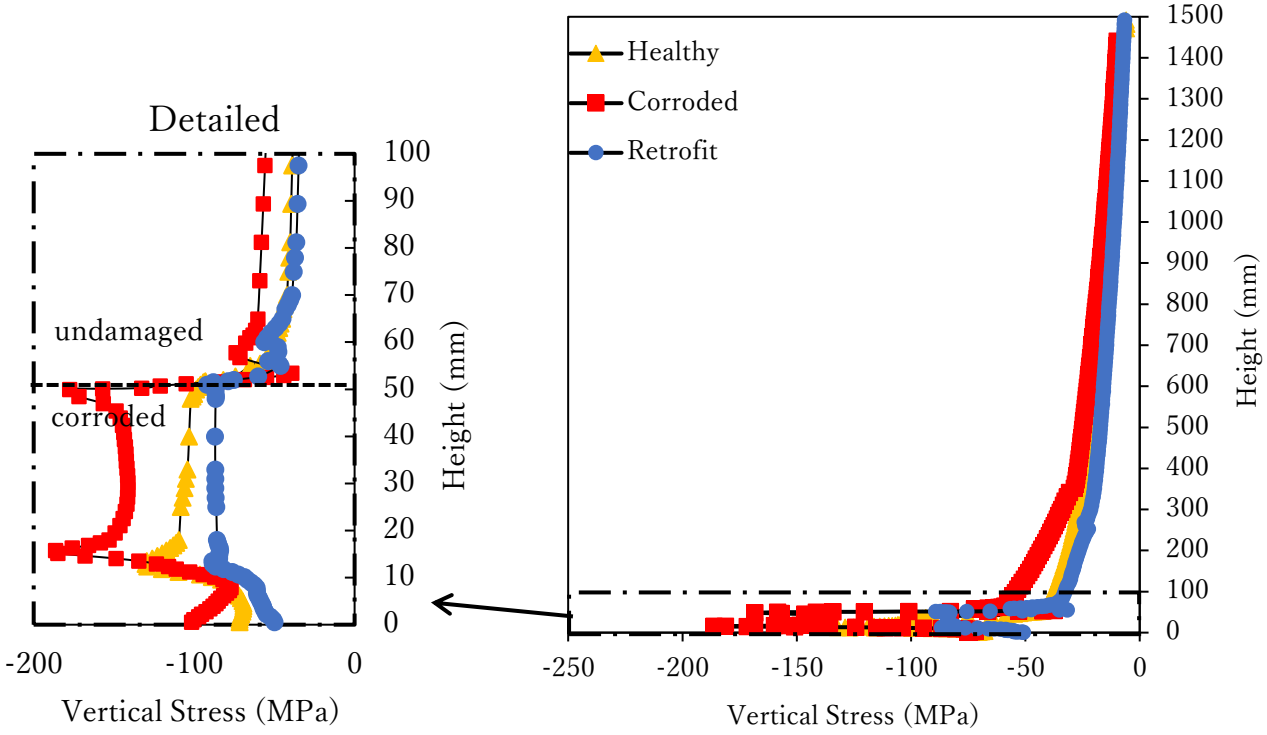


**Figure 3.3** Local stress distribution (CB) of corrosion effect on undamaged region

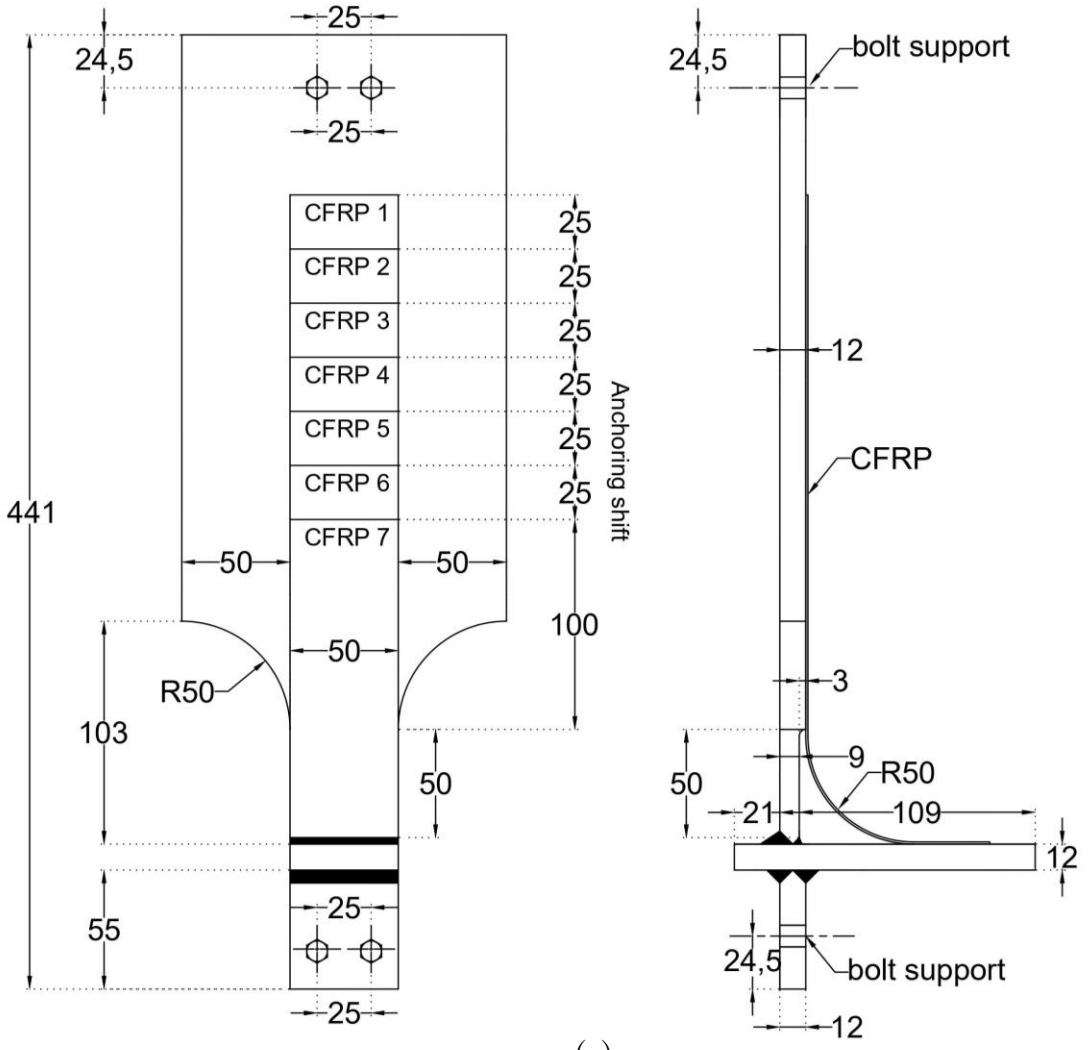


(a)

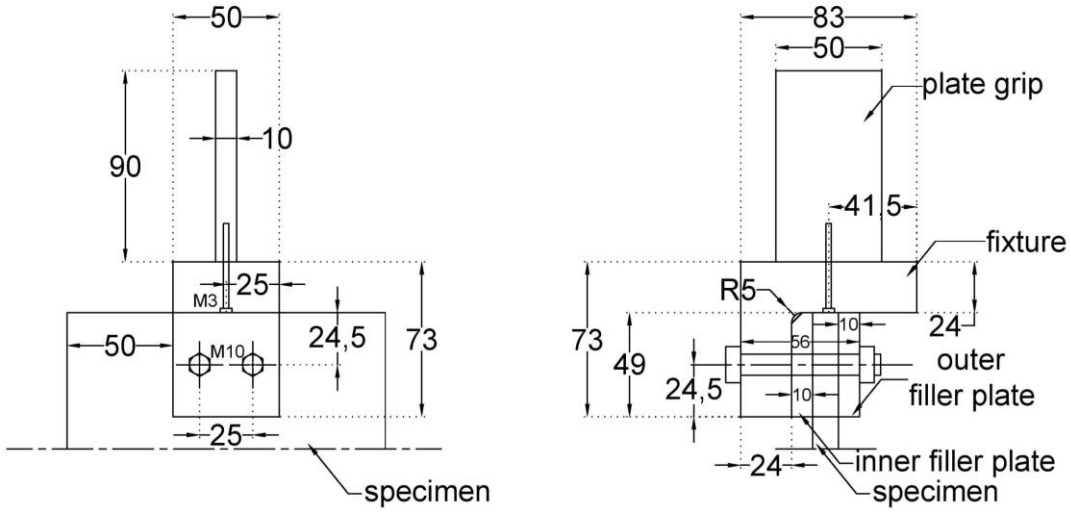


(b)

**Figure 3.4** (a) Compact specimen design; (b) Eccentric fixture part -upper section. (unit: mm)

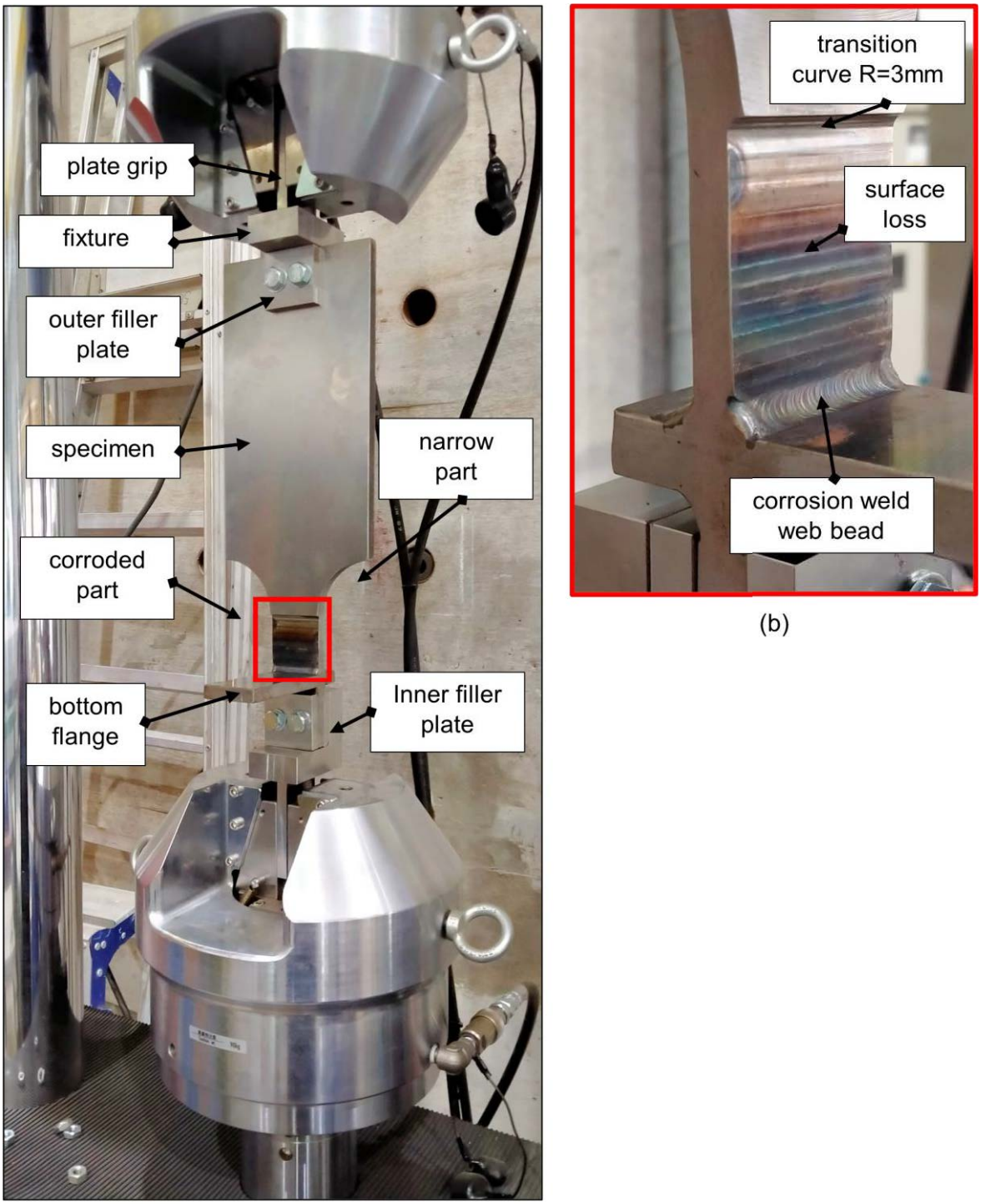


**Figure 3.5** (a) Setting placement of specimen before CFRP retrofit; (b) Detailed artificial corrosion part

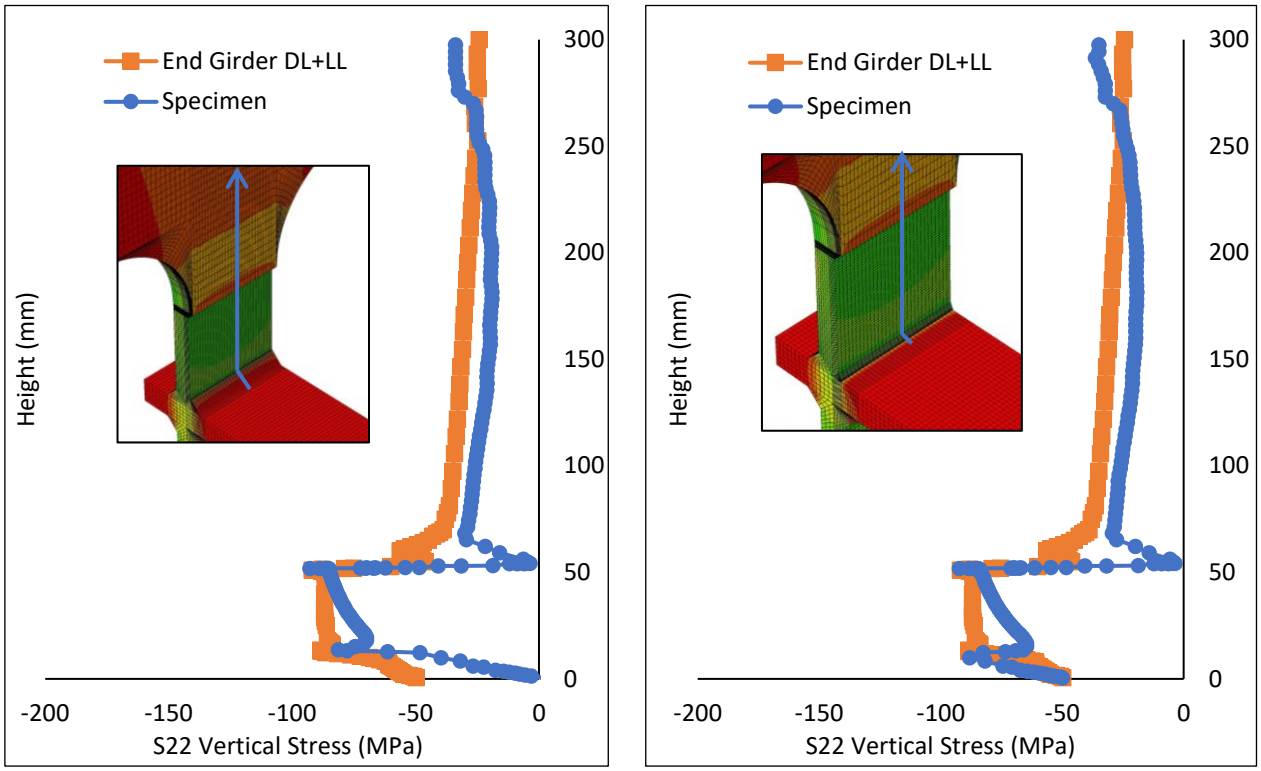


**Figure 3.6** Local vertical stress (S22) distribution comparison of sub-model retrofit girder ends and specimen. (a) original girder end weld; (b) adjustable weld bead

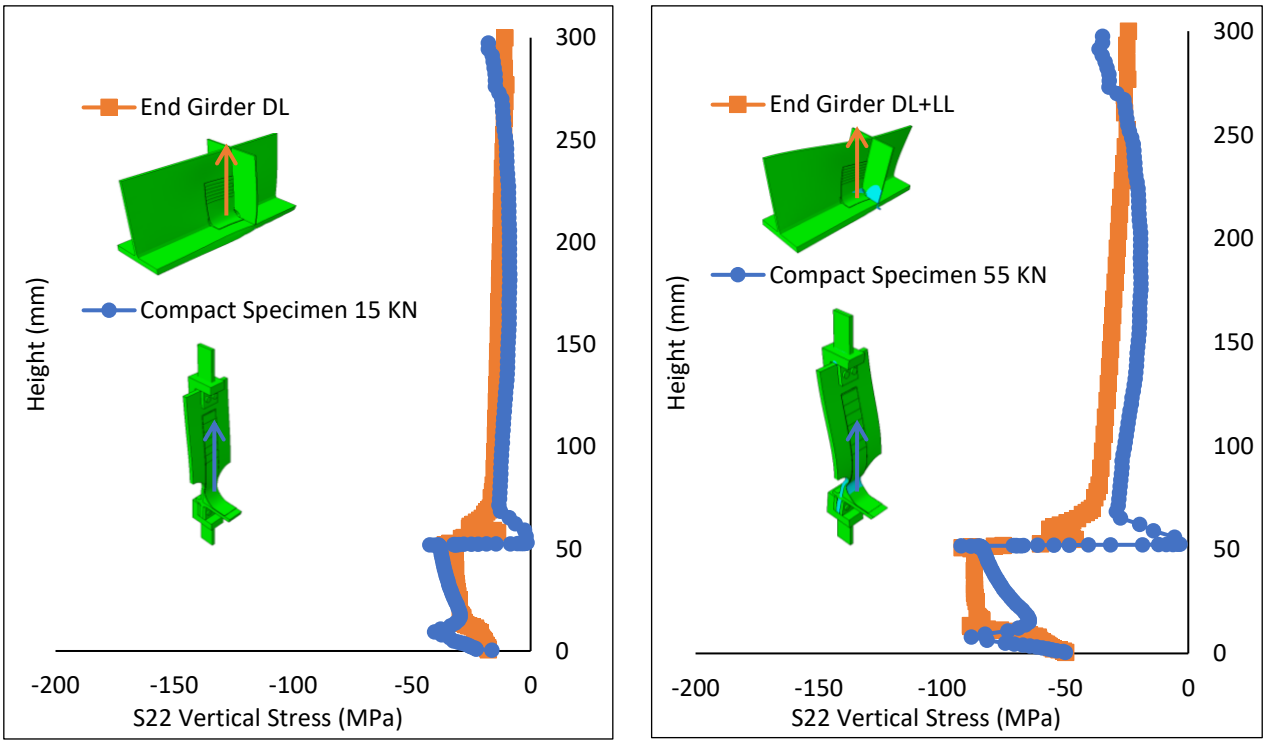


**Figure 3.7** Loading reproduction: (a) dead load (15 kN); (b) case 2 live load + dead load (55kN)

# Chapter 4

# Fatigue Durability Observation of Steel Girder Ends CFRP Reinforcement Specimen

## 4.1 Principle of Durability Assessment

For better performance and strength of retrofitted steel bridges, the CFRP reinforcement work must be assessed to predict fatigue life. Simply supported steel bridges are generally exposed to low amplitude loading by usual traffic conditions. As a result, bridge members mostly experience high-cycle fatigue (HCF) damage. Consequently, the girder ends retrofit part should have resistance in two aspects:

1) The low-stress amplitude under high-frequency becomes effectively determined by the microstructure strength level.
2) The localization of stress concentration of the CFRP retrofit part should be recognized.

It has long been established that a novel technique approach is necessary for evaluating and understanding the long-term durability limit for CFRP reinforcements. This study realizes the significance of durability issues in developing an experimental method to evaluate the local stress distribution in CFRP reinforcement for steel girder ends. The damage initiation variable is based on a difference in stress range equivalent to counting the influence of proportional loading. Additionally, the potentially damaged regions for retrofitting part of the girder ends would develop rapidly in fast-decreasing due to constant stressing in the long loading run. Then, accumulation of repeated modes leading to a dominant critical local concentration stress of the component would be considered as initiated of damage stage.

At low-stress amplitude, the fatigue life was dominated by damaged initiation, which leads to extended fatigue life. In contrast, damage propagation dominates at high-cyclic loads [1]. The author identified the regions in the fatigue life of CFRP reinforcement as stable damage growth (SDG) regions in which visible damage has been visualized and formed. The damage was growing slowly by constant-amplitude load fluctuation. Consequently, it demanded the fracture mechanics concept to bring the relationship between the damage variable and the cycle numbers established through an experiment [2,3,4,5]. Fan et al. also proposed repairing steel girder end corrosion using ultra-high-performance concrete and evaluating the fatigue life of damaged steel bridges. They proposed that the traffic load cycle should be associated with the highest cycle frequency for severe fatigue history. Moreover, they also considered the interval $i$ time of traffic loading, which is not capable in this research method [6]. Miyakoshi et al. found that in the tension-tension ($T-T$) high-cycle fatigue test, there is the possibility of stress threshold for transverse crack initiation with CFRP $(90)^{\circ}$ about $40-50\ MPa$ [7]. Then, from their result, the CFRP fatigue life can be predicted in the low-stress condition. Backe et al. found the fatigue life of CFRP due to first damage appearance at about 30% of the lifetime of failure. They explored fatigue behavior with various frequencies to obtain the target lifetime evaluation. In addition, the types of damage, such as crack

and delamination at CFRP, interacted [8]. The practical evidence was delivered from Kasra et al. experiment. They assessed the CFRP-repaired welded joints of the bridge due to distortion-induced fatigue life. Using a highly flexible adhesive, they applied the hot-spot stress method to estimate the fatigue life [9]. Finally, few researchers have tried to achieve the closest actual fatigue life condition to implement their result, especially in the steel bridge CFRP retrofit field. That was particularly important. Because there was no fatigue detail category for the steel-CFRP reinforcement part, the classification method (S-N) cannot predict its fatigue life. Then, the fatigue life analysis of this study is subjected to fill this gap.

Among mechanical and thermal properties of CFRP, it was sure which may be affected by fatigue damage, degradation of stiffness, e.g., detachment or delamination. It became one of the preferable indicators to specify the durability of structures. It is relatively simple to assess and has been well-correlated to accumulated damage in various load cases. CFRP damage typically experiences three-stage degradation in a rapid-slow-rapid path for CFRP under high-cycle fatigue loading [10-13]. Hagaragi et al. found that the damage initiation stage is more complex than the propagation and failure stages over many repetitive loads. The initiation period relies upon a few parameters, e.g., geometrical, loading, and stress concentration [14]. Most researchers showed that the CFRP part damage initiation period was detected due to fatigue cases occurring within a short period. Then, the corresponding CFRP reinforcement part under the damage initiation process, which accumulated during the component's service life, should be significant, and thus it is worth investigating.

Fatigue damage in the entire fatigue life is governed by the number of fluctuations in stress rather than maximum stress at some point; hence the stress amplitude $\sigma_a$ or stress range $\Delta\sigma$ and mean stress $\sigma_m$ are the most significant parameters in a fatigue life assessment. In practice, observation of constant stress-cycle series in the component's fatigue life is given to detect fatigue damage of CFRP retrofit part early.

The present experimental study was constructed to give adequate data to determine the dependence of CFRP fatigue durability by observing the damage initiation type. This objective can be explained based on elastic response over cycles. Therefore, the damage initiation response should remain essentially elastic even with the cyclic-fatigue stress producing a decreased CFRP part elastic modulus.

The range of stress can be established in terms of local stresses. Notably, various directional stress components can be used. Implementing vertical stress from the actual vertical stress of the target structure (steel girder ends) was recommended as full-scaled local stress distribution. Thus, this approach, known as the reproduction of local stress distribution explained in detail in Chapter 3. Moreover, only local shift stress must be selected as the fatigue limit for fatigue life analysis, particularly the cycle counting process. However, this is only meaningful in some instances when

the visual damage appears appropriately. The peak or valley in fatigue-cycle counting could be damage detected signal which typically contains local damage at the target point. By verifying for each cycle point whether a small local shift stress could indicate micro-damage growth. Hence, the fatigue life of the retrofit specimen should be expected to dominate by bending mode (mode I), driven by the eccentric axial load.

According to the experiment parameter, the damage initiation should be identified as the first damage nucleation in the out-of-plane CFRP part axis. However, the damage characteristics of initiation could be defined at different degrees, from microscopic to macroscopic observation levels. Since the stiffness degradation is a property of the durability parameter, the damage initiation is intensive to identify. Thus, this research proposed a new parameter related to the practical definition of CFRP damage initiation: "the period required to produce damage into visible size. This approach has a more sensitive method for monitoring and capturing CFRP structural degradation through damage initiation. Moreover, it was expected that damage initiation would occur within a short period corresponding to the actual separation or detachment of the reinforcement part in the specimen.

## 4.2 Experimental Setup

An upgrading method involved impregnating the resin to the carbon sheets. A carbon fiber-reinforced polymer (CFRP) was formed at the site to integrate the existing damaged steel structure that may be easily manually constructed. Various experiments, e.g., from Wakabayashi et al.; Miyashita et al.; Hidekuma et al.; [15,16,17], have confirmed the ability to 1) reduce stress and 2) increasing bearing buckling load increases with the amount of the fiber sheets. Therefore, the amount of CFRP sheets to be placed should be determined according to the amount of cross-section loss. This study provides the configuration of bonding layers of the method based on the Nippon Expressway Research Institute (NERI) [18]. Also, applying a polyurea resin of the highly expansive elastic putty to bonding layers suppresses the separation or peeling of CFRP. It is expected to improve the durability even in high vibration, the detailed sequence shown in Figure 4.1. The effect of the resin (FR-E9P) on the tensile rigidity of the entire CFRP is only around 5% because the elastic modulus of resin is less than 1/100 even though the volume of resin occupies 70%-80% of the carbon fiber. Therefore, only the cross-section area of the carbon fiber should be used for the calculation and analysis of CFRP.

As stated above, the CFRP sheet should be oriented so that fibers are aligned vertically: the same direction of principal stress in the web plate ends subjected to the reaction force. Since a girder web ends under reaction force dynamically defined as members subjected to an axial force (compressive force). Then, using the value of allowable compressive stress in "Design Manual II

11.5.2" ($\sigma_{140} = 140\ MPa$) was to control the load capacity of the retrofit specimen should be less than allowable stress.

### 4.2.1 Putty (FU-Z) Configuration

The highly expansive putty is applied to bond the steel plate to CFRP to prevent debonding between CFRP and the steel under high stress or buckling deformation. It also transfers stress properly from the steel of the fiber. Therefore, the thickness of putty plays an essential role in obtaining the required reinforcing effect. Miyashita et al. [16] The expected value of the minimum design thickness of putty (FU-Z) 0.8 mm is set and does not exceed 1.5 mm. Moreover, this study challenged the utilization of putty in compressive-compressive (C-C) high-cycle fatigue conditions to assess the elasticity of putty characteristics, as putty is low strength material with high-elongate capacity.

Former research from Wakabayashi et al. [15] studied the polyurea putty effect in buckling deformation. They found that the maximum load using polyurea putty is not significantly different from that without it. However, the polyurea putty retains the load from suddenly dropping when the displacement exceeds 45 mm. Then, the putty can help prevent debonding and improve flexibility in the CFRP reinforcement attached to the steel.

Further, Hidekuma et al. [17] determined that the thickness of adhesive layers without polyurea putty should be calculated using the following Equation 4.1.

$$h_e = \frac{t_p - t_s}{2} + \frac{1}{3}\left[\frac{t_c - t_p}{2} - nt_{cf}\right] \tag{4.1}$$

Where $h_e$ is thickness of adhesive layers, $t_p, t_c$ is the thickness of the specimen after primer coating and CFRP bonding, $t_{cf}$ is thickness of carbon fiber, and $n$ is the number of layers. Then, their research was attempted for no putty cases. They designed the material substitution with epoxy primer (FP-N9) and impregnation epoxy resin (FR-E9P). It was thicker by adding 1/3 of its initial thickness to avoid the significant error of stress concentration to epoxy primer as the first layer. However, their approach is capable in flat steel plate specimens, e.g., coupon specimens or corroded flange. Then, this study proposes a different approach in the specimen with no putty case, considering the degree of field application.

In the case of the specimen without polyurea putty (FU-Z), increasing the curve dimension in the anchoring place is possible. In the typical case, the curve (arc-like shape) $R = 50\ mm$ , placed at the weld bead joint as a countermeasure against corrosion. Therefore, epoxy putty (FB-E9S)

modulus elasticity was 4021 MPa, higher than FP-N9 and FR-E9P. It is more reasonable and practical to maintain the dimension of the curve to produce the inertia capacity against cyclic loading in a specimen without putty. The simple concept is to replace the flexibility of polyurea putty with more stiffness from epoxy putty under specification. Then, the curved of the specimen with putty decreased a little. The aligned linear dimension of epoxy putty in the specimen without putty was 25 mm. The specimen with putty was 21.5 mm, as shown in Figure 4.2(a-b). The polyurea putty was visible from the side view due to the attachment process, as shown in Figure 4.3(b). Finally, to construct the idea, a slight assumption was given. If the utilization of polyurea putty is neglected, then the CFRP would delaminate or detach due to incapable of keeping pace with the out-of-plane deformation of steel (bending mode case) if the damage initiates (debonding or detachment) under no putty CFRP configuration more than 2 million cycles. Then creating flexibility as a component for stress transfer of the steel CFRP retrofit component could be reconsidered. However, we can maintain the usage of polyurea putty material if the situation is conversely.

### 4.2.2 Frequency Determination

The natural frequency of the simple-span bridge structure is typically revealed by the residual vibration which remains after the load (vehicles) has left the span. The first vibration (bending mode) was predominant in all experiments performed. The following discussion was limited to considering this mode. While the live load is on the bridge span, the frequency of vibrations is generally not the bridge's natural frequency. From that point, it indicates that it is a force rather than a free vibration. It is assumed that this forced vibration is caused by the vertical oscillation of the vehicle mass on the bridge structure system. As a result, the forced vibration is most significant than the natural frequency of the structure. Referred to John M. Biggs et al. [19], the vibrations of the simple-span bridge with different span lengths are compared. These records of measurements depend upon the roadway's roughness, type of vehicle, and speed of vehicles. Then, the records can be interpreted in this fatigue experiment because of the actual condition appearing in the accelerations trace. In conclusion, due to the requirement of frequency input of cyclic loading in the fatigue experiment machine, the probable value was determined by simple-span bridge vibration field measurement.

The simple-span steel I girder bridge structure in field measurement was almost similar to the target bridge. It was the Gilbertville bridge, with a span length of 34 m compared to its target span of 40 m. These actual vibrations were not constant across the span, so the assumption length of the span contributed to the vibration associated with truck speed was generalized. Also, the 1$^{st}$

mode of natural frequency is strongly related to the span length of the bridge. Considering the result leads to a conclusion regarding the amplitude and frequency characteristic of CFRP-steel retrofit structure durability due to the type of vehicle and vehicle speed. The study adopted the 4 Hz vibration. Then, the records can be interpreted in this fatigue experiment because of the actual condition appearing in the accelerations trace. In conclusion, due to the requirement of frequency input of cyclic loading in the fatigue experiment machine, the probable value was determined by simple-span bridge vibration field measurement.

### 4.2.3 CFRP Modeling of Specimen

The study determined the load proportion of the cyclic experiment. The determination of cyclic load on the specimen was based on reproducing the local stress distribution method between the retrofit steel girder end and the retrofit specimen. Chapter 3 (3.3 Fatigue Load Reproduction) described a detailed discussion regarding this method. The finite element model of the retrofit specimen was constructed and then subjected to compressive loading in simulation. Referring to Nippon Expressway Research Institute (NERI) [18], the elastic modulus of the material of each element was conducted. For Epoxy Primer (FP-N9) $E = 2533$ MPa; Epoxy Putty (FB-ES9) $E = 4021$ MPa; Polyurea Putty (FU-Z) $E = 65$ MPa; CFRP-resin (FR-E9P) $E = 640000$ MPa; Steel $E = 210000$ MPa. As shown in Figure 4.4(a-c), the C3D8R element was applied for the rest of the elements except the CFRP part to capture an accurate stress concentration in a small mesh. However, CFRP thickness is small, 0.143 mm per layer. Then S4R element is applied with the fiber orientation for the general shell layer. The element joint was modeled as a monolith (tie constraint) with various material properties to support a simple attaching element.

### 4.2.4 Experiment Loading Strategy

To perform a durability experiment in fatigue, uncertain parameters, e.g., temperature and creep, should be clarified first. This study provided experimental conditions and measurement methods to accommodate the field conditions of the CFRP reinforcement component. Figure 4.5(a-c) presents the loading strategy to reproduce a state close to that fatigue experiment. The room temperature (ambient) experiment was set up near the testing machine used in the fatigue experiment. The temperature experiment aimed to observe the relationship temperature difference of the CFRP reinforcement part. Then, the effect of temperature changes on CFRP during cyclic loading could be clarified. Next, the creep experiment aimed to understand the amount of strain change caused by creep deformation that occurred in each part of the retrofit component under

constant load conditions. Because the durability experiment consists of extended time, this parameter should be clarified before the cyclic loading begin.

This experiment attached the strain gauge on the CFRP surface with a selected similar arrangement of each retrofit specimen, as shown in Figure 4.5(b). This study adopted four points of strain gauge on the CFRP surface. The selection of strain gauge points was based on specimen numerical analysis for high local stress locations on the CFRP. A thermocouple type T-G-0.65 from Tokyo Measuring Instrument was utilized. Moreover, the strain gauge type BFLAB-2-3-3LJCT-F for composite material (CFRP) manufactured by Tokyo Measuring Instrument adhered with an epoxy-based long-term measurement adhesive EB-2. The strain gauges were attached at the exact four locations as in the fatigue test (strain gauge 1, etc.), based on numbering in Figure 4.5(c). Two thermocouples were installed between the strain gauge attachment positions to generate a local temperature change of CFRP components.

The total strain ($\varepsilon^{Total}$) was developed from cumulative strain in the specimen. Then, the author also conducted a simple formula to generate or filter the mechanical strain ($\varepsilon^{M}$), as shown in Equation 4.2. The purpose of focusing in $\varepsilon^{M}$ is the geometric measure of deformation can represent the relative displacement between retrofit components in the material body.

$$\varepsilon^{M} \quad = \quad (\varepsilon^{Total} - \varepsilon^{creep}) \tag{4.2}$$

Where $\varepsilon^{Total}$ is total strain, $\varepsilon^{M}$ is mechanical strain, $\varepsilon^{C}$ is creep strain. The experiment used a fatigue machine, EHF-EV200k1 (a dynamic fatigue test system manufactured by Shimadzu Corporation). It applied a compressive load of 55 kN as a preload to fit the jig and fixtures in the same way as in the fatigue loading. Then, the loading maintained a compressive load of 15 kN as the minimum value (self-weight) during the fatigue test for 3 days and attached the strain gauge. The creep strain of the part was measured. The strain gauge was attached at the same position as the cyclic load, and the measurement was continued at a sampling rate of 0.1 Hz.

### 4.2.5 Self-weight reproduction experiment

Then, the local strain on the retrofit specimen should be saturated under isotropic pressure of self-weight before applying cyclic loading. The focus of the measurement was to make the strain saturated on the selected load (15 kN). The creep experiments were carried out at room temperature. Since no creep rupture was observed in this condition, the strain-time relationships are considered in two stages, as presented in Figure 4.6(a). In the first stage, the strain increased

following the saturated process of the fiber and resin for 1 day. Then, the creep strain rates slow down constantly, which is stable for an extended period in cyclic load. An elastic elongation mechanism was developed due to the compact specimen design under constant load to clarify the retrofit specimen's target location and deformation mode. In Figure 4.6(b), the creep strain at SG 3 - SG 4 is higher than SG 1 - SG 2. So that indicates the influence of vertical force acts perpendicular on the retrofit specimen is more severe at the transition curve (TC).

### 4.2.6 Temperature experiment

Next, the temperature strain experiment was conducted at 20°-30° Celcius. The purpose is to ensure temperature contribution due to free strain on the CFRP part. The first changes of temperature strain were based on the CFRP resin hardening process of the retrofit specimen without putty. Next, the dependence of thermoplastic behavior on the completion elastic modulus of CFRP reinforcement is compared and plotted in Figure 4.7. The heat from the hardening process influenced the raising of thermal strain for one day. Then, free thermal strain is expected to act on the elastic modulus change corresponding to the hardening process. The hardening process effect in ambient temperature is found to be independent for case room temperature around 20-30°C. However, this measurement reveals that the room temperature voltage change from the specimen was recorded as an observed strain change and plotted against temperature. The temperature change range is almost constant (±2°C) due to the completion of the hardening process. If the temperature range is small, the room temperature change is independent of CFRP parts. It is observed that the effective temperature strain was independent of the level of elastic strain, which defines the internal thermal activation. Measurements were taken every 30 seconds and continued for three days in the fall season.

The coupling strategies between creep and room temperature experiments were conducted. Next, the relevant condition of the loading strategies is proposed in Figure 4.8. The free thermal properties of CFRP material could be independent. Therefore, the creep strain was inducted into cyclic loading as a reference. The experiment was performed using the fatigue machine described before. The compression load with sinusoidal waveform is repeated at 4 Hz, as seen in schematic Figure 4.8. Also, the cyclic data will collect every 10.000 cycles. To apply the cyclic load of more than 1 million cycles is required 2 days or more at the shortest. The cyclic loading decided to stop at 3.5 million cycles that spent 10 days long. Then, strain measurement was performed intermittently so that the deformation of the retrofit specimen could be grasped in units of 10.000 cycles. The axial cyclic loading and loading point displacement were measured at a sampling rate of 100 Hz. The high-cyclic fatigue loading will continue until the damage initiation appears

visually. Then, the 1-2 points strain gauges are developed to discover the curve part's stiffening effect in the number of repetitions in fatigue loading. The local stress of the curve part should be monitored as a countermeasure of corrosion. Also, this curved part has various fiber alignments due to anchoring specifications and the thickest epoxy putty (FB-E9S), which the fatigue characteristics have not been discovered yet. The 3-4 points are designed to assess the high-stress concentration fatigue effect in the steel part due to the shifting thickness of the corroded steel part.

## 4.3 Experimental Results and Observations

Detachment and delamination are CFRP damage types that are difficult to inspect since they were concealed. Therefore, this study succeeded in using a strain gauge to detect the detachment under cyclic loading and support it with visible damage verification. Even so, destructive observation was developed to determine the delamination characteristics of CFRP reinforcement. The CFRP-retrofitted specimens (with putty and without putty) were high-cycle fatigue tested under a constant compressive load range $\Delta P = 40$ kN. The local stress of 4 points strain gauge at the CFRP part from all specimens was measured. The local stress at the curve part (SG1 & SG2) was approximately half smaller than at the transition curve (TC) (SG3 & SG4). These phenomena also support the finding from the previous study by Noor and Tamura [20]. The local stress at the CFRP transition curve has a higher value due to the transition zone of the corroded region to the healthy region. The condition is that the curved part should be installed together. The difference in local stress at each point provided a linear response to determine the severe location of CFRP reinforcement [21-23]. Then, the target investigation to maintain the elastic stress of the CFRP part in the current method is satisfied.

CFRP steel-reinforcement damage observation experiences three stages of degradation in a rapid-slow-rapid path for CFRP under high-cycle fatigue loading. Fatigue damage in the entire service life is governed by the number of fluctuations or cycles load in local concentration stress rather than maximum stress at some point; hence the constant local stress amplitude ($\sigma_a$) and the number of cycles ($N$) are the most significant parameters in a fatigue durability assessment. In the experiment, the cyclic local stress at the CFRP part from the specimen with polyurea putty and without polyurea putty (FU-Z) was almost similar. The difference of local stress from all point strain gauge positions was approximately not exceeding 5 MPa, even though the component of the retrofit specimen is different. This study found that using polyurea putty (FU-Z) was insufficient to decrease local stress concentration in elastic conditions. However, FU-Z will increase the flexibility against out-of-plane deformation (300%-500% elongation) in long cyclic numbers to

prevent the damage initiation of the CFRP reinforcement part. This experiment shows a limited deformation of viscoelastic material under constant amplitude fluctuation load.

### 4.3.1 Detachment Characteristics

Detachment is one of the damage initiation types of CFRP-strengthened steel. At the time of constant load, joint polymer particles separated due to the mode direction. The characteristics of damage initiation in the detachment of specimen no putty were rapidly recorded as a function of time. From the experiment specimen without putty, the detection of damage initiation is possible by using shifted local stress $\sigma_{SLS}$ characteristics. It indicated the change in micromechanics due to fatigue. Since the $\sigma_{SLS}$ was achieved by the separation of joint bonds perpendicular to the stress direction. Totally modulus elastic of CFRP holds a constant local stress level for an extended cyclic load. Also, it immediately dissipated a shifted local stress. It returned to the initiation stress level, while the modulus elastic of joint material transformed with time.

The separation of the joint bond due combination of local vertical stress and out-of-plane mode at specific cycles achieves the characteristic of detachment that occurred in the specimen without putty. The damage initiation stress signal was detected only at SG3. Moreover, the effect of rapid deformation of the detectable detachment was visually confirmed. The comparison of durability observation in local stress measured from $2.5x10^6 – 3.5x10^6$ cycles is shown in Figure 4.9. When the joint material was suddenly deformed by the influence of a long period (3 million cycles) of eccentric cyclic loading, the shifted local stress ($\sigma_{SLS}$) The elastic joint shall be the “impact during cyclic stress” behavior, even though the stiffness was not changed immediately or delayed, as shown in Figure 4.9a-2. The sudden change of local stress only detected at the surrounding location of strain gauge three was observed as a stress redistribution phenomenon due to the CFRP joint's separation. The shifted local stress was correlated to releasing the joint's modulus. This parallel arrangement of modulus elastic of each material's properties can be caused by a constant eccentric cyclic load effect. As there is no possibility it occurred independently. After the local area of joint material separated, the CFRP modulus elastic could be immediately returned to its initial condition. Because the local stress redistribution of detachment occurred in a short period, that indicated the impact stress during cyclic loading has been completed. So, the contribution of CFRP's high modulus elastic (640 GPa) could prevent the damaged part from losing its stiffness in the following cyclic loading. However, the detachment phenomena must be understood not only in geometrical findings only. The cyclic load amplitude was low but sufficient to influence the CFRP reinforcement structure material. It may result from a lack of flexibility in the specimen without polyurea putty (FU-Z) that exceeds earlier local fatigue durability damage. Otherwise, as

displayed in Figure 4.9b (1-3), the application of FU-Z could be stabilized the performance of the target retrofit part thanks to excellent elongation characteristics. The local stress of the specimen with putty is still linear in local stress data measured with the same cyclic level. The additional finding showed that the 1.05 mm thickness of FU-Z had a great response to durability performance, supporting the CFRP strengthening method solutions.

The reversible elastic local stress in compression (C-C) fatigue loading generally shows an elastic recovery of each detach damage. There are four shifted local stress ($\boldsymbol{\sigma_{SLS}}$) was detected in 3 million cycles. This initiation damage occurred between the urea primer (FP-UL1) and the CFRP resin (FR-E9P). In detailed Figure 4.9c the 1st damage detection was detected in 7 seconds long with 28 cycles (2991818 – 2991846). The one of cyclic stress was detected attached to the zero stress ($\boldsymbol{\sigma_0}$) which means no elastic modulus ($\boldsymbol{E_0}$) active. The cyclic impact effect was recognized where the elastic modulus consisted of bending stress concentration. In this investigation, CFRP material characteristics could be described as the control parameter after initiating the local damage. It was because it was required to improve the load capacity against eccentric cyclic compressive load when the CFRP part would damage due to that combination. The standard tensile strength value with aligned fiber direction is also specified as 1.900 N/mm$^2$ [16]. Then the separation of the CFRP joint has been proven not harmful to the CFRP part. The behavior of CFRP material can be adapted to the operating long cyclic load when experiencing initiation of detachment. The local damage characteristics of CFRP contributed as corroded steel reinforcement due to dissipating stress concentration and out-of-plane deformation in elastic conditions were discovered. Therefore, a specimen with putty indicated a strong bond of material. Also, as shown in Figure 4.9b (1-3), it can be interpreted that the fatigue life improvement of CFRP reinforcement by polyurea putty was related to the viscoelastic behavior. Using polyurea putty (FU-Z) is one of the factors that significantly improved the durability and strength of the reinforcement part.

Next, the effect of the long cycle ($\boldsymbol{N}$) showed that the interactions between cyclic fatigue and damage initiation are complex. These relationships are challenging to integrate into the service-life prediction model, as displayed in Figure 4.9(a-2) in 3 million cycles. The 2nd damage detection signal has different characteristics. It is received the decreasing of local stress 8 MPa, respectively. The element parts still have modulus elastic, so the detachment could not occur perfectly. The 3rd damage detection was detected in 9 seconds long, and it reached the zero stress ($\boldsymbol{\sigma_0}$). Which means that complete detachment occurred. The 4th damage detection was detected 11 seconds long and almost reached zero stress. The gap of local stress almost reached 2 MPa, respectively. All detachment process was detected in 31 second long with 124 cyclic damage loads.

The detachment process revealed the possibility of fully separating joint material in rapid conditions. From this result, the possibility of damage initiation detection could be less than 2% of total fatigue life. The strain gauge succeeds captured the initiation deformation mode of specimen no putty. The cyclic damage block was redistribution in a noticeably brief period.

In the final loading at 3.5 million cycles, the detachment characteristic showed a slight inclination of local stress. When the detachment is initiated, the progressive detachment will be defined next without an increase in compressive fatigue load. The inclination of local stress, as displayed in Figure 4.9(a-3), results from the slight out-of-plane displacement at the detached region. The instability of thin CFRP laminate due to detachment was measured as a change of local stress. The change of local stress during constant-amplitude cyclic-load fluctuation plays an essential role in determining the detachment effect after the initiation phase.

Moreover, it is also because the detachment slip maintains an elastic condition; the bond strength of the damaged joint transmits the residual stress to the effective bond joint area. It moves from the detachment plane toward the spread of the section. Also, CFRP part stiffness could be changed after half a million cycles.

### 4.3.2 Damage Visibility (Detachment)

The visible detachment location of damage in the specimen without putty was identified in this study. The location represented elastic stress concentration in the retrofit specimen. The joint Urea Primer and CFRP-resin separation was identified as damage initiation characteristics. The damage initiation was detected by visual inspection, as shown in Figure 4.10. It was only at the left side corroded web edge within the vicinity of the growth end. Thus, the elastic deformation in the corroded web was not uniform. This study confirmed this condition as “resin-rich zones” [24-26]. Then, The resin-rich zones are formed during the CFRP-resin construction process. The dry CFRP sheet is compressed in the wet resin (FR-E9P). This compression pulls the CFRP sheet close at the curve part for a bottom anchoring part, and a micro void could be formed between the CFRP joint and Urea Primer. A resin-rich zone is formed after the hardening process. Furthermore, the specimen's lack of flexibility triggers joint material separation due to the cyclic bending mode.

The detachment slit was measured at 2.02 mm, respectively, after the complete cyclic loading. Moreover, the length of damage growth at the upper side is about 14 mm, and at the bottom side is about 16 mm, as shown in Figure 4.10. After the joint separation, the damage could be growth in the matrix due to bending mode. It is because the high frequency of bending mode would reduce the strength of the matrix. The finding of potential damage location could be

recognized with particular conditions at the field. The top end of the corrosion part should be considered more. Detecting damage that occurs is not significant in destroying the retrofit part of the CFRP because this experiment maintains the fatigue in elastic conditions. It can be observed from Figure 4.10 that detachment during cyclic compression is dependent on the material treatment and stress concentration location. However, the visible detachment does not develop in a short period.

### 4.3.3 Interlaminar Failure (Delamination)

During the fatigue loading of the specimen without putty, a local stress ($\boldsymbol{\sigma_{LS}}$) concentration in vertical direction and magnification of detachment area created fiber–resin debonding condition. The process of forming internal delamination begins with the spreading of detachment. The delamination was detected after the end of the loading cycle (3.5 million cycles). To check the delamination process, cut the specimen under a specific point and use a microscope. To catch the micro delamination of the specimen. As shown in Figure 4.11 (a-b), the comparison of a cut section of the specimen with and without putty was observed. The strain gauge location (SG3) was considered to verify the strain result and visual damage. This study also verifies the contribution of the transition curve of the corrosion part. In Figure 4.11(a), the delamination was observed from the outermost layers (7 → 4 CFRP sheets). The delamination gaps were measured from the cut section at SG3 with 500x magnification. The gap widths were measured from 0.3 – 0.35 mm, respectively. The typical delamination in the bridging zone length under a long cyclic load was investigated. This characteristic is recognized as viscoelastic deformation of the tip zone with each load cycle. Compressive cyclic load denotes the traction stress at the beginning of detachment to generate the debonding. This study found evidence of delamination damage of the specimen without applying FU-Z after the detachment strike. The specimen with polyurea putty was safe from delamination, as shown in Figure 4.11(b). The contribution of putty material was noticed to control the internal delamination in the CFRP reinforcement structure. The putty's ability to elongate helped the specimen matrix (resin) sustain long eccentric cyclic loading.

The proposed study contributes to a better understanding of internal delamination at the transition curve of the corrosion region. The delamination was mainly caused by stiffness degradation after the joint separation. The bending of local stress flowed through all layers and caused damage in 50% of the layers, as displayed in Figure 4.11(a). It can be seen in this experiment that putty can prevent internal damage that occurs to the CFRP. When the CFRP is faced with a cyclic loading that affects the high elastic level at a point, it can allow the putty to avoid a situation in which a state of fatigue will occur. This assessment can be used as a reference in the CFRP

retrofit so that it knows the actual validity. Moreover, this experiment revealed that the CFRP part could hold the cyclic loading in a high-stress range during the delamination and detachment process.

Delamination might be developed inside the CFRP part component without being noticeable on the surface. Still, delamination failure in this experiment relied on the detachment initiation cycle, even though the local bending stress was dominant. The relationship failure phenomenon occurred when the material detached from its adjoining layer losing its elastic modulus ($\boldsymbol{E_0}$). Then, the adhesion between the CFRP sheet layer and resin (FR-E9P) causes separation. Because a low elastic modulus of resin bound together the CFRP sheet, in particular, compressive cyclic fatigue load applied aligned with CFRP sheets angle ($90^{o}$), and out-of-plane mode can cause the resin matrix to debond from the CFRP sheets. Indeed, the matrix was the weakest part of CFRP laminate. However, the specimen without polyurea putty survived until 3x106 cycles, indicating that the material of strengthened steel girder ends reached the fatigue life design ($2x10^{6}$ cycles).

## 4.4 Summary

The putty is flexible enough to prevent delamination and detachment under high-stress cyclic. However, although high frequency was applied, CFRP peeling has not occurred during the experiment. The result of HCF shows that it is low-strength material but high-elongation elastic material with good energy absorption capability.

Detachment and delamination at the end of the curved part were confirmed. In this research, the following findings were mainly obtained:

| | Fatigue Durability | Ending of Cycles |
|---|---|---|
| No polyurea putty (FU-Z) | No visual damage deformation was detected until 2.5 million cycles | A slight local stress inclination was confirmed at 3.5 million cycles due to detachment |
| | The local stress shift was confirmed at 3 million cycles, which indicated damage initiated in the compact specimen | Significant delamination was confirmed from 7 to 4 layers in the top-of-end corrosion after 3.5 million cycles (around SG 3). |

| | | |
|---|---|---|
| With polyurea putty (FU-Z) | Specimen with putty survived to complete all fatigue cycles at 3.5 million cycles with no damage | No damage was detected, and no local stress shift characteristics after 3.5 million cycles. |

To protect the CFRP part from initiation of microdamage, consider that the CFRP is a brittle material. It can be interpreted that the fatigue life improvement of CFRP reinforcement by added polyurea putty was related to flexibility behavior. Using polyurea putty is the factor that significantly improved the durability and strength of the reinforcement part due to long fatigue conditions.

The compact specimen with CFRP retrofit showed great high-cycle fatigue endurance. Finally, essential characteristics relating to the specimens CFRP strengthened without high elongation polyurea putty were investigated.

1. The proposed method provides a general method for determining service live load control for CFRP retrofitted steel girder ends safety prediction. It was also found that the maximum local compressive stress is reduced by an effective distance of bracing or with increases in the eccentricity of live load positions. The stress redistribution of retrofit web-ends has been discovered to determine the local stress shape characteristics of the damaged area under CFRP reinforcement.
2. The specimen's filler plate and fixture are vital in realizing eccentric compression cyclic loads. The elastic condition is still considered in this high cycle fatigue loading. In the following investigation, the out-of-plane behavior would induce the performance of retrofit members.
3. The result of HCF shows that polyurea putty (FU-Z) is low-strength material but high-elongation elastic material with good energy absorption capability. To protect the CFRP part from initiation of microdamage and shifted local stress ($\boldsymbol{\sigma_{SLS}}$), considering that CFRP is a brittle material. It can be interpreted that the fatigue life improvement of CFRP reinforcement steel girder ends by polyurea putty is related to the viscoelastic behavior of the polymer. Using polyurea putty is the factor that significantly improved the durability and strength of the reinforcement part.

## 4.5 References


[4.1] H. Fujiwara and M. Miyake, "Quantitative analysis on deterioration and remaining life of steel bridge painting based on field data," *Struct. Eng. Eng.*, vol. 20, no. 2, 2003.

[4.2] Japan Road Association. (JRA) (2012). Spesification for Highway Bridge (Part II Steel Bridges). ISBN978-4-88950-717-1 C2051

[4.3] M. Shenoy, J. Zhang, and D. L. McDowell, "Estimating fatigue sensitivity to polycrystalline Ni-base superalloy microstructures using a computational approach," *Fatigue Fract. Eng. Mater. Struct.*, vol. 30, no. 10, pp. 889–904, 2007.

[4.4] P. Colombi and G. Fava, "Fatigue behaviour of tensile steel/CFRP joints," *Compos. Struct.*, vol. 94, no. 8, pp. 2407–2417, 2012.

[4.5] H. Liu, X. L. Zhao, and R. Al-Mahaidi, "Fatigue crack growth simulation for CFRP bonded steel plates using boundary element method," *Compos. Civ. Eng. CICE 2006*, vol. 4, no. Cice, pp. 425–428, 2020.

[4.6] Fan, Z. T., Huang, W., & Negoita, A. (2022). Repairing Steel Girder End Corrosion Using Ultra-High Performance Concrete. Journal of Bridge Engineering, 27(1), 05021015.

[4.7] Miyakoshi, T., Atsumi, T., Kosugi, K., Hosoi, A., Tsuda, T., & Kawada, H. (2022). Evaluation of very high cycle fatigue properties for transverse crack initiation in cross - ply carbon fiber - reinforced plastic laminates. Fatigue & Fracture of Engineering Materials & Structures, 45(8), 2403-2414.

[4.8] Backe, S., & Balle, F. (2018). A novel short-time concept for fatigue life estimation of carbon (CFRP) and metal/carbon fiber reinforced polymer (MCFRP). International journal of fatigue, 116, 317-322.

[4.9] Ghahremani, K., Ranjan, R., Walbridge, S., & Ince, A. (2015). Fatigue strength improvement of aluminum and high strength steel welded structures using high frequency mechanical impact treatment. Procedia Engineering, 133, 465-476.

[4.10] D. Zhang, W. Huang, J. Zhang, W. Jin, and Y. Dong, "Prediction of fatigue damage in ribbed steel bars under cyclic loading with a magneto-mechanical coupling model," *J. Magn. Magn. Mater.*, vol. 530, no. January, p. 167943, 2021.

[4.11] J. Deng, J. Li, and M. Zhu, "Fatigue behavior of notched steel beams strengthened by a prestressed CFRP plate subjected to wetting/drying cycles," *Compos. Part B Eng.*, vol. 230, no. July 2021, p. 109491, 2022.

[4.12] A. Hosseini, J. Michels, M. Izadi, and E. Ghafoori, "A comparative study between Fe-SMA and CFRP reinforcements for prestressed strengthening of metallic structures," *Constr. Build. Mater.*, vol. 226, pp. 976–992, 2019.

[4.13] A. Li, S. Xu, H. Wang, H. Zhang, and Y. Wang, "Bond behaviour between CFRP plates and corroded steel plates," *Compos. Struct.*, vol. 220, pp. 221–235, Jul. 2019.

[4.14] Hagaragi, M., Mohan Kumar, M., & Sharma, R. S. (2021). Estimation of Residual Life and Failure Mechanism of Cracked Aircraft Wing Skin. In Fatigue, Durability, and Fracture Mechanics: Proceedings of Fatigue Durability India 2019 (pp. 493-513). Springer Singapore.

[4.15] D. Wakabayashi, T. Miyashita, Y. Okuyama, and N. Koide, "Study on Repair Method using CFRP for Corroded Steel Girder Ends."

[4.16] Miyashita, T., Nagai, M., Wakabayashi, D., Hidekuma, Y., Kobayashi, A., Okuyama, Y., ... & Horimoto, W. (2015, August). Repair method for corroded steel girder ends using CFRP sheet. In IABSE-JSCE Joint Conference on Advances in Bridge Engineering-III (pp. 21-22).

[4.17] Strengthening Effect of CFRP Bonded Steel Plate with Insufficient Bond Length. https://www.ndt.net/article/smar2019/papers/Th.3.B.8.pdf

[4.18] NERI (Nippon Expressway Research Institute). 2015. Design and installation manual for upgrading of steel structure with the use of carbon fiber sheet. Tokyo : NERI

[4.19] Vibration and Stresses In Girder Bridge. https://onlinepubs.trb.org/Onlinepubs/hrbbulletin/124/124.pdf

[4.20] Numerical Assessment of CFRP Retrofit Effect for Repairing Corroded Steel Girder Ends by Local Stress and Displacement Distribution. DOI: 10.37421/24720437.2022.08.123

[4.21] A. Li, S. Xu, H. Wang, H. Zhang, and Y. Wang, "Bond behaviour between CFRP plates and corroded steel plates," Compos. Struct., vol. 220, pp. 221–235, Jul. 2019.

[4.22] M. Lei, Z. Linyun, L. Shuqin, and W. Shui, "Eccentric Load Coefficient of Live Load Normal Stress of Continuous Composite Box-girder Bridge with Corrugated Steel Webs," Procedia Earth Planet. Sci., vol. 5, pp. 335–340, 2012.

[4.23] L. M. Gil-Martín, B. Šćepanović, E. Hernández-Montes, M. A. Aschheim, and D. Lučić, "Eccentrically patch-loaded steel I-girders: The influence of patch load length on the ultimate strength," J. Constr. Steel Res., vol. 66, no. 5, pp. 716–722, 2010.

[4.24] Koutsonas, S. (2018). Modelling race-tracking variability of resin rich zones on 90 composite 2.2 twill fibre curved plate. Composites Science and Technology, 168, 448-459. https://doi.org/ 10.1016/j.compscitech.2018.08.001

[4.25] Haesch, A., Clarkson, T., Ivens, J., Lomov, S. V., Verpoest, I., & Gorbatikh, L. (2015). Localization of carbon nanotubes in resin rich zones of a woven composite linked to the dispersion state. Nanocomposites, 1(4), 204-213. https://doi.org/10.1080/ 20550324.2015. 1117306

[4.26] Ahmadian, H., Yang, M., & Soghrati, S. (2020). Effect of resin-rich zones on the failure response of carbon fiber reinforced polymers. International Journal of Solids and Structures, 188, 74-87. https://doi.org/10.1016/j.ijsolstr.2019.10.004

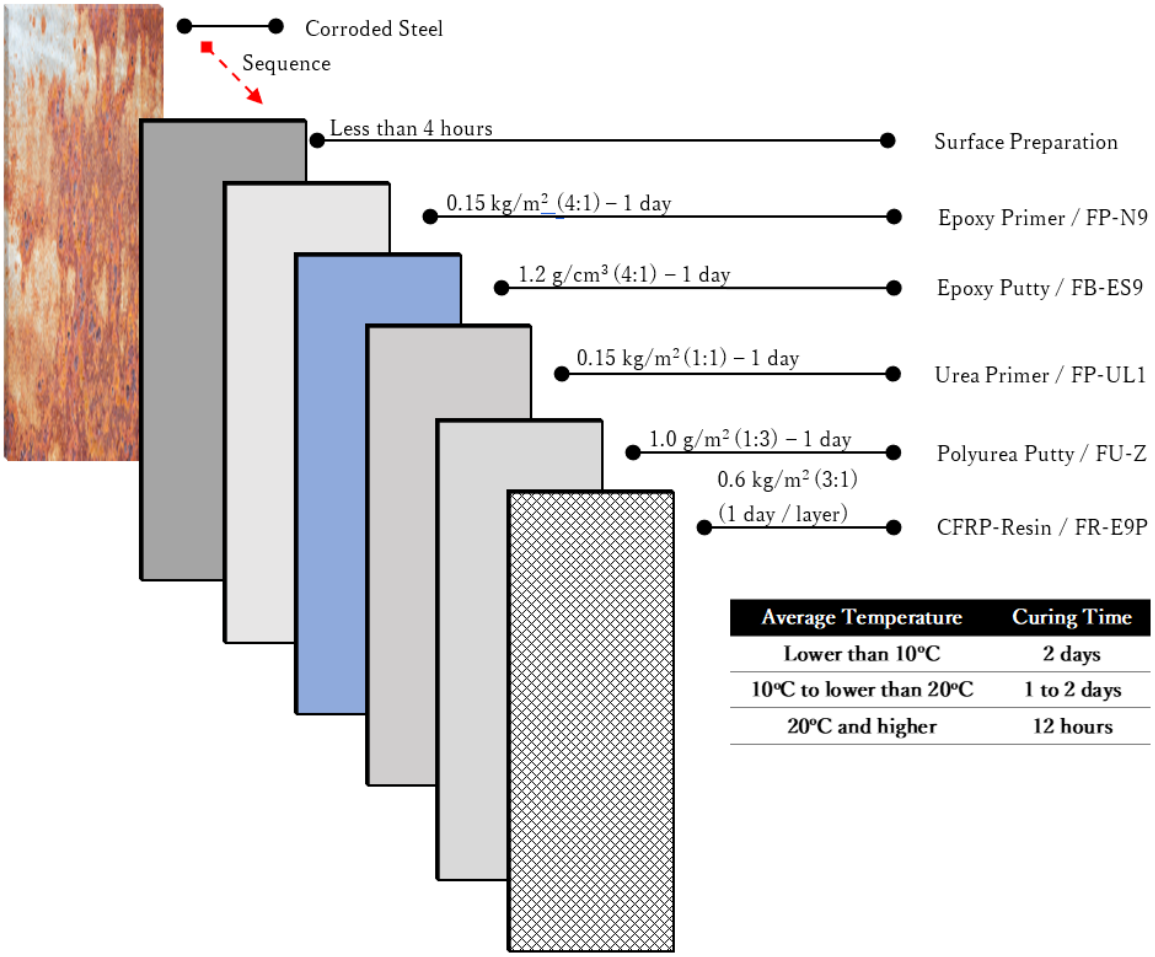


| Average Temperature | Curing Time |
|---|---|
| Lower than 10°C | 2 days |
| 10°C to lower than 20°C | 1 to 2 days |
| 20°C and higher | 12 hours |

**Figure 4.1** Configurations of each layer of CFRP bonding method and standard amount resin

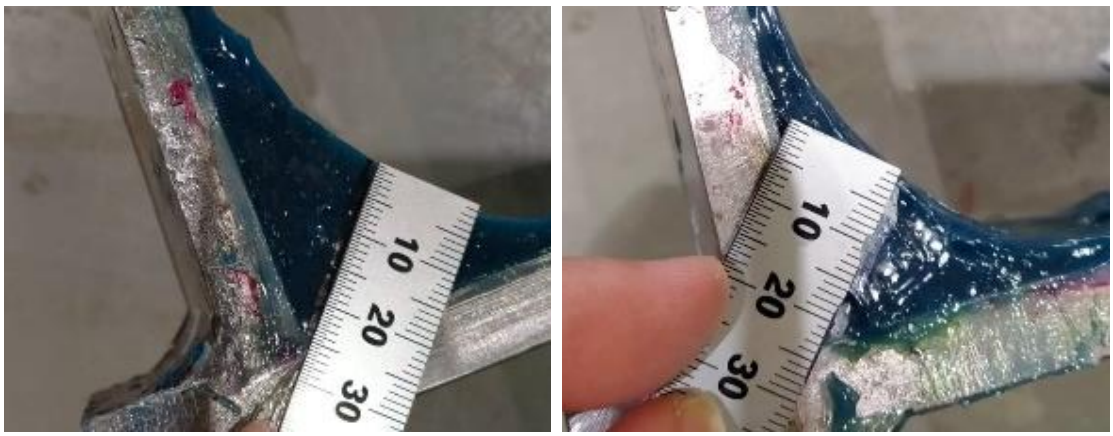


(a) (b)

**Figure 4.2** Comparison of (a) Epoxy putty in specimen without polyurea putty; (b) with polyurea putty

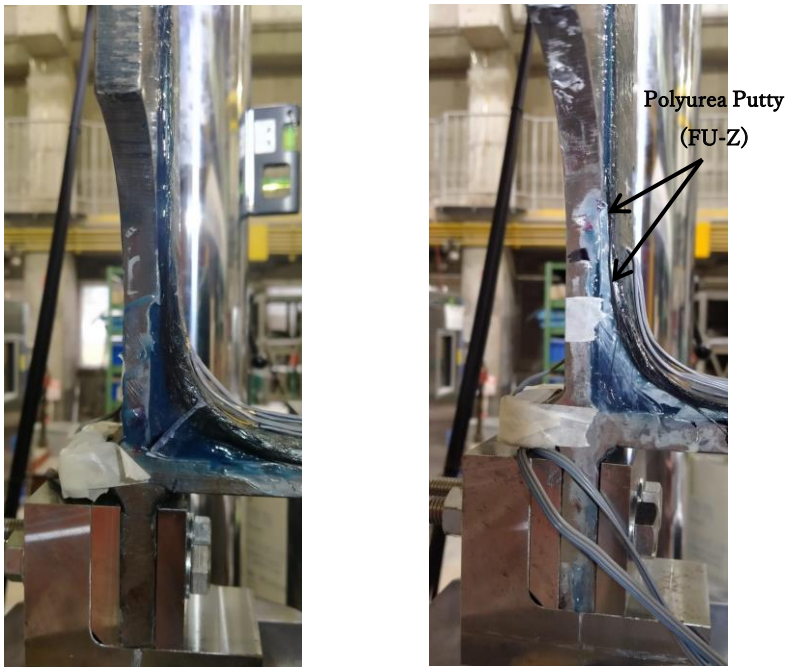


**Figure 4.3** Comparison of applied material: (a) Retrofit specimen without putty (b) with putty.

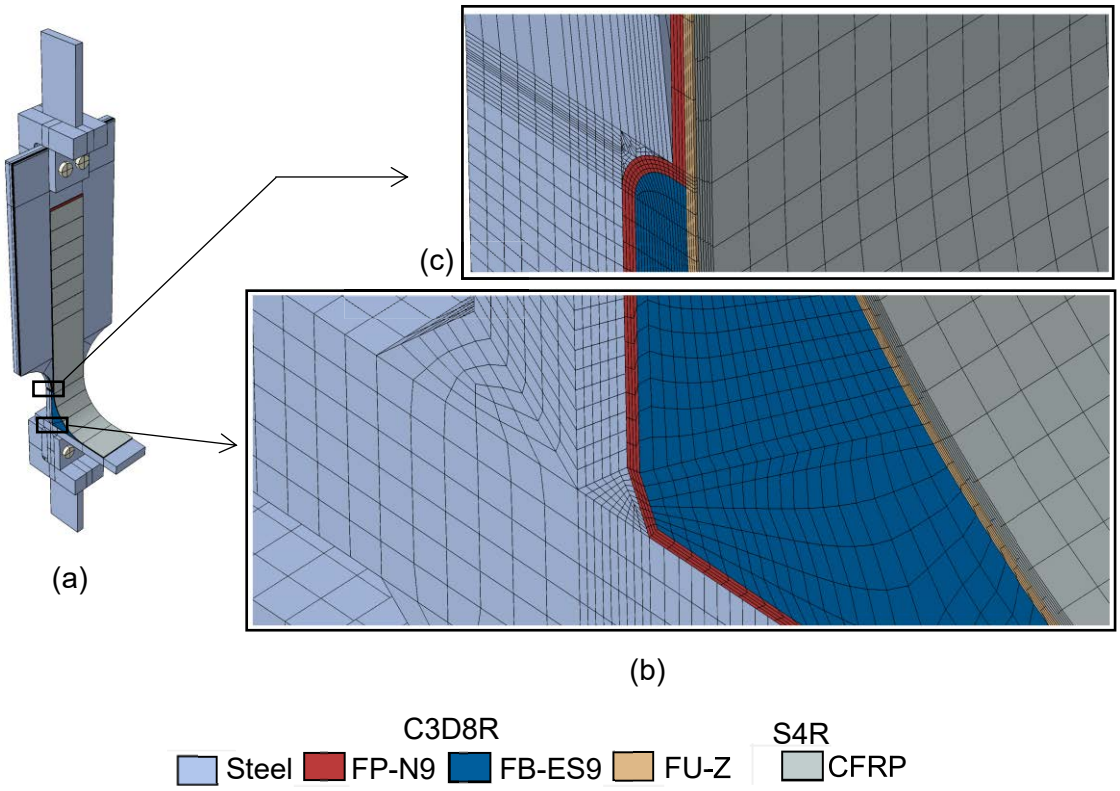


**Figure 4.4** (a) Retrofit specimen modeling; (b) Detailed mesh of corrosion weld part; (c) Detailed mesh transition curved part.

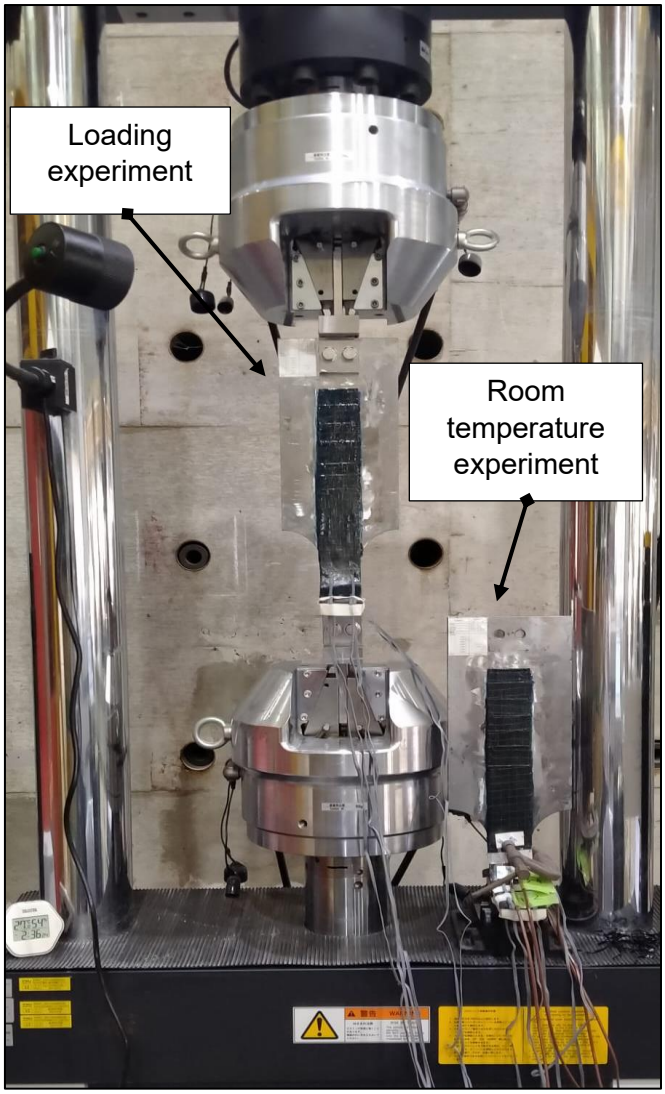


(a)

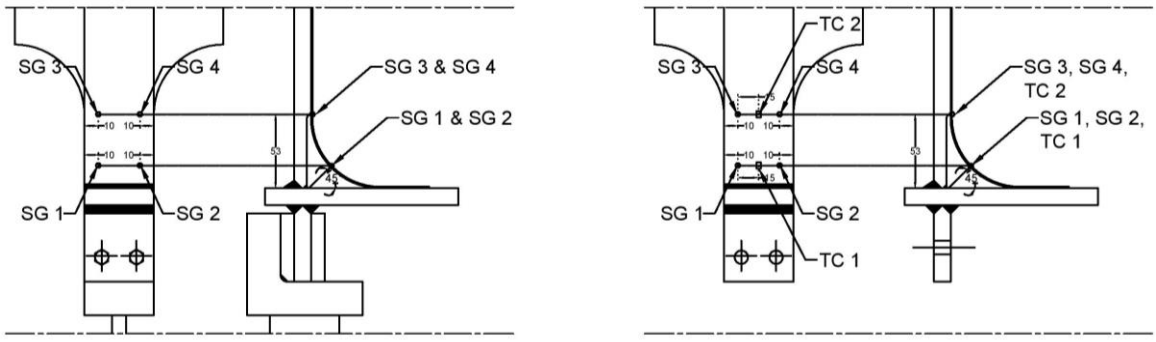


(b) (c)

**Figure 4.5** (a) Experiment condition; (b) Location of strain gauge (SG) at loading experiment; (c) Location of strain gauge (SG) and thermocouple (TC) at temperature experiment (unit: mm).

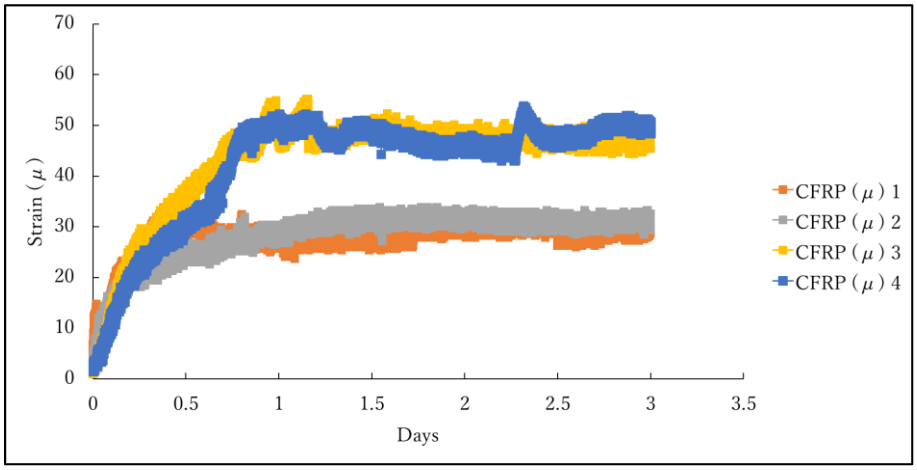


(a)

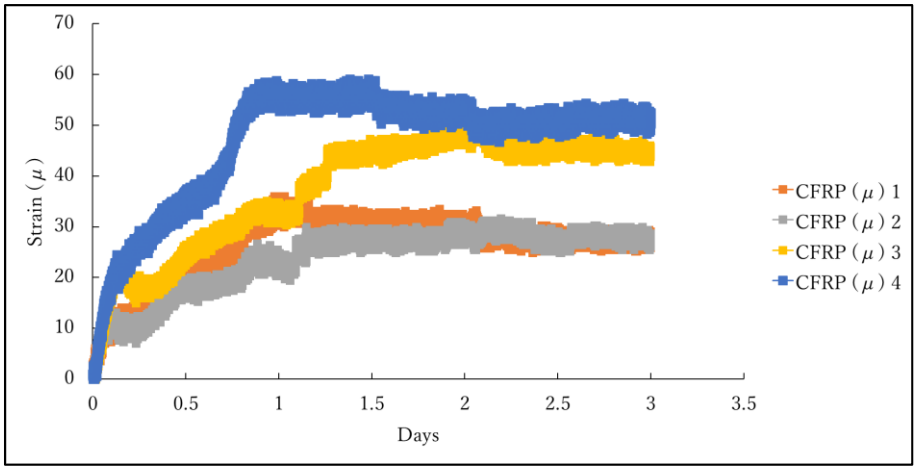


(b)

**Figure 4.6** (a) Creep strain of retrofit specimen without putty (15kN); (b) with putty (15 kN)

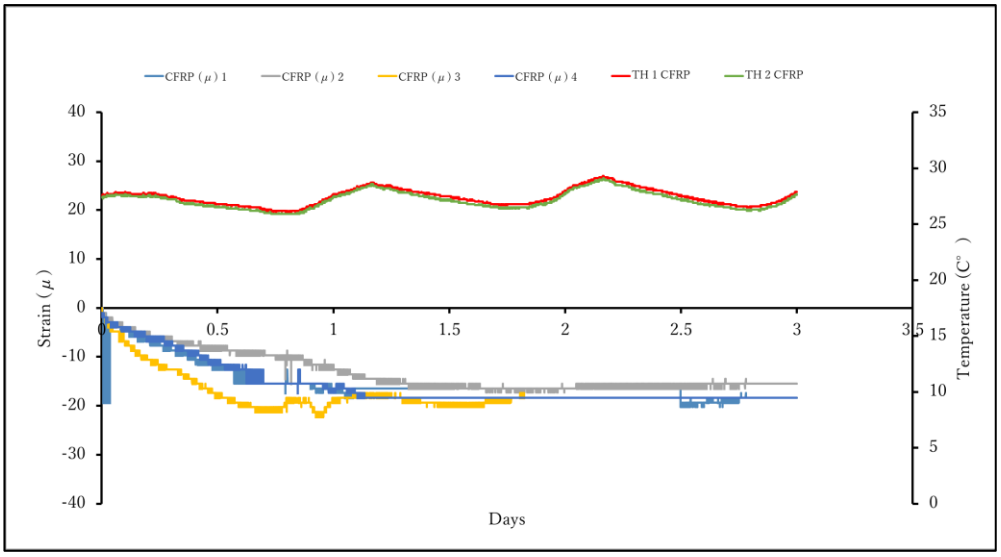


**Figure 4.7** Strain characteristics of room temperature on CFRP part

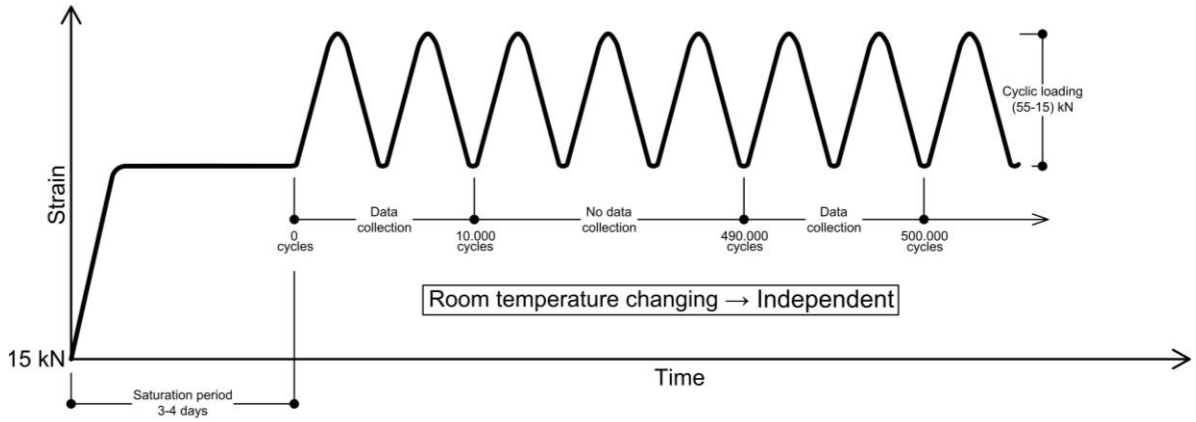


**Figure 4.8** Schematic loading strategies of fatigue durability experiment

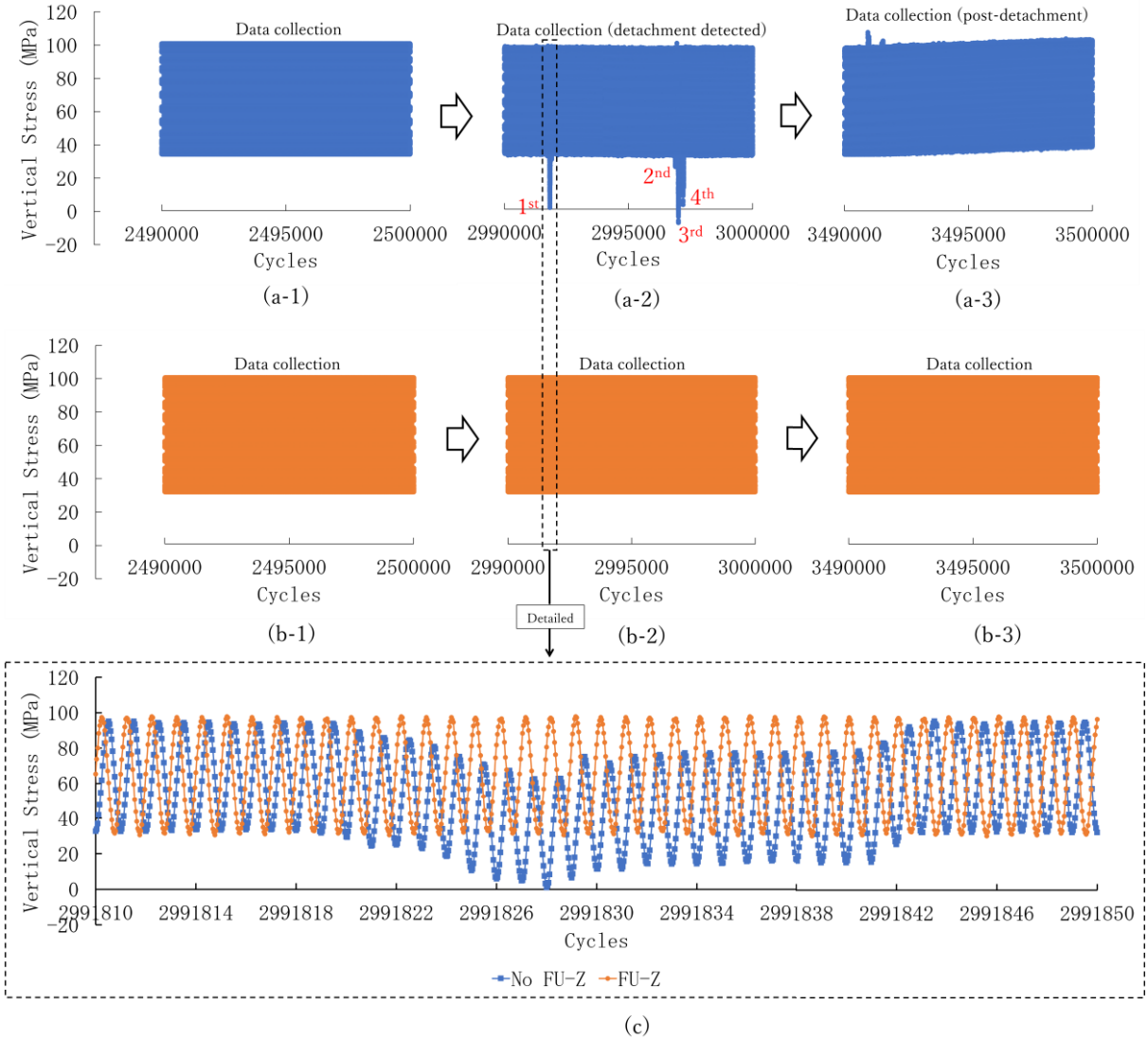


**Figure 4.9** Data collection of local stress at 2.5-3-3.5 million cycles: (a-1) local stress data specimen without putty in 2.5x106 cycles; (a-2) detachment detected data collection; (a-3) data collection of post damage initiation in 3.5x106 cycles; (b 1-3) specimen with putty; (c) detailed comparison cyclic loading with 1st damage initiation.

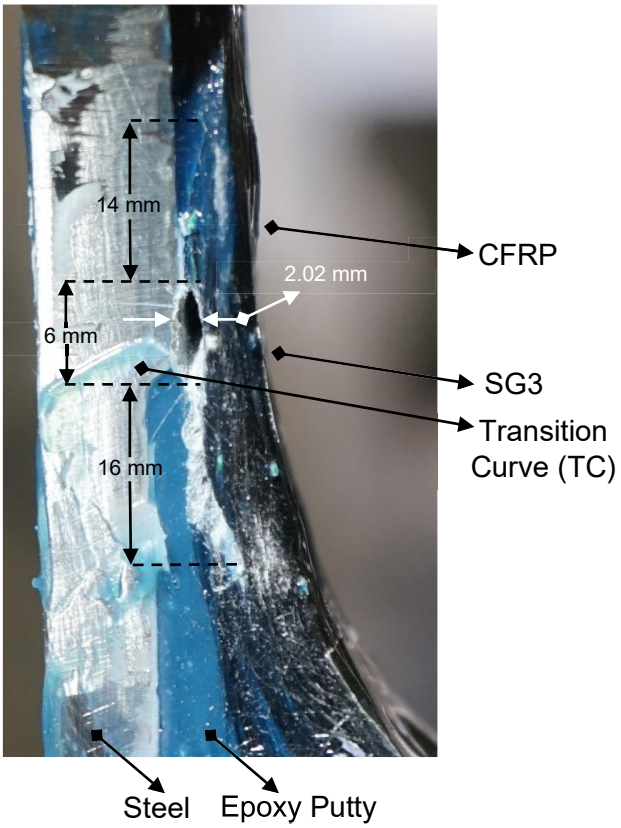


**Figure 4.10** Damage initiation as a detachment of interface CFRP reinforcement part in specimen without polyurea putty (FU-Z)

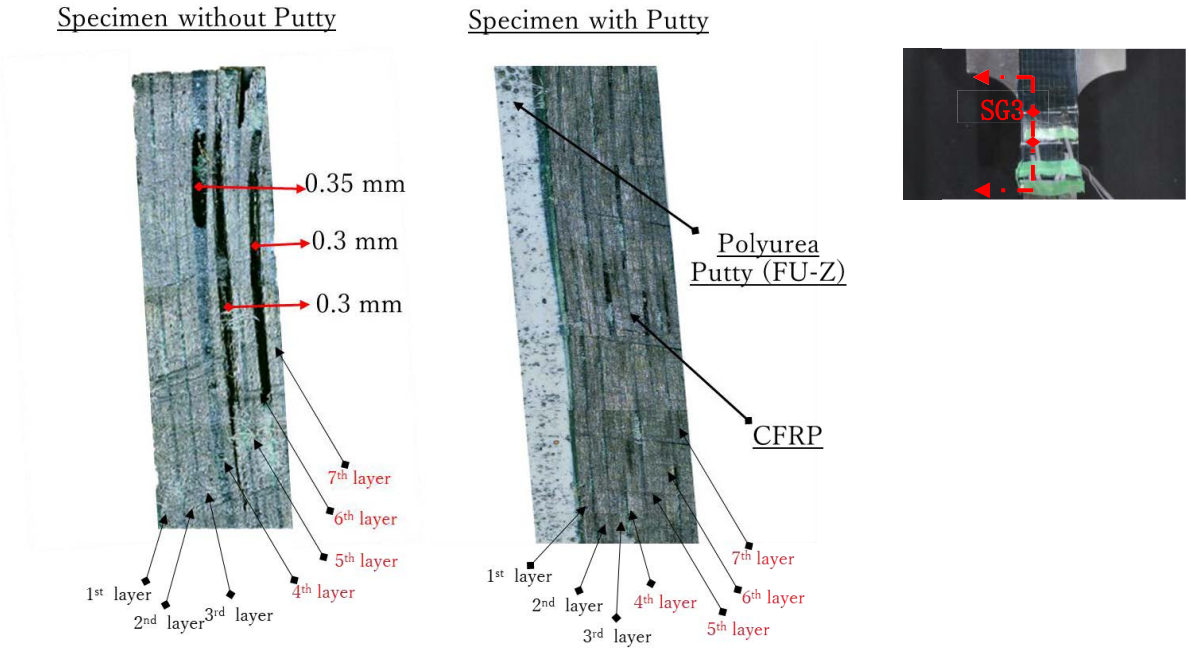


**Figure 4.11** Cut section of specimen: (a) specimen without putty – delamination observes; (b) specimen with putty.

# Chapter 5
# Conclusions and Recommendations

## 5.1 Conclusions

The assessment of the retrofit steel bridge was necessary to evaluate and accurately identify the "turning points". Technical evidence of fatigue durability resistance under elastic conditions (service life) could be recognized. Also, it was to generate the visual damage initiation characteristics in the CFRP retrofit girder ends specimen [1-25].

This research provides a new methodology for assessing the durability of Carbon Fiber Reinforced Polymer (CFRP) strengthening of corroded steel girder ends. The approach is based on detecting damage initiation characteristics to describe the fatigue durability of the CFRP reinforcement system. The study present suggested experiment procedure, including retrofitted specimen design and loading parameters. The assessment methods can be used in the CFRP retrofit steel girder ends service live durability determination model.

A CFRP reinforcement material consists of a CFRP sheet, primer, and epoxy adhesive, then typically provided as a system. Also, the correlation between material selection and structure life is observed. The fatigue durability specimen without putty (FU-Z) is applicable under 3 million cycles where local stress concentration occurs on the edge bond. However, bending stress transfers through the reinforcement part without putty could be less flexible than through the specimen with putty. That is why the damage initiation was detected earlier in the specimen without putty. This response suggested that material-saving in the fatigue durability of CFRP systems is possible and cost-effective. However, this study focuses on the service load conditions of the steel girder ends bridge. Then, the usability of polyurea putty (FU-Z) in the CFRP retrofit method should be clarified for another load condition, e.g., seismic load, wind load, and UV exposure. Also, the variety of target parts should be included, e.g., localized corrosion at a lower flange. In the CFRP field application for the reinforcement, the durability against service load was not the only factor influencing its performance. Then, the conclusions of this research are expressed as follows:

1. To identify the severe characteristics of local stress distribution and deformation at steel girder ends CFRP retrofit.

A numerical investigation was conducted to study the effect of bracing type at the bridge ends on the local stress distribution of steel plate girder bridges. Detailed modeling of CFRP retrofitted girder ends with different bracing were analyzed under self-weight and live load eccentrically applied in the lane over the exterior girder. Those analyses were carried out in healthy-corroded-retrofit conditions to identify their local behavior. The area of section loss at the inner side of the web ends plate was determined within the effective width ($12t_{web}$).

In a steel girder bridge with cross-beam bracing (CB), local stress in the bottom weld bead joint of the support part is slightly larger than cross-frame bracing (CF-V & CF-X). Indeed, the effect of cross-frame was more significant in steel girder bridges. However, the comparison results of the stress ratio were shown that the depth of surface loss ($t_{sd}$) was played an important role in categorizing the allowable stress of SM400 in the design ($\sigma_{140}$). Also, the characteristics of bending mode deformations showed transversal displacement towards the tension side. This coupling effect creates the potential damage region because local stress concentration was higher at the cruciform corner edge of the column girder ends. All CFRP retrofit sub-models in-plane local stress concentration contour occurred for ¼ the total horizontal direction and decreased following CFRP geometry. Then, the identification of severe regions at CFRP reinforcement of corrosion steel girder ends was recognized.

Finally, The CFRP curved part (R = 50 mm) plays a significant role in shifting the distribution peak of local stress. Higher local stresses were mainly generated at the top end of the corroded edge part. That corroded edge was recognized as the transition zone from the corroded to the uncorroded in the web girder ends region. Based on the stress distribution of CFRP retrofit cases, it was revealed that the transition zone has a jump in stress phenomena. Because the surface loss modeling on the girder ends produced stiffness deterioration, which could clarify why being under the material elastic modulus ($E$) still has residual local stress. The detailed results are discussed in Chapter 2.

2. To develop a novel experimental method of reproduction of CFRP retrofitted steel girder ends conditions.

There could be the possibility of insufficient fatigue machine specification to applicate a full-size retrofitted bridge target part. Then, only a small practical part was constructed as a compact specimen to interpret the fatigue experiment. The fixture and specimen design became key parameters to replicate the CFRP retrofit girder ends element conditions. Fixture design contains various functions: fixture planning, specimen layout strategy, and fixture element design. Therefore, the fixturing layout is essential to identify the technical parameter configuration in eccentric fatigue cyclic loading, which is the configuration of the retrofit specimens following the limitation of the fatigue machine. In addition, the filler plate also contributes to eccentricity reproduction during the fatigue experiment. Therefore, the simplification approach of the corroded specimen part was conducted. The limitation of duplicability of the corroded girder ends part, e.g., stiffener and scallop parts that reproduced a local stress shape. The comparison of vertical local stress distribution shape between the retrofit girder end and the retrofit specimen is successfully

generated, which increases the assessment accuracy. It is proven that the proposed compact specimen and fixture design maintained the CFRP-retrofit steel girder ends specimen in elastic condition.

The vertical local stress distribution shape method proposed a numerical simulation to determine the fatigue machine's loading. The conventional approach focused on the vertical local stress distribution correlation between retrofit girder ends, and the specimen was considered. This method can be reproduced characteristics target structure from the model target bridge to the experimental scale specimen. With this challenge, the novel fatigue experimental design is designed and evaluated in Chapter 3.

3. To observe high-cycle fatigue conditions due to its lowest durability location on the retrofitted specimen

In Chapter 4, the experimental-scale fatigue durability was performed to evaluate the strengthened damaged part of steel girder ends by recognizing the resistance behavior under long-run elastic loading. The study aims to make it possible to consider the location of fatigue initiation due to low-durability section parts. Retrofit specimens were designed to replicate the inner side corrosion of steel girder web ends. Applicability of a new bending fixture design to reproduce an actual eccentric compressive axial constant load by considering the compact specimen shape and dimensions was performed. Also, a strategy for fatigue strength evaluation is outlined, including polyurea putty application, loading frequency, and data collection methods.

The physical behavior response of CFRP reinforcement at corroded steel girder ends specimen under the service loads was observed well. It was respectable to mention that CFRP retrofit specimens impacted all local damage responses presented in this study without polyurea putty (FU-Z) application. Linear elasticity was the most significant of these characteristics since it described the initial response of the specimen to constant amplitude load fluctuations. The CFRP-damaged part can be returned to its original stress upon the damage initially appearing. When purely detachment damage was detected at the CFRP part, it could be recognized as an “impact stress”. This phenomenon was analyzed with detachment conditions to determine whether the joint material lost its elasticity during separation. Therefore, in time ($5x10^5$ cycles) the elastic modulus will be changed independently. This behavior was described when the local stress during the deformation stages does not exceed the elastic limit. In this process, the interlaminar stress of the CFRP joint led to redistribution for the instance cyclic period. Furthermore, some deformations were visible and permanent. However, owing to the high elastic modulus of CFRP, it can endure large amounts of cyclic loading so that the corroded steel girder is safe.

Two initial damage characteristics are found in the CFRP retrofit specimen without polyurea putty (FU-Z) under cyclic loading: detachment and delamination. The macroscopic initial damage location was at the corrosion edge. Since the elastic modulus of each element's strength is typically stronger than the joint itself, detachment is involved in the joints earlier than the delamination of CFRP layers. It took $3x10^6$ cycles to detect detachment so that the shifted local stress ($\sigma_{SLS}$) was announced as measured to monitor the detachment initiation of joints. During eccentric constant compression cyclic loading, the detached CFRP cannot resist its bonding interface (CFRP fiber-resin (FR-E9P)). It was investigated that the delamination within CFRP takes the exact location after detachment. Hence, understanding the impact of damage initiation will help the engineer safely estimate the durability of CFRP reinforcement at corroded steel girder ends against long periods of service life.

Finally, the numerical analysis in Chapter 2 confirms that the typical retrofitted steel girder ends parameters on the durability resistance are the corrosion depth and the CFRP curved part. Then, in Chapter 3, the novel method of reproduction of actual conditions by combining eccentric load, CFRP retrofit requirement, and a set of compact specimen designs was proposed. Also, its accuracy was confirmed. Furthermore, in Chapter 4, the combination of high-cycle fatigue and signal processing was considered for observed the durability of all specimens. First, an attempt was made to evaluate the retrofit specimen's room temperature effect and creep effect. Experimental on CFRP reinforcement steel girder ends system indicated that the procedure in this study could determine the response of deterioration in ambient conditions. The configuration of the strain gauge location was considered as well. Next, observation and evaluation of the damage initiation presence on the CFRP retrofit part were attempted. This study shows the possibility of evaluating CFRP reinforcement's durability resistance experimentally due to the steel girder end's service life condition. This study's fatigue durability observation indicates that the CFRP-repaired steel girder end specimens improved service life and have excellent fatigue durability if adequately constructed following current guidelines and specifications.

## 5.2 Recommendations

Based on the conclusions of this study, the following suggestions are made for a more accurate assessment of the structural performance of CFRP reinforcement steel girder ends.

I. Through this study, durability observation indicates that the CFRP-repaired steel girder ends' service life improvement has excellent fatigue durability. If adequately constructed following current guidelines and specifications (NERI) [5]. The result of the experiment was to present a new way of understanding the phenomena of CFRP reinforcement that

exceeded $\mathbf{2.5\,x\,10^6}$ cycles. This study contains the description of methods and procedures for estimating the elastic stress range of retrofit specimens from numerical analysis based on Specifications for Highway Bridges Part II, in detailed category D ($\Delta\sigma_f = \mathbf{100\ MPa}$) [4]. Then, to set out the practical method for engineers working on fatigue design of CFRP when assessing the influence of post-retrofit of corrosion part specific at the steel girder ends. This includes the practical implication of the ability of damaged CFRP joint (no FU-Z) against extreme cyclic loading. This will be helpful for fatigue durability evaluation and for engineers to adopt simple strength design rather than explain the concept to understand the details of the phenomena themselves.

II. The durability resistance is an essential parameter for assessing the performance of the CFRP strengthening part. The accuracy of repaired steel girder ends evaluation has been improved in recent years, including the present result. On the other hand, the durability of steel bridge members was not always affected by service life loads, so there is still room for further study. However, this study made it possible to assess the local behavior of CFRP-strengthened steel girder ends numerically. It is necessary to update the variation of surface loss location due to local corrosion at the steel girder ends. In particular, an analysis representing realistic many retrofit corrosion conditions is required. Furthermore, clarification of local stress and deformation modes of retrofit parts will enable accurate evaluation of durability resistance.

III. The compact specimen and fixtures also remain to be studied. In this study, the contribution of scallop and stiffener are neglected. However, the analysis and evaluation can be made from the fit-stress distribution method. The behavior on the durability test may contain a considerable amount of information. It is desirable to develop a variety of target that combines the results of many conditions. In the future, the compact specimen and fixtures should be capable of observing the variation of actual loading, e.g., seismic and wind load. It is essential to consider the CFRP retrofit location at the steel bridge's support, which makes it vulnerable to deterioration since it is promising to conduct experiments that reproduce other phenomena occurring on the CFRP retrofit part.

IV. The engineer should count the serviceability limit state aspect to avoid damage initiation, like in the present study. The strength limits state, stability limit state, and extreme limit state on the CFRP retrofit component are a necessity. In other considerations, the wet conditions experiment is recommended to provide the engineer with a basis for evaluating exposure selection because the current study only considers dry (ambient) conditions. The

wet environment is characterized by exposure and accumulation of moisture at the surface of CFRP reinforcement or interface of CFRP reinforcement. Also, the exposure at this temperature correlates with long-term durability response. A further experiment shall utilize the ultraviolet rays (UV A) due to extended exposure to the CFRP reinforcement to the sun. The durability test provides the influence of oxidation penetrating in the retrofit steel girder ends.

## 5.3 References


[5.1] Tamaki, Y., Shimozato, T., Tai, M., Fuchiwaki, H., & Taira, H. (2019). A Study on Washing Effect of Steel Girder Bridges Under Airborne Salt Environment in Subtropical Okinawa Areas. , 26(102), 102_43-102_55. (In Japanese)

[5.2] Tamakoshi, T., Yoshida, Y., Sakai, Y., & Fukunaga, S. (2006, October). Analysis of damage occurring in steel plate girder bridges on national roads in Japan. In Proceedings of the 22th US–Japan Bridge Engineering Workshop, Seattle, WA, USA (pp. 23-28).

[5.3] Fisher, J. W., Yen, B. T., & Wagner, D. C. (1987). Review of field measurements for distortion-induced fatigue cracking in steel bridges. Transportation Research Record, (1118).

[5.4] Specifications For Highway Bridges Part II Steel Bridges Japan Road Association March 2012.pdf.

[5.5] NERI (Nippon Expressway Research Institute). 2015. Design and installation manual for upgrading of steel structure with the use of carbon fiber sheet. Tokyo : NERI

[5.6] Pham, N. V., Miyashita, T., Ohgaki, K., Hidekuma, Y., & Harada, T. (2021). Repair Method and Finite Element Analysis for Corroded Gusset Plate Connections Bonded to CFRP Sheets. Journal of Structural Engineering, 147(1). 04020310

[5.7] Nirbhay, M., Dixit, A., Misra, R. K., & Mali, H. S. (2014). Tensile test simulation of CFRP test specimen using finite elements. Procedia Materials Science, 5, 267-273.

[5.8] Bagale, B. R., & Parvin, A. (2021). Fiber-Reinforced Polymer Strengthening of Steel Beams under Static and Fatigue Loadings. Practice Periodical on Structural Design and Construction, 26(1), 04020046.

[5.9] M. Shenoy, J. Zhang, and D. L. McDowell, “Estimating fatigue sensitivity to polycrystalline Ni-base superalloy microstructures using a computational approach,” Fatigue Fract. Eng. Mater. Struct., vol. 30, no. 10, pp. 889–904, 2007.

[5.10] P. Colombi and G. Fava, “Fatigue behavior of tensile steel/CFRP joints,” Compos. Struct., vol. 94, no. 8, pp. 2407–2417, 2012.

[5.11] H. Liu, X. L. Zhao, and R. Al-Mahaidi, “Fatigue crack growth simulation for CFRP bonded steel plates using boundary element method,” Compos. Civ. Eng. CICE 2006, vol. 4, no. Cice, pp. 425–428, 2020.

[5.12] D. Zhang, W. Huang, J. Zhang, W. Jin, and Y. Dong, “Prediction of fatigue damage in ribbed steel bars under cyclic loading with a magneto-mechanical coupling model,” J. Magn. Magn. Mater., vol. 530, no. January, p. 167943, 2021.

[5.13] D. Wakabayashi, T. Miyashita, Y. Okuyama, and N. Koide, “Study on Repair Method using CFRP for Corroded Steel Girder Ends.”

[5.14] A. Hartman, C. Bennett, A. Matamoros, and S. Rolfe, “Innovative retrofit technique for distortion-induced fatigue cracks in steel girder web gaps,” Bridg. Struct., vol. 9, no. 2–3, pp. 57–71, 2013.

[5.15] B. Bhattacharya and B. Ellingwood, “Continuum damage mechanics analysis of fatigue crack initiation,” Int. J. Fatigue, vol. 20, no. 9, pp. 631–639, 1998.

[5.16] M. Quaresimin and M. Ricotta, “Fatigue behaviour and damage evolution of single lap bonded joints in composite material,” Compos. Sci. Technol., vol. 66, no. 2, pp. 176–187, 2006.

[5.17] M. May and S. R. Hallett, “An assessment of through-thickness shear tests for initiation of fatigue failure,” Compos. Part A Appl. Sci. Manuf., vol. 41, no. 11, pp. 1570–1578, 2010.

[5.18] F. Magi, D. Di Maio, and I. Sever, “Damage initiation and structural degradation through resonance vibration: Application to composite laminates in fatigue,” Compos. Sci. Technol., vol. 132, pp. 47–56, 2016.

[5.19] T. K. O’Brien, A. D. Chawan, R. Krueger, and I. L. Paris, “Transverse tension fatigue life characterization through flexure testing of composite materials,” Int. J. Fatigue, vol. 24, no. 2–4, pp. 127–145, 2002.

[5.20] M. Marco, E. Giner, M. H. Miguélez, and D. González, “On the effect of geometrical fiber arrangement on damage initiation in CFRPs under transverse tension and compression,” Compos. Struct., vol. 274, no. July, p. 114360, 2021.

[5.21] T. Skinner, S. Datta, A. Chattopadhyay, and A. Hall, “Fatigue damage behavior in carbon fiber polymer composites under biaxial loading,” Compos. Part B Eng., vol. 174, no. May, p. 106942, 2019.

[5.22] J. Deng and M. M. K. Lee, “Fatigue performance of metallic beam strengthened with a bonded CFRP plate,” Compos. Struct., vol. 78, no. 2, pp. 222–231, 2007.

[5.23] F. W. Panella and A. Pirinu, “Thermal and ultrasonic analysis of fatigue damaged CFRP samples under traction and bending load,” Procedia Struct. Integr., vol. 28, no. 2019, pp. 1709–1718, 2020.

[5.24] M. M. A. Ammar, B. Shirinzadeh, P. Zhao, and Y. Shi, “An approach for damage initiation and propagation in metal and carbon fiber hybrid composites manufactured by robotic fiber placement,” Compos. Struct., vol. 268, no. February, p. 113976, 2021.